Electrocatalytic Degradation of Industrial Wastewater Using Iron Supported Carbon-Cloth Electrode via Electro-Fenton Oxidation Process

IKENNA CHIBUZOR EMEJI

216165288

A thesis submitted in fulfillment of the requirements for the

Doctor of Philosophy: Engineering: Chemical

Department: Chemical Engineering

Faculty of Engineering and Technology

Vaal University of Technology Vanderbijlpark

Supervisor/Promoter: Prof. PO. Osifo

Co-supervisor/Promoter: Dr. OM. Ama

Date: February 2021

DECLARATION

Name: **Emeji, Ikenna Chibuzor**

Student number: **216165288**

Degree: PhD in Chemical Engineering

Electrocatalytic Degradation of Industrial Wastewater Using Iron Supported Carbon-Cloth Electrode via Electro-Fenton Oxidation Process

I declare that the above thesis is my work, except where it is stated otherwise and it has not been submitted to another university for any other degree.

Signature:

Date: February, 2022

Place: Vaal University, Vanderbijlpark

DEDICATION

To the loving memory of my dear wife – Pastor Mrs Nwamaka Francisca Emeji

Acknowledgment

I humbly wish to express my sincere gratitude to my supervisor, in the person of Prof. P.O. Osifo, for his support, guidance, and fatherly role during the course of this program. May God Almighty bless him and grant him good health, long life, and prosperity. To my co-supervisor, Dr. OM. Ama, I say thank you, and may the horizon of opportunities always serve you.

Special thanks also go to my colleagues in "The Thermochemical Processes and Waste Utilisation research Group, department of chemical engineering, Vaal University of technology" for their positive contributions, and encouragements especially during research meetings, which enable me to develop a thick skin to pursue the program to completion. I would also like to thank the National Centre for Nanostructured Materials, Council for Scientific and Industrial Research for providing a conducive atmosphere during this period and allowing me to use their facilities.

My sincere gratitude goes to my lovely kids (Ikenna David, Tochukwu Divine, and Adanna Delight, Emeji) for their prayers and continuous support in all aspects, throughout this work. You are all amazing for always being there for me. I fondly love you all. To my siblings (Uchechukwu Obinna Emeji, Ugochukwu Ihenacho Chukwunonye, and Lucky Kelechi Chukwunonye), I am indebted to you all for the sacrifice, patience, and understanding you showed during this program. May God Almighty bless you all?

Finally to my friends Dr. Ephraim Igberase, Dr. Uyiosa Osagie Aigbe, and Chief Obed Amadi, may 'Chukwu-Okike Abiama Puru Ime Ihe Nile' continue to bless you all for the special roles each of you played in my life that enable me to complete this program.

LIST OF PUBLICATIONS

Book

Igberase, E., Osifo, P.O., Seodigeng, T. and **Emeji, I.** 2021. Enhanced Chitosan Material for Water Treatment. Springer International Publishing

Book Chapters

Emeji I.C., Ama O.M., Aigbe U.O., Khoele K., Osifo P.O., and Ray S.S. 2020. Electrochemical Cells. In: Nanostructured Metal-Oxide Electrode Materials for Water Purification. Engineering Materials, Springer, Cham

Emeji, I.C., Ama, O.M., Aigbe, U.O., Khoele, K., Osifo, P.O. and Ray, S.S. 2020. Properties and Synthesis of Metal Oxide Nanoparticles in Electrochemistry. In: Nanostructured Metal-Oxide Electrode Materials for Water Purification (pp. 85-96). Springer, Cham

Khoele, K., Ama, M.O., **Emeji, I.C.,** Anku, W.W., Ray, S.S., Delport, D.J., Osifo, P.O. 2020. Dynamic Degradation Efficiency of Major Organic Pollutants from Wastewater. In: Nanostructured Metal-Oxide Electrode Materials for Water Purification. Engineering Materials. Springer, Cham

Khoele K., Ama O.M., Delport D.J., **Emeji I.C.,** Osifo P.O., Ray S.S. (2020) The Essence of Electrochemical Measurements on Corrosion Characterization and Electrochemistry Application.

In: Ama O., Ray S. (eds) Nanostructured Metal-Oxide Electrode Materials for Water Purification. Engineering Materials. Springer, Cham

Anku, W.W, Ama, O.M., **Emeji, I.C.,** Aigbe, U.O., Osibote, A.O., Osifo, P.O., Ray, S.S.(2021) Functionalized Nano-Magnetics for Environmental Applications. Functionalized nanomagnetic materials for environmental applications, Editor(s): Chaudhery Mustansar Hussain, Sudheesh K. Shukla, Girish M. Joshi, In Micro and Nano Technologies, Functionalized Nanomaterials Based Devices for Environmental Applications,Elsevier, 2021, Pages 127-145: https://www.sciencedirect.com/science/article/pii/B9780128222454000015

Journal Publication

Emeji, I.C., Ama, M.O., Osifo, P.O, Ray, S.S., García-Rodríguez, O. and Lefebvre, O. 2019. Electrochemical preparation of iron-supported carbon-cloth electrode and its application in the in-situ production of hydrogen peroxide, *International Journal of Electrochemical Science*, 14. 9355 – 9368

Emeji, I.C., Ama, O.M., Khoele, K., Osifo, P.O. and Ray, S.S. 2021. Electro-Fenton Degradation of Selected Antiretroviral Drugs Using a Low-cost iron-modified carbon-cloth electrode. *Electrocatalysis*, 12 : 327–339

ABSTRACT

Human immunodeficiency virus (HIV) and acquired immune deficiency syndrome (AIDS) causes morbidity and mortality in infected patients. These epidemics are significantly reduced and treated globally with antiretroviral drugs (ARVDs). However, the eventual disposal of the ARVDs, either by excretion or otherwise, enables them to end up as emerging hazardous contaminants in our environment. Of all the available methods to remove ARVDs from our water bodies, electrochemical methods are reckoned to be one of the most effective. As a result, it is imperative to acknowledge the interactive behavior of these pharmaceuticals on the surface of the electrode. In this study, iron nano-particles were deposited on the carbon cloth electrode by electrodeposition using chronoamperometry techniques. The synthesized electrode was characterized using scanning electron microscopy (SEM), energy-dispersive x-ray spectroscopy (EDX), and x-ray photoelectron spectroscopy (XPS) microanalysis. The electrochemical characterization of the material was also carried out using cyclic voltammetry (CV) and electrochemical impedance spectroscopy (EIS). The electrode's electrocatalytic activity toward the generation of hydrogen peroxide (H_2O_2) through a two-electron oxygen reduction reaction was assessed.

Furtherance to this is the electrochemical degradation of nevirapine (NVP), lamivudine (LVD), and zidovudine (ZVD) in wastewater as a pharmaceutical model compound for organic pollutants in 50 mM K_2SO_4 electrolyte at a pH of 3. The SEM and EDX analysis showed the formation of iron nanoparticles within the matrix structure of the carbon cloth (CC) electrode. The XPS enlightened the presence of oxygen functional groups in the electrode's structure. EIS results are indicative that the modified electrode has a decreased charge transfer resistance (Rct)

value as compared to the bare CC electrode. On the other hand, the CV result fosters good conductivity, enhanced current and large surface area of the modified electrode. More active and anchor sites were discovered on the iron-supported CC electrode which resulted in higher catalytic activity for the generation and accumulation of H_2O_2. The concentrations of "*in-situ"* generated H_2O_2 were found to be related to the current density supplied to the device after quantification. Although the accumulated H_2O_2 concentration appears to be low, it's possible that side reactions depleted the amount of H_2O_2 produced. As a result, the oxygen reduction reaction (ORR) through 2e- has a higher electrocatalytic activity with the improved iron assisted CC electrode than bare CC electrode. The electrochemical degradation studies conducted with the modified CC electrode by electro-Fenton process show a decrease in the initial ARVDs concentration (20 mg/L) as compared with the bare electrode. Their rate constants were 1.52 x 10^{-3} $mol^{-1}min^{-1}$ for ZVD, 1.20 x 10^{-3} $mol^{-1}min^{-1}$ for NVP and 1.18 x 10^{-3} $mol^{-1}min^{-1}$ for LVD. The obtained removal efficiencies indicate that the iron nanoparticle in the synthesised improves the degradation efficiency.

Table of Contents

NOMENCLATURE

AIDS	Acquired immune deficiency syndrome
AOPs	Advanced oxidation processes
ARVDs	Antiretroviral drugs
BOD	Biological oxygen demand
BOD_u	Ultimate BOD
B.I.	Biodegradability index
CBOD	Carbonaceous biochemical oxygen demand
CC	Carbon cloth electrode
CE	Counter electrode
CME	Chemically modified electrode
COD	Chemical oxygen demand
CRAs	Chemokine receptor antagonists
CV	Cyclic Voltammetry
DO	Dissolved oxygen
E	Potential
EAOP	Electrochemical Advanced Oxidation Processes
EC	Emerging contaminants
EDS	Energy-dispersive X-ray spectroscopy
Epa	Anodic peak potential
Epc	Cathodic peak potential
EU	European Union

FIs	Fusion inhibitors
Fe/CC	Iron-supported carbon-cloth electrode
HAART	Highly active antiretroviral therapy
H_2O_2	Hydrogen peroxide
HIV	Human immunodeficiency virus
I	Current
INIs	Integrase inhibitors
Jo	Current density
K_2SO_4	Potasium tetra oxo sulphate (VI)
LVD	Lamivudine
MBR	Membrane bioreactor technology
MF	Microfiltration
µg/L	Microgram per liters
NF	Nanofiltration
ng/L	Nanogram per liters
NVP	Nevirapine
NRTIs/NtRTIs	Nucleoside and nucleotide reverse transcriptase inhibitors
NNRTIs	Non-nucleoside reverses transcriptase inhibitors
$OH^{\bullet}$	Hydroxyl radicals
ORR	Oxygen reduction reaction
PGSTAT	Potentiostat/Galvanostat
PIs	Protease inhibitors
ppm	Part per million

Rct	Charge transfer resistance
RE	Reference electrode
RO	Reverse osmosis
Rt	Retention times
SA	South Africa
SEM	Scanning electron microscope
t	Time
TDS	Total dissolved solids
TOC	Total organic carbon
UF	Ultrafiltration
WWTP	Wastewater treatment plant
WE	Working electrode
XPS	X-ray photoelectron spectroscopy
ZVD	Zidovudine

LIST OF TABLES

LIST OF FIGURES

Chapter 1: Introduction

Water reclamation from industrial and domestic wastewater is of global importance. Reclaimed water can be recycled for reuse and, therefore, can satisfy global water demand, as long as the wastewater is adequately treated. Treated wastewater effluents can be used for a good number of purposes such as toilet flushing, agricultural and irrigation purposes, industrial processes, and even for drinking and cooking purposes. However, the water must be accessible and safe. Access to a regular supply of clean water is part of our human needs. South Africa, which is situated in an arid region, lacks sufficient clean water to meet the needs of the people, especially those in the rural areas. The situation is further compounded by persistent periods of long droughts in recent times. This led the majority of people in South Africa to depend on groundwater obtained from aquifers and wells, which are often polluted. Water pollution occurs as a result of population increase, industrialization, rapid economic development, and water shortage. As a result, issues concerning water sustainability, usage, and management can be found almost in every sector of the world. There is a global prediction that water demand will increase by 55% during the period range of 2010 to 2050. However, this statistical global increase will see the water demand, from the manufacturing sector, increasing by about 400%. Also, the water demand in the electricity sector will increase by approximately 140% and in the domestic sector; the increase in water demand will be 130% (Water, U.N., 2015.)**.**

To avoid the risk of drinking contaminated water, the South African government has amended an act called the National Water Act 36 of 1998, Gazette No. 19182, and published it in the government gazette of September 6th, 2013. The act introduces stringent wastewater effluent disposal measures and made it mandatory for industries: (1) to treat effluents to acceptable

standards and limits before allowing the effluents into the water source as given in Appendix II, (2) to make effluent purification an integral part of the industrial process, and (3) to use certain prescribed amounts of water as permitted. Also, the Act imposes certain duties on the users, thereby, maintaining a balance between demand for water and water quality. These duties are designed to control water pollution, but because there are no incentives attached to compliance with these rules, industries tend to default. That is why the United Nations, suggested that protection of water quality from all sources of untreated wastewater, be they domestic, industrial or agricultural, is a prerequisite for ensuring sustainable development, poverty alleviation, job creation, human and ecosystem health and people's well-being (Water, U.N., 2014). However, technological advancement and working mechanisms of industries (e.g. pharmaceutical, chemical, and agricultural industries) have made them the major producers of enormous amounts of industrial wastewater. Manufacturing industries produce on daily bases, a variety of new chemicals that can be used for disease treatment in the health sector, cleaning in the domestic and industrial sector, controlling pests to increase food production in the agricultural sector, and purification of water in the water sector among others. Apart from the beneficial purposes of these chemicals, some of them are very toxic and highly hazardous and can seriously be harmful to the environment and human health. These new products are known as emerging contaminants (EC) and are regarded as a wider range of active organic micro-pollutant resulting from man-made chemicals. They include pharmaceuticals and veterinary medicines (prescribed and non-prescribed drugs), personal care products (such as soaps, cosmetics, disinfectants, toothpaste, etc.), industrial chemicals (such as benzene, dioxins, and PCBs), pesticides and herbicides and many other emerging compounds (Archer, 2017)**.**

As consumption of these chemicals increases, their environment concentration also increases as widely detected in recent times. Van Boeckel and co-workers in 2014 reported that there is a 36% increase in the global consumption of antibiotic drugs during the early period of 2000 to 2010. He went further to suggest that 76% of the increment in global antibiotic drug consumption is among the BRICS countries which include Brazil, Russia, India, China, and South Africa. Researchers such as Rehman *et al.* 2015, Camacho-Muñoz *et al.* 2014, and Luo *et al.* 2014, have identified various pharmaceutical products in water bodies around the world. In South Africa (SA), effluents from plant treating wastewater are the major source of pollution that deteriorates the water quality. Through this source, pharmaceutical products have been found to gain entry into the water bodies as reported by (Agunbiade and Moodley, 2016; Matongo *et al.,* 2015(a); Matongo *et al.,* 2015(b); and Swanepoel *et al.,* 2015). The presence of these pharmaceuticals in aquatic environments, even if they occur only in traces (sub nano or micro levels (ng/l or µg/l)), has led to great concern over their toxicological effect on exposure to humans and ecosystems. Jones and co-workers in 2001 identified microbial resistance to antibiotics and feminization or masculinization of aquatic organisms as the likely risk of exposure, among others. Generally, ECs have been identified to have endocrine-disrupting properties as pharmaceuticals in water may have an unintended effect on fishes (Nibamureke *et al.,* 2019). Although there are no given limits for some of these pharmaceutical contaminants in SA, it has been suggested by the United States Environmental Protection Agency (US.EPA, 2007), that these pharmaceuticals will be regulated shortly. Measuring the pharmaceutical micro-pollutants as biological oxygen demand (BOD), SA has no given limits; but, the European Union (EU) stipulated a guideline that targets BOD limits of 3.0 to 6.0 mg/l for aquatic life to be employed (Chapman, 1996). As for the chemical oxygen demand (COD), SA guidelines for

industrial effluents are targeted to be within the range of 0 to 30 mg/l as stipulated in their water quality guidelines of 1984 (Chapman, 1996; DWAF, 1996). Although the Maximum Contaminant Level (MCL) for chemicals in wastewater were shown in Appendix III, the effluent standards as given by DWAF, (DWAF, 1998) were presented in Appendix I.

To avoid the risk posed by these pharmaceutical micro-pollutants in our water bodies, it has become mandatory to develop treatment processes that will completely remove or reduce them from our environment. These treatment processes will allow pharmaceutical wastewater to be treated before their discharge to the environment (Edokpayi *et al.,* 2017), thereby minimizing pollution problems and protecting groundwater with other receiving water bodies from contamination. Conventional treatment techniques such as adsorption, oxidation, biological process, precipitation, coagulation, sedimentation, and sand filtration (Zazouli and Kalankesh, 2017; Pramanik *et al.,* 2017) have been reported to be ineffective since they require high energy, produces toxic sludge and intermediates that need further purification before disposal. Non-biodegradable micro-pollutants are recalcitrant to microorganism and are also very difficult to be removed by these treatment methods. Better and efficient purification technologies for water/wastewater treatment can eliminate the enumerated water associated problems. As a result, micro-pollutant removal using advanced oxidation processes (AOPs), Ozonation, and membrane bioreactor technology (MBR) are becoming more widely accepted (Garrido-Cardenas *et al.,* 2020). For this reason, the electro-Fenton process will be examined for the complete removal of organics from synthesized antiretroviral wastewater.

1.1 Problem Statement

In the world today, there is an increasing rate in human usage and consumption of pharmaceutical products. This rate will keep increasing because of improving health care systems and longer life expectations of people. Excreted pharmaceutical products in the form of the parent compound, intermediates, or metabolites enter into the wastewater treatment plant (WWTP) where removal should be done. Their general occurrence in the effluent of WWTPs is a problem. The inability of WWTPs to remove completely these micro-pollutants maybe as a result of the application of ineffective traditional treatment processes. It may also be because the pollutants are recalcitrant and, therefore, very difficult to break down by chemical and biological processes. Another suggestion is that the treatment plant may lack robustness if not designed for such activities, allowing the micro-pollutants to exist in trace amounts in the WWTPs effluents.

Stringent legislation has made it impossible for such effluents to be discharged into our water sources since they cannot support aquatic life and cannot be used for irrigation purposes. Such effluents are characterized by high chemical and biological oxygen demand. As a result, it is imperative to develop a treatment process that will completely remove or reduce these micro-pollutants to its allowable limits. Deziel *et al.* 2014, suggested that one major strategy in finding a lasting solution for the removal of wastewater micro-pollutants is through the combination of already existing treatment processes such as advanced oxidation processes (AOPs), biologically activated sludge and advanced membrane technology. Also, recent studies have shown that electro-Fenton is one of the most promising methods of recalcitrant organics removal from wastewater. However, in this study, the electro-Fenton process will be used to degrade and

remove selected recalcitrant pharmaceuticals such as zidovudine (ZVD), lamivudine (LVD) and nevirapine (NVP) antiretroviral drugs (ARVDs).

1.2 Objective

The main aim of this study is to use electro-Fenton process for the treatment of wastewater containing antiretroviral organics through the development of iron (II) deposited on carbon cloth electrode

1.2.1 Specific objectives

The basic objectives of this study are:

I. To synthesise composite iron-supported carbon-cloth (Fe/CC) electrode via electrodeposition, this will serve as a catalyst in the heterogeneous electro-Fenton treatment of antiretroviral wastewater

II. To characterise the surface morphology of the synthesized Fe/CC electrode using SEM, XPS, and EDS

III. To use electrochemical measurements such as electrochemical impedance (EIS) and cyclic Voltammetry (CV) to characterise the synthesised iron-supported CC electrode

IV. To determine the performance of the electrochemical process with respect to the synthesised Fe/CC electrode for the treatment of antiretroviral organics.

1.3 Project Scope

This work covers the synthesis of the iron-supported carbon-cloth electrode using iron (II) sulfate heptahydrate ($FeSO_4 \cdot 7H_2O$) as the source of iron. It also covers the characterisation of the synthesised electrode and the degradation studies of antiretroviral organics of ZVD, LVD, and NVP in water using the electro-Fenton process. On this note chapter 1 reports on; introduction, problem statement, objectives, and project scope. Chapter 2 deals with the literature review; hence, it reports antiretroviral drugs (ARVDs) in general, available techniques for the removal of organics from industrial wastewater, modified electrode, electrochemical techniques, and reversibility. It also gives a summary of the electrochemical cell operations detailing the electrifying processes occurring at the solution-electrode interface. Chapter 3 gives the methodology on how the active iron salts precursor was impregnated to the CC electrode to acquire the desired electrode modification. The procedure of electrode testing, sample collection and characterisation was also reported. Chapter 4 highlights the electrocatalytic activity of the synthesised electrode toward the "*in-situ"* generation of hydrogen peroxide (H_2O_2) via oxygen reduction reaction (ORR) by two electrons. Chapter 5, however, is the applicability of the synthesised CC electrode in the degradation of antiretroviral wastewater effluents containing organics from NVP, LVD, and ZVD. Finally, Chapter 6 covers general conclusions, and recommendations

REFERENCES

AGUNBIADE, F.O. AND MOODLEY, B. 2016. Occurrence and distribution pattern of acidic pharmaceuticals in surface water, wastewater, and sediment of the Msunduzi River, Kwazulu Natal, South Africa. *Journal of Environmental Toxicology and Chemistry*, 35 (1) : 36–46.

ARCHER, E., PETRIE, B., KASPRZYK-HORDERN, B. AND WOLFAARDT, G. M. 2017. The fate of pharmaceuticals and personal care products (PPCPs), endocrine disrupting contaminants (EDCs), metabolites and illicit drugs in a WWTW and environmental waters, *Journal of Chemosphere*, 174 : 437–446.

CAMACHO-MUNOZ, D., MARTIN, J., SANTOS, J.L., APARICIO, I. AND ALONS0, E. 2014. Concentration evolution of pharmaceutically active compounds in raw urban and industrial Wastewater, *Journal of Chemosphere*, 111 : 70–79.

CHAPMAN, D. 1996. Water quality assessments: A guide to use biota, sediments and water in environmental monitoring (2nd edn) E & FN Spon. London. 609.

DEPARTMENT OF WATER AFFAIRS AND FORESTRY (DWAF). 1996. South African water quality guidelines.

DEPARTMENT OF WATER AFFAIRS AND FORESTRY (DWAF). 1998. Quality of Domestic Water Supplies, Assessment Guide 1. 2nd edn. Pretoria. RSA.

DEZIEL N. 2014. Pharmaceuticals in wastewater treatment plant effluent waters. Scholarly Horizons: University of Minnesota, *Morris Undergraduate Journal*, 1 (2) : 12.

EDOKPAYI, J.N., ODIYO, J.O. AND DUROWOJU, O. S. 2017. Impact of wastewater on surface water quality in developing countries: a case study of South Africa. *Water Quality* : 401–416.

EPA, U. 2016. Contaminant Candidate List (CCL) and Regulatory Determination-Final CCL 4 Chemical Contaminants.

GARRIDO-CARDENAS, J.A., ESTEBAN-GARCIA, B., AGUERA, A., SANCHEZ-PEREZ, J.A., AND MANZANO-AGUGLIARO, F. 2020. Wastewater treatment by advanced oxidation process and their worldwide research trends. *International Journal of Environmental Research and Public Health*, 17 (1) : 170.

JONES, O.A.H., VOULVOULIS, N. AND LESTER, J. N. 2001. Human pharmaceuticals in the aquatic environment a review. *Journal of Environmental Technology*, 22 (12) : 1383–1394.

LUO, Y., GUO, W., NGO, H.H., NGHIEM, L.D., HAI, F.I., ZHANG, J., LIANG, S. AND WANG, X. C. 2014. A review on the occurrence of micropollutants in the aquatic environment and their fate and removal during wastewater treatment. *Journal Science of the Total Environment*, 473: 619–641.

MATONGO, S., BIRUNGI, G., MOODLEY, B. AND NDUNGU, P. 2015a. Occurrence of selected pharmaceuticals in water and sediment of Umgeni River, KwaZulu-Natal, South Africa. *Journal of Environmental Science and Pollution Research*, 22 (13) : 10298–10308.

MATONGO, S., BIRUNGI, G., MOODLEY, B. AND NDUNGU, P. 2015b. Pharmaceutical residues in water and sediment of Msunduzi River, kwazulu-natal, South Africa. *Journal of Chemosphere*, 134 : 133–140.

NIBAMUREKE, M.C.U., BARNHOORN, I.E. AND WAGENAAR, G. M. 2019. Assessing the potential effects of nevirapine in South African surface water on fish growth: A chronic exposure of Oreochromis mossambicus. *The South African Journal of Science*, 115 (3–4) : 1–6.

PRAMANIK, B.K., SHU, L., AND JEGATHEESAN, V. 2017. A review of the management and treatment of brine solutions, *Journal of Environmental Science: Water Research and Technology*, 3 (4) : 625–658.

REHMAN, M.S.U., RASHID, N., ASHFAQ, M., SAIF, A., AHMAD, N. AND HAN, J. I. 2015. Global risk of pharmaceutical contamination from highly populated developing countries. *Journal of Chemosphere*, 138 : 1045-1055.

SWANEPOEL, C., BOUWMAN, H., PIETERS, R. AND BEZUIDENHOUT, C. 2015. Presence, concentrations and potential implications of HIV-anti-retrovirals in selected water resources in

South Africa, *Journal of Water Research Commission, WRC Report*, 2144 (1) : 14.

U.S. ENVIRONMENTAL PROTECTION AGENCY. 2007. Method 1694 : Pharmaceuticals and Personal Care Products in Water, Soil, Sediment and Biosolids by HPLC/MS/MS, EPA-821-R-08-002.

VAN BOECKEL, T.P., GANDRA, S., ASHOK, A., CAUDRON, Q., GRENFELL, B.T., LEVIN, S.A. AND LAXMINARAYAN, R. 2014. Global antibiotic consumption 2000 to 2010: an analysis of national pharmaceutical sales data, *Journal of the Lancet infectious diseases*, 14 (8) : 742–750.

WATER, U. N. 2014. A Post-2015 Global Goal for Water: Synthesis of Key Findings and Recommendations from UN-Water. Paris.

WATER, U. N. 2015. Water for a sustainable world. The United Nations World Water Development Report.

ZAZOULI, M.A. AND KALANKESH, L. R. 2017. Removal of precursors and disinfection by-products (DBPs) by membrane filtration from water; a review, *Journal of Environmental Health Science and Engineering*, 15 (1) : 25.

Chapter 2: Literature review

2.1 Wastewater micro-pollutant

An increase in water usage gives rise to wastewater quantity. Discharges from industrial, agricultural, and domestic sources add micro-pollutants to the ecosystem. Water pollution occurs when water containing toxic micro-pollutants such as organic pollutants, inorganic pollutants, solids, pathogens, and nutrients enter the water body as shown in Figure 2.1. Polluted water can destroy plants around the ecosystem; harm people, and animals who consume it. According to Krishnan *et al.* 2017, wastewater is generally categorized by properties such as total dissolved solids (TDS), turbidity, chemical oxygen demand (COD), biological oxygen demand (BOD), dissolved oxygen (DO), hardness, pH, and color. Since these characteristics vary, efficient removal methods are required that allow effluent discharge within established environmental regulatory limits. Prevention of water sources from pollution and the protection of public health by safeguarding water supplies against the spread of diseases are the two fundamental reasons for treating wastewater.

Wastewater containing organics undergo degradation and decomposition by bacterial activity. Carson and Mumford (2002), identified sources of organic micropollutants as cosmetics, pesticides, new Organic Chemicals, synthetic detergents, synthetic fibers, plastics, paints, food additives, pharmaceuticals, insecticides and volatile organic compounds (VOCs). Most of these synthetic compounds pose dangers to man and the environment hence are toxic and biorefractory, in other words, they are resistant to microbial degradation. Also, in this category is “oil” which enters the water body through oil spills, and wastewater from refineries. Oil spreads

over the water surface, thereby reducing the amount of dissolved oxygen entering into it and also covers algae preventing it from photosynthesizing properly. Fish and wildlife will eventually die because their food is poisoned from oil spills.

Figure 2.1: Wastewater entering the aquatic system

2.2 Antiretroviral drugs

Pharmaceuticals are generally defined as prescribed medication used to treat and prevent diseases, thus improving the quality of life. Pharmaceuticals such as antiretroviral drugs (ARVDs) are used for the treatment and prevention of human immunodeficiency virus (HIV) infection (Günthard *et al.,* 2016). HIV is retroviruses that attack body cells, naturally responsible for defence against illness, in the body's immune system. The mechanism of the HIV attack system is to fuse and incorporate its genes into the human DNA, where it replicates itself thereby diminishing and destroying the immune system (LaRosa and Orange, 2008). The collapse of the

body's immune system leads to Acquired immune deficiency syndrome (AIDS). Available data suggest that the HIV epidemic started in the mid-1970, during which escalation was rampant and approximately 100,000-300,000 persons were infected (Mann, 1989). According to UNAIDS (UNAIDS, 2018), 36.7 million people are globally estimated to be living with HIV. South Africa has the highest HIV scourge in the world, with 20% of the global number of people living with HIV, 15% of new infections, and 11% of AIDS-related deaths. HIV is transmitted through blood or bodily secretions contaminated with HIV-1 and HIV-2 (Cohen and Gay, 2010; Bhopale, 2012). Other ways of transmission are through unprotected sexual contact, drug injection with non-sterile needles, and unscreened blood products.

However, ARVDs do not kill or cure HIV and AIDS but rather prevent it from multiplication, by suppressing it to an undetectable level (Ying *et al.,* 2016). Combinations of three or more antiretroviral drugs (ARVDs) available as highly active antiretroviral therapy (HAART) are used to prevent mortality and morbidity in pregnant women and with the avoidance of breastfeeding resulted in the elimination of mother-to-child transmission of HIV (Tonwe-Gold, 2007). Generally, compounds often used to treat HIV/AIDS includes nucleoside and nucleotide reverse transcriptase inhibitors (NRTIs/NtRTIs) such as lamivudine, tenofovir and zidovudine, non-nucleoside reverse transcriptase inhibitors (NNRTIs) such as efavirenz, nevirapine, and delavirdine, protease inhibitors (PIs) such as atazanavir, darunavir, and saquinavir, integrase inhibitors (INIs) such as raltegravir; fusion inhibitors (FIs) such as enfuvirtide; and chemokine receptor antagonists (CRAs) such as maraviroc (Bhopale, 2012). There is a tremendous increase in the global intake of pharmaceutical antiretroviral drugs. This sensational scale-up of HIV/AID treatment by many nations has lowered deaths associated with AIDS from 1.5 million in 2010 [1.3 million–1.7 million] to 1.1 million [940 000–1.3 million] in

2015 (UNAIDS, 2018). After using these medications for curative purposes, they end up as hazardous substances in our environment. It has been reported that South Africa has the most extensive antiretroviral therapy in the world. Since South Africa uses more of these compounds than any other nation, a larger amount of ARVDs is potentially discharged into the South African wastewater system. In water bodies, these antiretroviral drugs release organics which are regarded as micro-pollutant. Wood *et al.* 2015, reported that lamivudine, zidovudine, and nevirapine were detected in surface waters and effluents of WWTP in these concentration levels; lamivudine (0.09 – 0.24 µg/L), zidovudine (0.45 – 0.97 µg/L) and nevirapine (0.24 – 1.48 µg/L).

These assertions of Wood *et al.* 2015, were supported by Schoeman *et al.* 2015, who reported that antiretroviral pharmaceuticals such as nevirapine and efavirenz were detected in the influent and effluent of SA WWTP at a concentration of about 2100 and 17400 ng/L. According to him, treated effluents from WWTPs contain nevirapine and efavirenz at concentrations as high as 350 and 7100 ng/L respectively. He, therefore, concluded that WWTP only removes to an extent some of the antiretroviral (about 50%). Another researcher, Fick *et al.* 2007, reported that the antiretroviral drug - oseltamivir is not degraded or removed during conventional wastewater treatment and therefore persistent in surface waters for a longer period. Vanková, (2010), carried out a biological treatment of synthetic wastewater of three antiretroviral drugs, lamivudine, nevirapine, and zidovudine in a closed bottle system and reported that these drugs were non-biodegradable, toxic, and inhibitory to activated sludge bacteria, hence refractory in the environment. Conventional treatment of antiretroviral drugs may result in intermediates which according to (Dantas *et al.,* 2007), inhibit the growth of microorganisms in WWTP thus affecting their removal efficiency. Other researchers such as Prasse *et al.* 2010, and Kummerer, (2008) also reported that there is incomplete or partial removal of antiretroviral drugs entering WWTP.

Consequently, detailed information about lamivudine, zidovudine, and nevirapine drugs that release an increased concentration of organics into our environment is given in the subsection below.

2.2.1 Nevirapine (NVP)

Nevirapine is a low aqueous solubility drug with a general molecular formula $C_{15}H_{14}N_4O$, CAS No.129618-40-2 and molecular structure indicated in Figure 2.2a. For maximum solubility in aqueous buffers, nevirapine should first be dissolved in DMF and then diluted with the aqueous buffer of choice. It is lipophilic and has a molar mass of 266.30 g/mol with other of its properties indicated in Table 2.1. This antiretroviral drug which is used for HIV/AIDS treatment belongs to the non-nucleoside reverse transcriptase inhibitors (NNRTIs) group. Nevirapine is regarded as one of the first option drugs for triple schemes during pregnancy and prophylaxes of vertical HIV transmission as reported by Pereira *et al.,* 2007. These drugs stop HIV from multiplying by preventing the reverse transcriptase (RT) enzyme from working. The most common side effect of nevirapine as indicated by David and Hamilton, 2010, are skin rash although in some patients it causes fatal and severe hepatotoxicity (chemical-driven liver damage).

2.2.2 Lamivudine (LVD)

General molecular structure, molecular formula and CAS No. for lamivudine are shown in Figure 2.2c, $C_8H_{11}N_3O_3S$ and 134678-17-4. Another common name of Lamivudine is 3TC and it exerts antiviral effects by acting as a DNA chain terminator (Quercia *et al.,* 2018). They also belong to the first group of nucleoside reverse transcriptase inhibitor (NRTI) that was officially

accepted for the treatment of HIV-1 infection in 1995 and hepatitis B virus (HBV) infection in 1998 (Quercia *et al.,* 2018; Bhatt *et al.,* 2008). Lamivudine also is lipophilic and hence not recommended for the aqueous solution to be stored for more than one day. For long term storage, it was suggested that lamivudine should be stored as supplied at -20°C. See Table 2.1 for other properties of Lamivudine

2.2.3 Zidovudine (ZVD)

Zidovudine with a general molecular formula $C_{10}H_{13}N_5O_4$ was reported as the first antiretroviral drug used for the treatment of HIV infection (Fischl *et al.,* 1987). It has a structural formula as indicated in Figure 2.2b, a CAS No.30516-87-1 and like other NRTIs, zidovudine completely blocks viral replication by inhibiting the activities of the viral reverse transcriptase-an enzyme that HIV uses to make a DNA copy. This action improves the immunologic function and clinical abnormalities of the patient associated with AIDS. Common side effects associated with AZT include increased body fat synthesis, discoloration of fingernails and toenails, nausea, and DNA damage (Butanda-Ochoa *et al.,* 2017). More severe side effects include anaemia, leukopenia, and bone marrow suppression (Alzahrani, 2015). Zidovudine is soluble in organic solvents such as ethanol, DMSO, and dimethylformamide (DMF), which should be purged with an inert gas.

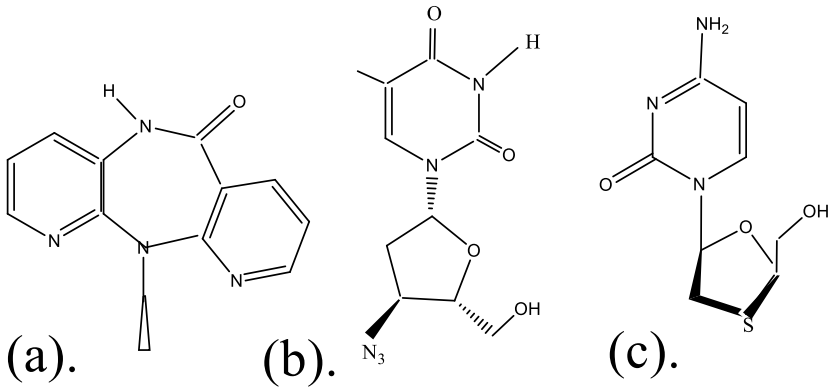

Figure 2.2: Structures of (a) Nevirapine (b). Zidovudine and (c) Lamivudine

2.3 Parameters for characterizing wastewater quality

2.3.1 Dissolved Oxygen (DO)

Waste substances in water are food for microorganisms. Microbes, therefore, demand oxygen to survive as they degrade these waste matters to form BOD or COD, which is the amount of oxygen used by microorganisms as they feed upon substances in wastewater (Gray, 2002). Hence, Dissolved Oxygen (DO) is oxygen dissolved in water and this is what all aquatic organisms demand to stay alive. DO is expressed in milligram per liters (mg/L) or part per million (ppm). According to Brown, (1985), dissolved oxygen can also be depleted through respiration (from fish and aquatic plants), direct chemical oxidation, and outflow of water. If the oxygen in water decreases to a low level, that fishes begin to die, then the region becomes "septic", hence at DO less than 2 ppm fishes die (Brown, 1985). After this point, even if all the organics and nitrogenous compounds are consumed, the DO will continue to be low until reaeration is performed naturally by the diffusion of air into the river. According to the Bureau of Indian Standards (BIS), the Dissolved Oxygen of wastewater should be within the range of 4 - 6 mg/L (Siddiqui and Waseem, 2012). The concentration of DO in the water sample is influenced significantly by temperature, salinity, and atmospheric pressure. Hence, as the water gets warmer, it holds less oxygen; as the water gets saltier, it holds less oxygen and as you increase altitude, water holds less oxygen. Therefore, total oxygen demand is the total amount of oxygen required to oxidize biodegradable and non-biodegradable organic matter along with few oxidizable organic substances, hence, TOD > COD > BOD. Estimation of oxygen demanded by microbes is through the following methods:

2.3.2 Theoretical oxygen demand (ThOD)

Oxidation of organic matter in the presence of oxygen results in the generation of carbon dioxide, water, and other inorganic products, such as ammonia, hydrogen sulfide, etc. The products of such processes depend on the elemental composition of the organic matter as given in Equation 2.0. Theoretical oxygen demand is, therefore, the amount of oxygen demanded by microbes to completely oxidize a known compound to CO_2 and H_2O, and it can be estimated by theoretical calculation that depends on simple stoichiometric principles. Materials containing carbon compounds, which serve as a food source to the microorganism, are sources of carbonaceous biochemical oxygen demand (CBOD). A stoichiometric equation for the oxidation of carbon-containing organic matter was represented in Equation (2.1).

$$C_\alpha H_\beta O_\gamma N_\delta + \left[\propto + \frac{\beta}{4} - \frac{\gamma}{2} + \delta\right] O_2 \rightarrow \alpha CO_2 + \frac{\beta}{2} H_2O + \delta NH_3 \quad (2.1)$$

Using glucose to represents carbonaceous compound containing organic matter, the biochemical reactions as microorganism (bacteria) feeds on it is same as respiration which occurs within a cell as shown in Equation 2.2.

$$C_6H_{12}O_6 + 6O_2 \longrightarrow 6CO_2 + 6H_2O \quad (2.2)$$

Stoichiometrically, from Equation 2.2, 6 moles of oxygen were in demand per 1 mole of glucose (gluc.) consumed by the bacteria. Hence, $(\frac{6\text{mol } O_2}{1\ molglc})$. Multiplying this by their molecular weights,

$\frac{6\text{mol } O_2}{1\ molgluc}$ x $\frac{32\text{g } O_2}{1\ molO_2}$ x $\frac{1\text{ mol gluc}}{180\ ggluc}$ = 1.067 g O_2/g gluc. = 1.067 mg O_2/mg gluc.

If 100 mg/L of glucose were dumped into the river, you can multiply by COD equivalent to knowing the amount of oxygen that microbes will consume per liter. Hence

$\frac{100\ mgGlc}{l}$ x $\frac{1.067\ mgO_2}{mgGlc}$ = 106.7 mg O_2/L. This is, therefore, the oxygen in demand by microbes, to consume 100 mg/l of glucose dumped into the river.

2.3.3 Biological Oxygen Demand

Typical wastewater treatment plant depends on microorganisms in the wastewater to decomposed waste. In biological oxidation processes, organic micro-pollutants are oxidized by certain microorganisms into carbon dioxide and water using dissolved oxygen which resulted in ultimate BOD (BOD_u). This process is a very slow one and also time-consuming, as a result, another parameter BOD_5 was universally adopted as a measure of relative pollution. Hence, Biochemical Oxygen Demand (BOD_5) is the amount of dissolved oxygen required by microorganisms to biologically degrade organic components in water under aerobic conditions for 5 days of incubation at 20 ^oC. The BOD value is commonly expressed in milligrams of oxygen consumed per liter of the sample during 5 days of incubation at 20 ^oC. Hence, the presence of enough oxygen promotes the aerobic biological decomposition of organic waste by microorganisms (Tchobanoglus *et al.,* 2003). The typical range of BOD_5 in domestic wastewater ranges from 100 to 300 mg/L (Abdalla and Hammam, 2014)

2.3.4 Chemical oxygen demand (COD)

The amount of oxygen needed by microbes to consume all chemicals both organic and inorganic in the water is called the Chemical Oxygen Demand (COD). It is an empirical laboratory method used to measure the total organic matter (biodegradable and non-biodegradable) contained in a water sample. In other words, the (COD) test determines the oxygen required for the chemical oxidation of organic substances with the aid of strong chemical oxidants. It is measured in mg of oxygen equivalent per liters (mg O_2/l or mg/l). Currently, most COD tests use potassium dichromate as the oxidant. In the colorimetric method, organic matters are digested/consumed by potassium dichromate in acid solution, (Equation 2.3). Digestion is performed on the samples with a set amount of the oxidant, sulfuric acid, and heat (150 °C). This means the organics in the sample reacts with potassium dichromate, thereby reducing orange color dichromate ions ($Cr_2O_7^{-2}$) to green trivalent chromium ions (Cr^{+3}) (Clesceri *et al.*, 1998)

$$C_nH_aO_bN_c + dCr_2O_7^{-2} + (8d + c)\,H^+ \longrightarrow nCO_2 + ((a+8d-3c))/2\,H_2O + cNH_4^+ + 2dCr^{+3} \quad (2.3)$$

Where $d = \frac{2n}{3} + \frac{a}{6} - \frac{b}{3} - \frac{c}{2}$

Both chromium species can absorb light or radiation in the visible region of the spectrum but at different wavelengths. While the dichromate ions are visible at 420 nm, the trivalent chromium ion Cr^{3+} is at 600 - 620 nm. In water analysis, the COD will always be higher than the BOD because COD measures both biodegradable and non-biodegradable organics. Hence, the BOD_5-to-COD ratio is called the "Biodegradability index" (B.I.) and it is utilized to quantify the

biodegradability of the effluent (Dahamsheh and Wedyan, 2017). It has been reported that the B.I. for municipal wastewater varies from 0.4 to 0.8 and the ratio can exceed 10 for industrial wastewater (Dahamsheh and Wedyan, 2017). However, B.I for raw wastewater can be used to determine treatment technology. If BOD/ COD is > 0.6 then the waste is fairly biodegradable and can be effectively treated biologically (Abdalla and Hammam, 2014). If the BOD/COD ratio is between 0.3 and 0.6, then seeding is required to treat it biologically, because the process will be relatively very slow. If BOD/COD < 0.3, wastewater is considered toxic and cannot be biologically treated (Abdalla and Hammam, 2014), hence chemical pre-treatment methods have to be deployed first to increase the biodegradability of the wastewater.

2.4 Available techniques for the removal of organics from industrial wastewater

Industrial wastewater usually contains organic and inorganic matter in varying degrees of concentration. The majority of effluents from the industry is toxic, mutagenic, carcinogenic, or simply hardly biodegradable and enters water bodies through discharge. These industrial effluents must be treated to meet certain standards of purity before they can be discharged into waterways. The techniques available for the treatment of wastewater are many and vary in different countries with the same aim of waste minimization and toxicity reduction. However, around the globe, there is an increase in domestic and industrial wastewater discharge without any form of treatment or after primary treatment only.

In China, a highly industrialized country, Dhote *et al.* 2012, reported that about 55% of all sewage is discharged without treatment. Kazora and Mourad, 2018 indicated that the majority of sub-Saharan African nations do not have wastewater treatment technologies, hence discharge wastewater directly to water bodies without treatment. Another researcher Momba *et al.* 2006, reported that in South Africa, municipal sewage treatment plants have operational deficiencies as they are insufficiently maintained allowing pollution to enter various water bodies. Conventional wastewater treatment methods such as filtration, evaporation recovery, chemical precipitation, chemical oxidation or reduction, electrochemical treatment, application of membrane technology, and biological treatment processes have been the major technique used in treating wastewater. While undergoing these treatment processes, wastewater goes through the following processes, preliminary treatment, primary treatment, secondary treatment, and tertiary treatment. However, it was discovered that conventional techniques are ineffective in the complete removal of micro-pollutants, particularly organic matter (Rajasulochana and Preethy, 2016). As a result, new green technical methods have been developed superior to conventional methods. Out of them are membrane bioreactors (MBR), and advanced oxidation process (AOP). Due to the presence of multiple contaminants in wastewater, a combination of two or three techniques was advised to be employed to get a better-treated effluent (Rajasulochana and Preethy, 2016).

2.4.1 Membrane Bioreactor (MBR)

Membrane technology is a recent technology used in treating industrial wastewater. Its application enables different filtration processes to be used with each process using a semi-permeable membrane. These membranes, in operating principle, act as a filter (physical barrier) that will let water flow through but effectively removes suspended solids, viruses, bacteria, and

other unwanted substances. In such a way, they are used for the creation of process water from surface water or wastewater. Membrane bioreactors can, therefore, be regarded as a biologically activated sludge process that integrates active microorganisms with semipermeable membranes for the disintegration and removal of organics. Although wastewater treatment by membrane technology is well established, there is the need to improve in terms of separation properties, energy demand, and costs. For water to penetrate through these membranes, an electric potential should be introduced across it. This should be accompanied by high trans-membrane pressure on the feed side and a steady concentration gradient.

For membrane configurations and classifications, in terms of placement of membrane inside the bioreactor, the MBR systems are of two configurations, the submerged configuration, and the external configuration (Mert *et al*., 2018). In the external configuration, the membrane module is placed outside the bioreactor tank and the permeate flux generally varies between 50 and 120 Lh^{-1} m^{-2} with the trans-membrane pressure (TMP) in the range of 1 to 4 bar MBR (Gupta *et al.*, 2008). Likewise, the submerged configuration gives a membrane module that is submerged in a proper aerated bioreactor tank. Operation is at lower flux which varies from 15 to 50 Lh^{-1} m^{-2} with trans-membrane pressure (TMP) of about 0.5 bar (Gupta *et al.*, 2008). Due to high permeate flux density; the submerged system is less prone to membrane fouling than the external system. In terms of pressure-driven filtration/separation processes, the membrane process is classified as reverse osmosis (RO), nanofiltration (NF), ultrafiltration (UF), and microfiltration (MF) (Abd El-Ghaffar and Tieama, 2017). Based on membrane pore size and mechanism of operation, membrane filtration processes are divided into a porous membrane and non-porous membrane. While UF and MF are porous membranes, NF and RO are non-porous membranes. According to materials of construction, membranes can also be classified into

organic polymeric membranes and ceramic membranes, although metallic membranes also exist. Polymeric membrane materials are organic materials such as polyethersulphone, polypropylene, polyvinylidene di-fluoride, polyacrylonitrile, polyamides, and polyethylene. Each of these materials is characterized by unique properties such as their degree of hydrophobicity, flexibility, pH, oxidant tolerance, and strength. MF and UF membranes are often constructed from these materials and that is why they have desirable resistance properties (Abd El-Ghaffar and Tieama, 2017). Another type of membrane is cellulose membranes. The membrane is liable to biodegradation and as a result of this uniqueness, they are operated at a narrow pH range of about 4 to 8. To control biodegradation, fouling and membrane damage, chlorine doses less than 0.5 mg/L should be added during its filtration process. In terms of shapes, design, and manner in which the membrane is arranged inside the modules, the membrane can come in four different configurations – tubular, spiral, hollow fiber, and flat sheet (El-Ghaffar and Tieama, 2017; Drioli *et al.,* 2006). In recent times, researchers such as El-Ghaffar and Tieama, (2017), and others, have demonstrated the efficiency of using MBR to treat wastewater

2.4.2 Advanced oxidation methods

Advanced Oxidation Process (AOP) is a chemical treatment method used for the removal of problematic organic matter in the industrial management of wastewater. The basic principle of AOP is the generation of hydroxyl radicals ($OH^{\bullet}$), which is a powerful oxidant that mineralizes efficiently pollutants/recalcitrant organics contained in wastewater. As illustrated in Table 2.1, the hydroxyl radicals ($OH^{\bullet}$) has a very high oxidation potential which is only lower than that of fluorine (F_2) (Tang *et al.,* 2013). Its oxidation characteristics are non-selective and highly

reactive, allowing the simultaneous treatment of multiple contaminants. According to Hisaindee *et al.* 2013, there are different kinds of AOPs and they are classified into irradiation processes and non-irradiation processes. Hence, for all AOPs, the effectiveness of the process depends profoundly on the efficiency by which $OH^{\bullet}$ is generated. As a result, the most frequently studied and utilized for many applications are AOP using hydrogen peroxide, AOP using Fenton's Reagent, Fenton-Like, and Photo Fenton Processes, Ozonation, and AOP with the application of irradiation using UV-VIS light at a particular wavelength (Krishnan, 2017). The focus in this study was on the use of electrochemical methods to produce hydroxyl radical, hence electrochemical Advanced Oxidation Processes (EAOP). Electro-Fenton was the first technology that was considered as an EAOP because of the production and active role of hydroxyl radical on the oxidation of organics (Brillas *et al.,* 2009).

Table 2.1: Oxidizing potential for some oxidizing agents

Oxidizing Agent	Oxidation Potential (V)
Fluorine	3.06
Hydroxyl radical	2.80
Oxygen (atomic)	2.42
Ozone	2.08
Hypochlorite	1.49
Chlorine	1.36
Chlorine	1.36

Hydrogen Peroxide	1.78
Chlorine Dioxide	1.27
O_2	1.23

2.4.3 Electro-Fenton Process (EFP)

This is a technology that uses electrochemical reactions to remove organic micro-pollutants. The use of electrochemical processes for wastewater treatment has generated much interest in recent years because of their environmental compatibility and simplicity. The process was found to be efficient in degrading and removing pollutants from various kinds of industrial wastewaters (Ciardelli and Ranieri, 2001). The efficiency of the processes in pollutant removal depends strongly on the nature of the materials used as electrodes. Therefore, electrode materials with good mechanical and chemical stability are often preferred for the generation of the required radicals. This technology is based on the promotion of, either the electrochemical regeneration of iron (II) from iron (III) species on the cathodic surface or the cathodic formation of hydrogen peroxide from oxygen reduction reaction. Therefore, when oxygen or air is continuously bubbled into the cathode chamber of an aqueous medium in an electrochemical cell with correct parameters, it picks up two electrons and becomes reduced to peroxide as shown in Equation 2.4 (Panizza and Oturan, 2011; Naimi and Bellakhal, 2012; Cuerda-Corre *et al.,* 2020). By this reaction, hydrogen peroxide is continually generated "*in-situ"* in the acidic media. So, hydroxyl radicals (HO•) are produced "*in-situ"* when Fenton reagents (Fe^{2+} and H_2O_2) are combined (Naimi and Bellakhal, 2012) according to Equation 2.5. The regeneration of Ferrous ions (Fe^{2+}) can occur either by cathodic reduction of ferric ions (Fe^{3+}) (Naimi and Bellakhal, 2012) Equation

2.6, or by ferric ions (Fe^{3+}) oxidation of an organic radical (Rosales *et al.*, 2012) (Equation 2.7), or Fenton-like reaction of ferric ions (Fe^{3+}) with H_2O_2 (Rosales *et al.*, 2012) (Equation 2.8).

$$O_2 + 2H^+ + 2e^- \longrightarrow H_2O_2 \text{ (acidic)} \quad (2.4)$$

$$Fe^{2+} + H_2O_2 \longrightarrow Fe^{3+} + OH^- + HO\bullet \quad (2.5)$$

$$Fe^{3+} + e^- \longrightarrow Fe^{2+} \quad (2.6)$$

$$Fe^{3+} + R \longrightarrow Fe^{2+} + R^+ \quad (2.7)$$

$$Fe^{3+} + H_2O_2 \longrightarrow Fe^{2+} + HO_2\bullet \quad (2.8)$$

$$2H_2O \longrightarrow O_2 + 4H^+ + 4e^- \quad (2.9)$$

$$\text{Organics} + HO\bullet \longrightarrow \text{intermediates} + CO_2 + H_2O \quad (2.10)$$

The anodic reaction in the application of electric current between two electrodes gives the oxidation of water to molecular oxygen (Cuerda-Correa *et al.*, 2020) (Equation 2.9) coupled with the production of hydrogen peroxide (Equation 2.4) which is necessary for Fenton's reaction. Organic micro-pollutants become destroyed and mineralized forming carbon dioxide, water, and intermediates (Equation 2.10). This is because of the (HO•) radicals produced in the aqueous media, abstract hydrogen from the organics by the process of oxidation. On the other hand, external energy source, in the form of UV light and ultrasound light (λ = 320 - 400 nm), can be used to illuminate the Fenton process to enhance micro-pollutant degradation efficiency resulting into photo-Fenton (PF) process. However, the effectiveness of EFP in the destruction of toxic waste and non – biodegradable effluents has been demonstrated as shown in the literature. Notable is the work of Naimi and Bellakhal, who in 2012 applied EFP in a 250 ml undivided cell

to remove 17β-Estradiol micro-pollutant in acetonitrile solution using carbon felt cathode and the platinum anode at a pH of 3, current density 200 mA and Fe^{2+} concentration of 0.2 mM.

2.5 Hydrogen Peroxide (H_2O_2)

H_2O_2 is an odorless and colorless water-soluble liquid reliably used as an oxidant in chemical synthesis (Ranganathan and Sieber, 2018). It was first identified as a product of barium peroxide with nitric acid in 1818 by Thenard (Campos-Martin *et al.*, 2006). The molecular structure of H_2O_2 is non-polar, with bent molecular shape and this permits it to be involved in both oxidation and reduction reactions. It is stored in an aqueous form and in a dark-colored container to avoid it reacting with light. H_2O_2 has a low molecular weight of 34.0147 g/mol which enables it to serve more effectively as an oxidizing agent than any other oxidant such as dinitrogen monoxide or nitric acid. On decomposition, as shown in Equation 2.11, it has an explosive reaction and gives only water and oxygen as the only reaction products, which makes it one of the most valuable, environmentally benign, and cleanest oxidants available. This characteristic of H_2O_2 has increased its demand, hence its direct usage in many large-scale applications of human life as a safe oxidizing agent as shown in Figure 2.3. Apart from the anthraquinone autoxidation method of producing H_2O_2, it can also be produced by chemical catalysis which is its direct synthesis from hydrogen and oxygen using a variety of catalysts (Campos-Martin *et al.*, 2006). One of the most important applications of hydrogen peroxide is its current usage in domestic wastewater treatment.

$$2H_2O_2 \longrightarrow O_2 + 2H_2O \qquad (2.11)$$

Not only was H_2O_2 used in the efficient removal of total organic carbon (TOC) and hypochlorite (Kosaka, *et al.*, 2001), it was also used in the advanced oxidation process (AOP) as a source of hydroxyl radicals the second most powerful oxidant available after fluorine. In recent times, Hydrogen peroxide can be easily produced "*in-situ"* by electrochemical synthesis using only air, water, voltage supply, and simple electrodes (Peralta *et al.*, 2013; Peralta-Hernández and Godínez, 2014). In particular, the desire to avoid transportation, handling, and storage of concentrated hydrogen peroxide solution, electrochemical synthesis is most preferable.

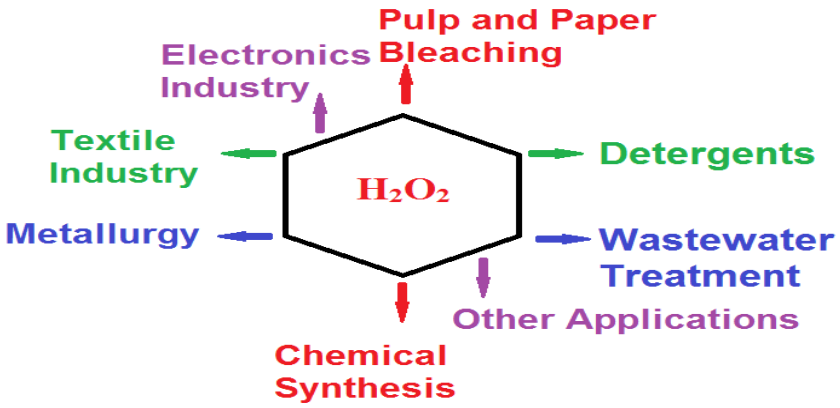

Figure 2.3: Principal uses of hydrogen peroxide

2.6 Electrochemical techniques

These are experimental methods developed to study the processes of electron transfer in an electrochemical cell at the interface of an electrode and its solution. Mass transfer of electroactive species (ionic movement) within the bulk of the solution gives rise to current flow; hence electron exchange between the electrode and the electroactive species resulted from the

oxidation and reduction process. The variables involved in electrochemical techniques are potential (E), current (I), and time (t). Either the potential or the current at the WE is controlled while the other is observed as a function of time, serving as the analytical signal. Some of the electrochemical techniques carried out in this research are:

2.6.1 Chronoamperometry

In chronoamperometry techniques, the potential is applied to the working electrode while current signals were observed as a function of time. Hence, for the diffusion-controlled process occurring at the electrode surface, chronoamperometry can be used to monitor current–time dependence. However, working in a still electrolytic environment so that flux to the electrode surface is strictly diffusion-controlled, application of reduction potential from an initial value of V_1 where no Faradaic current occurs to a set potential (V_2) which is significantly more negative on the WE, will result to a rapid current rise as the electroactive species near the electrode surface became depleted by electrolysis. Sufficiently applied negative potential will results in a complete conversion of reactant to a product as demanded by the Nernst Equation. Hence at V_2, the average concentration of reactants within the vicinity decreases, and Cottrell equation, describes the observed current (planar electrode) as a function of $t^{-1/2}$ in the relationship shown by Equation 2.12.

$$i = nFAC_0 \left(\frac{D_O}{\pi t}\right)^{1/2} = kt^{-1/2} \qquad (2.12)$$

Where n = stoichiometric number of electrons involved in the reaction;

F = Faraday's constant, A = electrode area (cm^2), C_o = bulk concentration of electroactive species (mol/cm^3) and D_o = diffusion constant for electroactive species (cm^2/s).

Thus, a plot of i vs. $\frac{1}{\sqrt{t}}$ yields a straight line. Such plots allow the estimation of the diffusion coefficients of the species to be obtained.

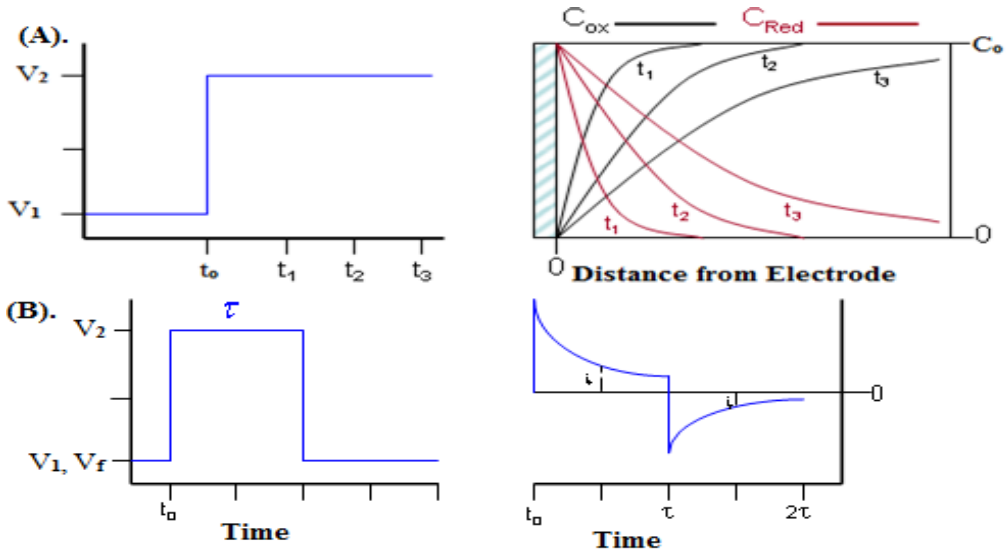

Figure 2.4: Chronoamperometry (a) A single potential step application and response, (b) A double potential step application and response

However, Chronoamperometry experiments can either be a single potential step, in which only the current resulting from the forward step as described above are recorded, or double-potential step, in which a second potential step (V_f) is applied following a period, usually designated as τ, at the step potential (V_2) (Figure 2.4)

2.6.2 Linear Sweep Voltammetry (LSV)

Linear Sweep Voltammetry (LSV) is an electrochemical technique that involves sweeping the potential of the working electrode linearly from a lower limit (V1) where no electrochemical reaction occurs to an upper limit (V2) or from upper to lower potential with scanning not repeated. The resulting signal is recorded as cell current measured as a function of time and as a function of potential as indicated in the peak-shaped voltammogram of Figure 2.5. The decay of the current after the peak rise is controlled by diffusion. The peak height is dependent upon the concentration of the electroactive species. Elgrishi *et al.* 2017, suggested that the characteristics of the linear sweep voltammogram depend on several factors such as:

- The rate of the electron transfer reaction(s)
- The chemical reactivity of the electroactive species and
- The voltage scan rate

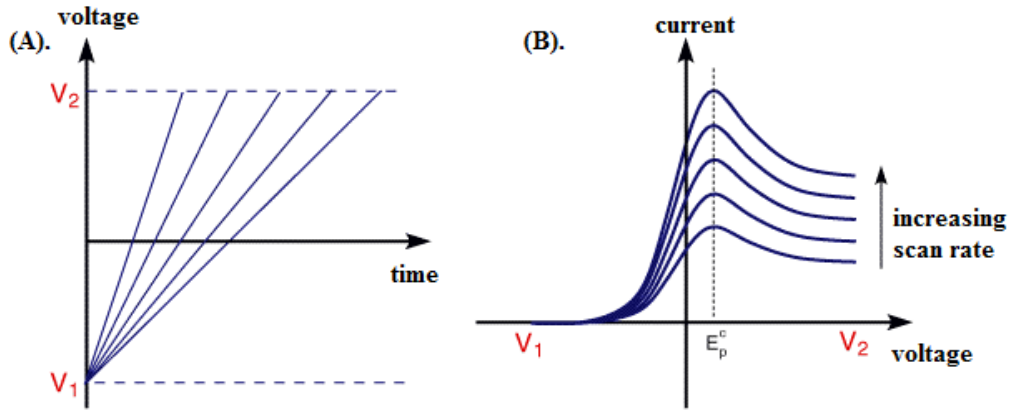

Figure 2.5: Linear increase of the potential vs time as depicted by Elgrishi *et al.*, 2017

2.6.3 Cyclic Voltammetry (CV)

This electrochemical technique is the most widely used in electrochemistry. The CV is used to measure the current-response of an electrode when a triangularly-shaped voltage is applied to the electrode in an unstirred solution (Nicholson and Shain, 1965). Typically, cyclic voltammetry consists of an electrolytic solution containing the analyst with a stationary electrode connected to a PGSTAT. Applying a sufficiently positive or negative voltage will force an electron transfer to occur at the interface. If the forward sweep (from A to F) as shown in Figure 2.6A, has sufficiently negative potential, a cathodic reduction process occurs until a peak is reached. The analyte O, therefore, gains an electron and became reduced to form new species R. As analyte is steadily depleted near the electrode surface to form new species, additional analyte via diffusion moves to the electrode surface from the bulk solution to replenish the depleted ones. The produced new species continues to grow on the electrode surface, forming a diffusion layer which slows down the mass transport of the analyte to the electrode surface.

As the rate of diffusion from the bulk solution to the electrode surface becomes slower, the current decreases as shown from (D to F). After reaching the switching potential (F), the scan direction is reversed, and the potential is scanned in the positive direction from (F to H) resulting in the anodic oxidation process. In this region, the formed species lose an electron and become oxidized. As the concentrations of the new species at the electrode surface became depleted, the concentration of the analyte at the electrode surface increased, satisfying the Nernst equati0on. The forward and reverse current has the same shape. The case is different as shown in Figure 2.6B when the initial forward potential scan is in the positive direction (from a, to d) given rise to the anodic oxidation process. Concerning Figure 2.6, the parameters of greatest important during

cyclic voltammetry measurement are the peak cathodic potential (E_{pc}), the peak anodic potential (E_{pa}), the peak cathodic current (i_{pc}), and the peak anodic current (i_{pa}).

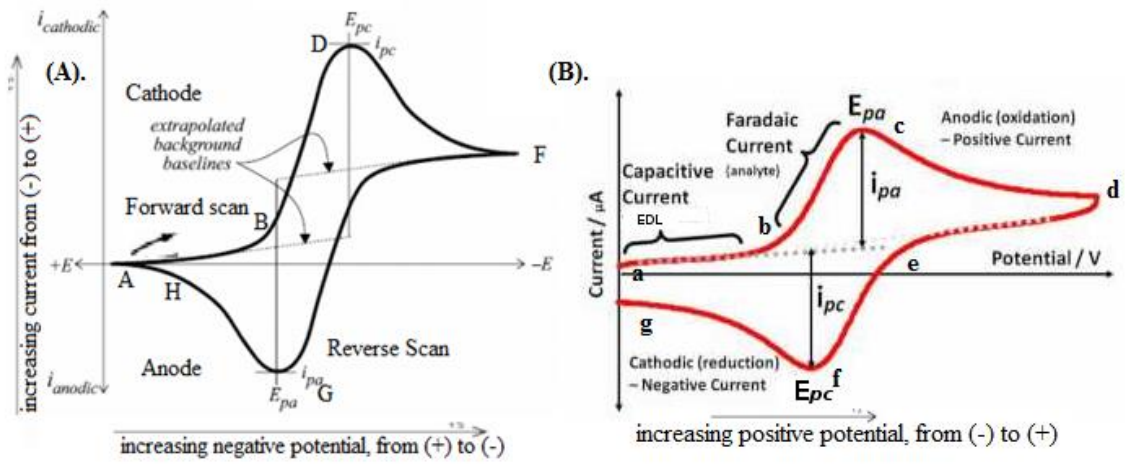

Figure 2.6: A cyclic voltammogram showing (A) a sufficiently negative potential forward sweep from (A to F) (B) a sufficiently positive potential forward sweep from (a to d)

2.7 Electrochemical Reversibility

Electrochemical reversibility is a concept used when the surface concentrations of *O/R* redox couple species obey the Nernst equation (Equation 2.17) at any potential difference applied at the electrode-solution interface. Electrochemical reversibility is defined by the following

2.7.1 Reversible System

The reversible system is characterized by fast electrode kinetics and a "large" value of the electrochemical rate constant (k^o). In other words, large k^o means increased mass transport to the electrode surface due to the "stretching" of the diffusion layer (Bard and Faulkner, 2001). For fully reversible O/R redox couple, peak current (Ip) was given by Randles – Sevčík equation (at 25^{o}C) as indicated in Equation 2.13. The corresponding potential for which the current reaches a peak value is given by Equation 2.14. If on assumption D_O=D_R=D, then the anodic-cathodic peak separation is given by Equation 2.15, at 25^{o}C. The peak – to – peak separation can be used to determine the number of electrons transferred in the process as well as a criterion for Nernstian behavior. However, both the cathodic and anodic peak potentials are independent of the scan rate.

Larger overpotential (ΔE_p) is disadvantageous for a redox reaction. (Nicholson, 1965) suggested that smaller values of ΔE_p results in a faster redox reaction, which indicates a higher electrocatalytic activity. The peak potential (E_p) is found to be related to the formal potential (E^o) of the redox process, which is centered between cathodic peak potential (E_{pc}) and the anodic peak potential (E_{pa}), Equation 2.16. For a simple one-electron reversible redox couple, the reverse-to-forward peak current ratio is equal to unity (Saber *et al.*, 2016; Haque *et al.*, 2013) (Equation 2.17).

$$i_p = 0.446\, nFAC\sqrt{\frac{nFVD}{RT}} = (2.69\, x10^5)n^{3/2}ACD_o^{1/2}V^{1/2} \qquad (2.13)$$

$$E_p = E^O + \frac{RT}{nF}\left(ln\left(\sqrt{\left(\frac{D_R}{D_O}\right)^{\pm 1}}\right) - 1.109\ (\pm 1)\right) \qquad (2.14)$$

$$\Delta E_p = E_{pa} - E_{pc} = \frac{59.2}{n} mV \quad (2.15)$$

$$E^O = \frac{E_{pa} + E_{pc}}{2} \quad (2.16)$$

$$\frac{i_{pc}}{i_{pa}} = 1 \quad (2.17)$$

Where n is the number of electrons involved, A is an area of the electrode in cm^2, D_O is the diffusion coefficient of the oxidized analyte in cm^2/s, v is the scan rate in (V/s) and C the bulk concentration in ($moles/cm^3$).

2.7.2 Irreversible System

Irreversible systems display sluggish electron transfer. It is characterized by a "small" value of rate constant (k^o), slow electrode kinetics, and very small exchange current density (jo) (Bard and Faulkner, 1980). The Nernst equation is not applicable in the case of an irreversible process. This is because the sluggish transfer of electron is insufficient to maintain surface equilibrium and thus the oxidized and reduced species are not at equilibrium. Such a system has peak-to-peak separation (ΔE) larger than 200 mV (Emeji *et al.,* 2019). To observe current flowing in an irreversible process, the application of an overpotential is required to strongly activate the charge-transfer reaction at the interface either in cathodic or in anodic section.

The peak current (Ip) of an irreversible electrode process, as shown in Figure 2.7, can be calculated by a modified Randles – Sevčík equation as shown in Equation 2.18. The corresponding peak potential is given in Equation 2.19

$$i_p = (2.99\, x10^5) n(\alpha n_a)^{1/2} A C D_O^{1/2} V^{1/2} \quad (2.18)$$

$$E_p = E^o - \frac{RT}{\alpha nF}\left[0.78 - \ln\frac{k^o}{D^{1/2}} + \ln\frac{\alpha nFv}{RT}^{1/2}\right] \quad (2.19)$$

Where ∝ denotes the electron transfer coefficient and n, the number of electrons transferred in the rate-determining step and k^o is the standard electrode reaction rate constant in cms^{-1}. Generally, for irreversible processes, the peaks are reduced in size and widely separated, and they are characterized by a shift of peak potential with the scan rate. According to Chandra *et al.* 2008, Laviron's equation was used to analyze the peak potential of the irreversible process.

Laviron suggested that a graph of Ep vs. (log v) as indicated in Equation 2.20 and 2.21, yields two straight lines with a slope equal to $-2.303RT/\alpha nF$ for the cathodic peak, and $2.303RT/(1-\alpha)nF$ the anodic peak. From these slopes, αn values can be calculated. The apparent heterogeneous electron transfer rate constant k^o could be determined using Equation 2.22. With Equation 2.23 and 2.24, αn values can also be calculated with Va and Vc denoting the potential scan rates at intercepts of the straight-line fits to anodic and cathodic data. Thus:

$$E_{pc} = E^o + \left[\frac{2.303RT}{nF}\right]\log\left[\frac{RTk^o}{nF}\right] + \left[\frac{-2.303RT}{\alpha nF}\right]\log v \quad (2.20)$$

$$E_{pa} = E^o + \left[\frac{2.303RT}{nF}\right]\log\left[\frac{RTk^o}{nF}\right] + \left[\frac{2.303RT}{(1-\alpha)nF}\right]\log v \quad (2.21)$$

$$\log k^o = \alpha\log(1-\alpha) + (1-\alpha)\log\alpha - \log RT/nFv - \alpha(1-\alpha)\left[\frac{nF\Delta E_p}{2.303RT}\right] \quad (2.22)$$

$$\frac{\alpha}{(1-\alpha)} = \frac{v_a}{v_c} \tag{2.23}$$

$$k^o = \frac{nF\alpha v_c}{RT} = \frac{(1-\alpha)nFv_a}{RT} \tag{2.24}$$

2.7.3 Quasi-reversibility

The voltammograms of a quasi-reversible process exhibit a large peak-to-peak separation compared to reversible processes. For this process, ΔEp is greater than (0.059/n) mV when the scan rate (v) increases (Haque *et al.,* 2013). The peak current increases with the scan rate ($v^{1/2}$) but it is not linear. In the reversible process, the current is controlled purely by mass transport but in the quasi-reversible process, the current is controlled by both the mass transport and charge transfer kinetics. The Randles–Ševc´ik equation for a quasi-reversible system is Equation 2.25

$$i_p = \pm\left(2.65x10^5\right)n^{3/2}\mathrm{ACD}^{1/2}v^{1/2} \tag{2.25}$$

According to Haque *et al.* 2013, when the peak current ratio (i.e reverse-to-forward peak current ratio) is greater than unity, ((i_{pc}/i_{pa}> 1) the system is said to correspond to a quasi-reversible system as indicated in Figure 2.7.

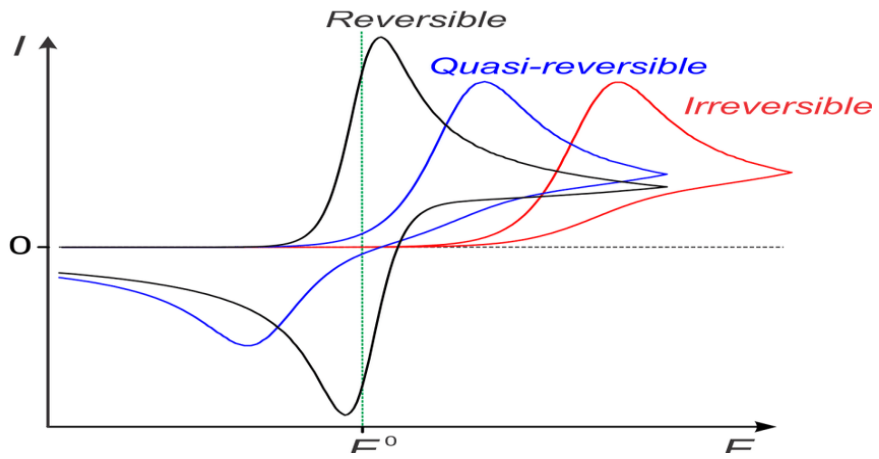

Figure 2.7: Examples of reversible, quasi – reversible and irreversible Cyclic Voltammetry. Source: Lee, (2014).

2.8 Electrochemical Cell

A typical electrochemical cell contains two electrodes and an electrolyte (Martinson *et al.*, 2014). They are devices that use spontaneous chemical reactions to produce clean electricity or, conversely, use electricity in the form of electrical energy to bring about non-spontaneous useful chemical reactions. The electrochemical cell can be designed either to be divided or undivided. Undivided cells are more straightforward to set-up with both oxidation and reduction taking place within the same compartment. Watts *et al.* 2015, demonstrated that the undivided cell setup as shown in (Figure 2.8a) is designed in such a way that the products formed from the redox reaction will not react with the electrodes. On the other hand, divided cells as shown in Figure 2.8b require a more specialized setup with electroactive species to be oxidized placed in the anodic compartment, while species to be reduced is placed in the cathodic compartment.

The cathodic and anodic chambers are separated with a semi-porous membrane such as sintered glass frit, porous porcelain, polytetrafluoroethylene, an ion-selective membrane or salt bridge. The purpose of the divided cell is to "separate" the chemistries at the two electrodes (Pletcher *et al.*, 2017) hence permitting the diffusion of ions via the membrane and restricting the flow of the products and reactants. Other functions of the porous membrane are to complete the electric circuit and maintain electrical neutrality on both sides of the electrode compartment. The two resulting half-cells may utilize the same or different types of electrolytes. Electrolyte, therefore, is an ionic substance that permits ions to migrate between the electrode compartments, thereby sustaining the system's electrical neutrality. The two types of electrolytes are strong and weak electrolytes.

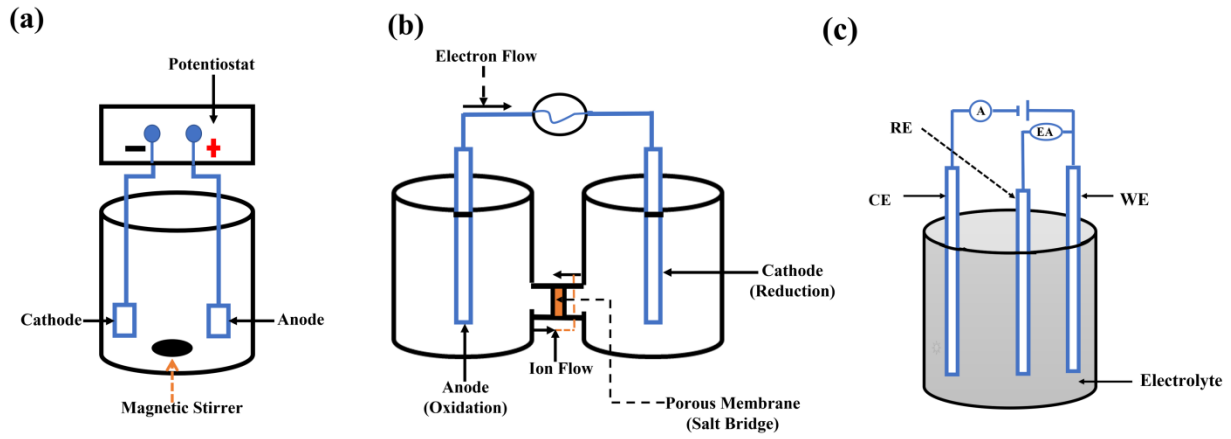

Figure 2.8: (a) Undivided Cell (b) Divided cell (c) 3-electrode cell electrochemical cell with E_A as the applied voltage, WE, CE and RE as the working, counter and reference electrodes respectively

Those electrolytes which completely ionize or dissociate into ions are known as strong electrolytes. Some of the examples of strong electrolytes are hydrochloric acid (HCl), sodium

hydroxide (NaOH), and potassium sulfate (K_2SO_4). Weak electrolytes, on the other hand, are those electrolytes that dissociate partially in an aqueous medium. Some of the examples of weak electrolytes are acetic acid (CH_3COOH), carboxylic acid (H_2CO_3), ammonia (NH_3), ammonium hydrosulphide (NH_4OHH_2S) (Tro, 2018). Electrochemical reactions occurring in a cell are between the electrolyte, electrodes, and an external substance (as in fuel cells that may use hydrogen gas as a reactant).

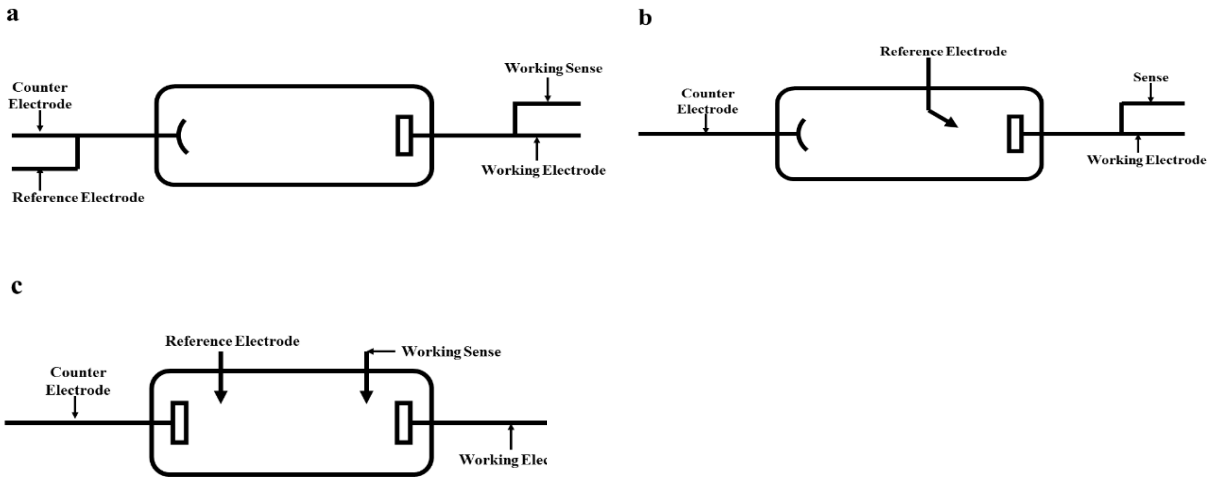

Figure 2.9: (a) Overview of 2-electrode setup (b) Overview of 3-electrode setup (c) Overview of 4-electrode setup

Electrodes are used to perform specialized roles in electrolytic cells; hence cells can be configured or set up to have two, three, or four electrodes, depending on the type of experiment to be conducted. The most basic form of cell configuration is the two-electrode cell configuration, which usually has the electrode under investigation as the working electrode (WE) and the electrode necessary to close the electrical circuit, the counter electrode (CE). The

electrode where the chemistry of interest occurs is the WE. The physical set-up for two-electrode mode is shown in Figure 2.9a with working (W) and working sense (WS) leads connected to the working electrode (WE) called the cathode and Reference (R) and counter (C) leads connected to the second electrode called the anode. In this type of setup, the counter electrode has two major responsibilities. It completes the circuit permitting charges to be circulated throughout the cell and it sustains the same interfacial potential despite the flow of free electrons. The role of circulating current with constant voltage supply, is, therefore, better utilized by two separate electrodes. Thus, this kind of setup is usually employed when one wants to examine and analyze properties such as electrolyte conductivity or to characterize semiconductor devices. For three-electrode cell configurations, the cell setup consists of the working electrode (WE), a counter electrode (CE), and a reference electrode (RE) as depicted in Figure 2.9b. In this setup, the RE is most often positioned in such a way as to measure and control the working electrode potential (which has both Working and Working Sense leads attached, without allowing the passage of free flow electrons. The RE is expected to sustain the electrochemical potential value at low current density.

Furthermore, since the RE allows the passage of so small current, the potential drop across the space separating the reference and the working electrode (iRU) is often very negligible. Hence, the three-electrode system gives a much more stable reference potential value than others with additional compensation of iR drop-in solution. Therefore, in the three-electrode setup, the major role of the CE is to allow the passage of all free electrons required to stabilize any current detected at the working electrode. Hence, maximum potentials at the CE are needed to achieve such a task. The most uncommon cell configuration is the four-electrode cell configuration**,** which has the Working Sense lead decoupled from the working electrode, as

shown in Figure 2.9c. In a 4-electrode mode, working electrode potentials are not being measured but rather the effect of an applied current or some barrier on the solution itself was measured. A 4-electrode cell setup is generally used to analyze processes occurring within the electrolyte, between two measuring electrodes separated by a membrane (EIS03, 2011).

2.9 Types of Electrochemical Cells

The two main types of electrochemical cells and they are galvanic cells (also called voltaic cells) and electrolytic cells.

2.9.1 Galvanic cells

A galvanic cell is a device that utilizes spontaneous oxidation-reduction reaction to produce an electric current; hence it is also called a voltaic cell (Oon, 2007). Spontaneous redox reactions are exothermic reactions. They change the energy liberated by a spontaneous reduction and oxidation reaction into electrical energy used to do work. Thus, in galvanic cells, the redox half-reactions typically occur in different compartments called half-cells. As depicted in Figure 2.8b, the porous barrier connects the two half-cell allowing ions to migrate between the two chambers while also retaining their electrical neutrality. The potential difference between the two electrodes (voltage) enables electrons to migrate from the reduced to the oxidized through an outer circuit, hence producing an electric current. The metal that is more readily oxidized serves as an anode with oxidation half-reaction occurring there while the cathode is the electrode at which the reduction half-reaction occurs. Using zinc (Zn) and copper (Cu) for illustration, the basic principles of the galvanic cell are represented in the following cell notation of Equation

2.26 and 2.27 (Holze, 2012). (Note that cell notation has its cathode displayed on the right-hand side and the anode on the left)

$$Zn|ZnSO_4\,(aq)||CuSO_4\,(aq)|Cu \quad (2.26)$$

$$Zn(s) + Cu^{2+}\,(aq) \rightarrow Zn^{2+}\,(aq) + Cu(s) \quad (2.27)$$

The ionic flow (electricity resulting from positive charge) is migrating from left to right once the zinc rod is immersed into its aqueous electrolytic solution of zinc (II) sulfate. As the reaction continues, the zinc rod melts with the appearance of massive copper metal. These conversions occur automatically, with all the energy released in the form of heat that can be dissipated. Conclusively, in Galvanic cell (aka Voltaic Cell), a chemical redox reaction is spontaneous as the change in Gibb's energy is less than zero (ΔG is < 0), hence electrode potential is greater than zero ($E^o > 0$). Electrons, therefore, migrate from the anode, the negative terminal to the cathode, the positive terminal (where electrons are gained). Examples of galvanic cells are (a) dry cell (i.e. non-rechargeable batteries) and (b) Daniel cell

2.9.2 Electrolytic Cell

The electrolytic cell, on the other hand, is an electrochemical cell that drives a non-spontaneous redox reaction through the application of an external source of electrical energy. In electrolytic cells, only a single compartment is employed in its applications. This kind of cell is mostly used to disintegrate chemical compounds, in a series of chemical operations called electrolysis. Examples of where this kind of cell is used are in rechargeable batteries, to divide solid metals from its metallic compound, to divide other chemical compounds such as water, to electroplate

metals and too impressed current cathodic protection. The main differences between galvanic and electrolytic cells are outlined in Table 2.2. However, all electrolytic cells contain three main parts: two solid electrode conductors in contact with its ionic conductors (electrolytes).

The negative charge electrode is always the cathode while the positively charged is the anode. These two electrodes are manufactured from substances that take part in the chemical reaction of which zinc, copper, and silver are examples. Also, like graphite, silicon, or platinum, they can be produced from chemically inert materials, thus they are generally regarded as active electrodes. First, the battery from the external source supply's electrical energy which sends the electrons onto the cathode, making it negatively charged.

Table 2.2: Correlation between galvanic and electrolytic cells

Galvanic cell	Electrolytic cell
1. ΔG is < 0, $E^o cell > 0$	$\Delta G > 0$, $E^o cell < 0$
2. A Galvanic cell transforms chemical energy into electrical energy.	An electrolytic cell transforms electrical energy into chemical energy.
3. A Galvanic cell transforms chemical energy into electrical energy.	An electrolytic cell transforms electrical energy into chemical energy.
4. A spontaneous redox reaction occurs	Electrical energy from external source

here which gives rise to the generation of electrical energy	initiates redox reaction, hence reaction is not spontaneous
5. The cell is configured to have the two electrodes in different half-cells compartments, linked together via salt bridges or porous partition	The cell is configured to have both electrodes in the same compartment having the same electrolyte.
6. The anode is the negative pole while the cathode is the positive pole. An oxidation reaction occurs at the anode, while that at the cathode is a reduction.	The cathode is the negative pole while the anode is the positive pole. An oxidation reaction occurs at the anode, while that at the cathode is a reduction.
7. Oxidized species are the source of electrons supplied and they move from anode to the cathode	External source supplies the electrons and forced them onto the cathode and eventually come out through the anode.

Pulling out electrons from the anode makes it positively charged. Once this occurs, a Redox reaction is initiated. Hence, an oxidation reaction occurs at the anode, allowing electrons to migrate freely, and becoming attracted toward the positive electrode. Consequently, electrons accumulate at the cathode where reduction takes place.

2.10 Electrochemical Cell Electrodes

Electrodes are typically good electric conductors, carrying currents to non-metallic solids, liquids, or gases. In solid conductors, the current is carried by electrons. Some examples of solid conductors are zinc, carbon, and iron. In liquids and gases, the current is being carried by molecules that have acquired either positive or negative charges called ions. Examples include hydrogen ion (H^+), hydroxyl ion ($OH^{\bullet}$), etc. According to Inzelt, (2015), there are numerous ways of classifying electrodes, hence enumerated. The electrode where reduction chemical reaction takes place is called the cathode and that where oxidation chemical reaction occurs is called the anode. Classifying electrode based on whether migratory ionic species across the boundary at the interface or not, we have a non-polarisable electrode which represents electrodes that allow mass transfer at the interface and polarisable electrode which does not allow any charge transfer at their interface. Based on the electrode size, electrodes can consequently be classified into microelectrodes, and ultra-microelectrodes. In terms of functional grouping, electrodes are classified as working, counter, and reference electrodes.

On the other hand, electrode surfaces can be modified to incorporate an electrochemical function either not possible or difficult to achieve using conventional electrodes. The targeted improvement includes increased selectivity, sensitivity, and improved resistance to fouling, chemical, and electrochemical stability. Durst, (1997) suggested that chemically modified electrode (CME) are electrodes made of a conducting or semiconducting material which is coated with a selected monomolecular, multimolecular, ionic, or polymeric film of a chemical modifier and that employing Faradaic (charge-transfer) reactions or interfacial potential differences (no net charge transfer) exhibits chemical, electrochemical, and/or optical properties

of the film. The distinguishing feature of a CME is that the substance coated on the electrode surface is electroactive, endowing the electrode with desirable properties in a rational chemically designed manner. Several methods used to chemically modify electrodes are chemisorption**,** covalent bonding, coating by thin films, cross-linking, dip-coating, electrochemical polymerization, spin coating (spin casting) and electrochemical deposition (Durst, 1997). In this study, electrochemical deposition is used to modify the electrode. Electro-deposition is also called electroplating and it is used to coat a conductive metal with a thin layer of material (Wang *et al.,* 2018). It is a process that assembles solid materials from ions in a solution. In this study, chronoamperometry techniques from PGSTAT were used for electrodeposition.

2.10.1 Working electrode (WE) and carbonaceous material

This is the electrode where the reaction of interest takes place. It changes from experiment to experiment to supply separate potential windows or to minimize/upgrade surface adsorption of the species of interest. The selection of WE depends either on the reduction and oxidation performance of the targeted species and the background current over the potential area needed for the measurement. A PGSTAT is used to control the applied potential of the working electrode as a function of the reference electrode potential. Carbonaceous materials in recent times have attracted considerable interest as an electrode material due to their commercial availability, good electrical conductivity, chemical and thermal stability, adsorption properties, relatively inexpensive cost, flexibility, and high surface area (Peng *et al.*, 2019).

Carbonaceous material has many possible forms of existence; hence, it can be utilized as WE materials in different forms such as, carbon felt, activated carbon felt, carbon cloth, activated carbon, carbon nanotube, etc. Also, their porous nature, surface properties, and electronic

conductivity have made them excellent catalyst support (Yang *et al.*, 2011). As support, their large surface area with varying pore size distribution and different surface functionalities can be utilized. Banuelos *et al.* used iron-modified activated carbon electrodes (Fe/AC) to obtain higher efficiency of discoloration and degradation in the EF and PEF processes of a typical dye aqueous solution (Banuelos *et al.*, 2015). In this study, a highly porous and lightweight structured carbon cloth electrode was used to anchor iron (II) catalyst for the heterogeneous EF process of treating pharmaceutical wastewater.

2.10.2 Counter electrode (CE) and boron-doped diamond (BDD) electrodes

The counter electrode is also known as an auxiliary electrode. It is the electrode used to complete the electrical circuit in the electrochemical cell (Fowowe, 2011). Its major duty is to provide a different path for the current to pass so that only an insignificant amount of current migrates through the reference electrode. Commonly, they are called inert electrode and they do not take part in an electrochemical reaction. Current regarded as free flow electrons migrate between the Working electrode and the counter electrode. To make certain that the kinetics of reaction taken place at the CE do not obstruct those reactions happening at the WE, the surface area of the CE must be larger than the surface area of the WE (Tian *et al.*, 2016). When studying a reduction reaction at the WE, an oxidation reaction occurs at the CE. As such, the CE should be chosen to be as inert as possible.

In this study, while the platinum electrode was used as CE during the iron (II) electrodeposition process, BDD was used as CE during the pharmaceutical wastewater

degradation. However, electrochemical oxidation using the BDD electrode has been realized as one of the most effective methods used for the degradation of refractory (Yu *et al.,* 2014). The most useful property of BDD electrodes is their ability to generated hydroxyl radicals ($OH^{\bullet}$) that allow the complete degradation of organics at high anodic potentials in wastewater treatment. As suggested by Yu *et al.* 2014, using BDD in an electrolytic cell, resulted in water being oxidized to hydroxyl radical formation and adsorbed on the electrode surface as illustrated in Equation 2.28

$$H_2O + BDD \longrightarrow BDD(HO\bullet) + H^+ + e^- \quad (2.28)$$

$$BDD(HO\bullet) + R \longrightarrow BDD + CO_2 + H_2O + H^+ + e^- \quad (2.29)$$

$$BDD(HO\bullet)\ ads \longrightarrow BDD + \frac{1}{2}O_2 + H^+ + e^- \quad (2.30)$$

Hence, organics (R) oxidation (equation 2.29) follows as any organics within this zone undergoes combustion, then oxygen evolution as shown by Equation 2.30. Patel *et al.* 2013, enumerated the following properties that made BDD the most efficient material for electro-oxidation of wastewater

- Extreme overpotential for oxygen and hydrogen evolution
- High chemical and electrochemical stability, especially the high electrochemical stability under severe conditions
- Corrosion stability in very aggressive media
- Possibility to anodically produce hydroxyl radicals with high current efficiency without any modification of electrodes

- An inert surface with low adsorption properties and a strong tendency to resist deactivation (Swain, 1994).

Apart from these advantages, BDD has a limitation, which is the high price of conductive diamond anodes thwarting the widespread use of BDD on a large scale.

2.10.3 Reference Electrode (RE)

RE is an electrode with constant potential and negligible current. Their potential is normally used to refer to the potential of other electrodes. Laboratory most commonly used reference electrodes, in aqueous media are silver-silver chloride Ag/AgCl electrode, the saturated calomel electrode (SCE), and the standard hydrogen electrode (SHE). These RE's, in solution, are mostly isolated by a porous membrane. RE's derived from Ag^{+}/Ag couple is the most often used in non-aqueous solvents, hence, a very high input impedance on the electrometer (> 100 GOhm) together with the CE, enables current flowing through the reference electrode to be maintained close to zero (ideally, zero). The half-reaction for the Ag/AgCl reference electrode and its half-cell notation is shown in Equation 2.31 and 2.32. In the same manner, the half-reaction that occurs inside the saturated calomel (SCE) reference electrode and the shorthand notation for the SCE half-cell is given in Equation 2.33 and 2.34.

$$AgCl\ (s) + e^{-} \longrightarrow Ag(s) + Cl^{-}(aq) \qquad (2.31)$$

$$Ag(s)\ /\ AgCl(s)\ //KCl\ (aq),\ AgNO_3\ (aq) \qquad (2.32)$$

$$Hg_2Cl_2(s) + 2e^{-} \longrightarrow 2\ Hg\ (l) + 2\ Cl^{-}\ (aq) \qquad (2.33)$$

$$Pt(s)\ /\ Hg(l)\ //\ Hg_2Cl_2(s)\ /\ KCl\ (aq,\ sat‘‘d) \qquad (2.34)$$

2.11 Electrode Potential (E^o)

The electrode potential, *E* (SI unit is Volts) is the electric potential difference of an electrochemical cell. It is the potential value delivered by an electrode to its interfacial boundary with the electrolyte. In an electrochemical cell, each electrode exacts an electric potential at the interface with the electrolyte due to charged species that are transported over the interface. The difference between the two electrode potentials gives the cell potential (Equation 2.35). When current moves across any given cell, the resulting electrodes potential should be steady to maintain a precise potential value for the electrode under analysis. Following the recommendations of IUPAC, the Standard hydrogen electrode (SHE) should be used as the reference point electrode. Hence, hydrogen is assigned a reference standard electrode potential of zero which all other electrodes are measured against. When SHE acts as the cathode, the half-cell reaction obtained is depicted in Equation 2.36.

$$E^0_{cell} = E^0_{cathode} - E^0_{anode} \tag{2.35}$$

$$2H^+ (aq) + 2e^- \longrightarrow H_2 (g) \quad E^0_{cathode} = 0.000V \tag{2.36}$$

If the SHE is connected to an electrode in another half-cell, the cell potential (the difference in potential energy) can be used to determine the standard electrode potential of the other half cell. E^0_{cell} is positive for reactions occurring spontaneous and negative for a non-spontaneous reaction. Given in Figure 2.10 are the standard potential of some common metals and non-metals.

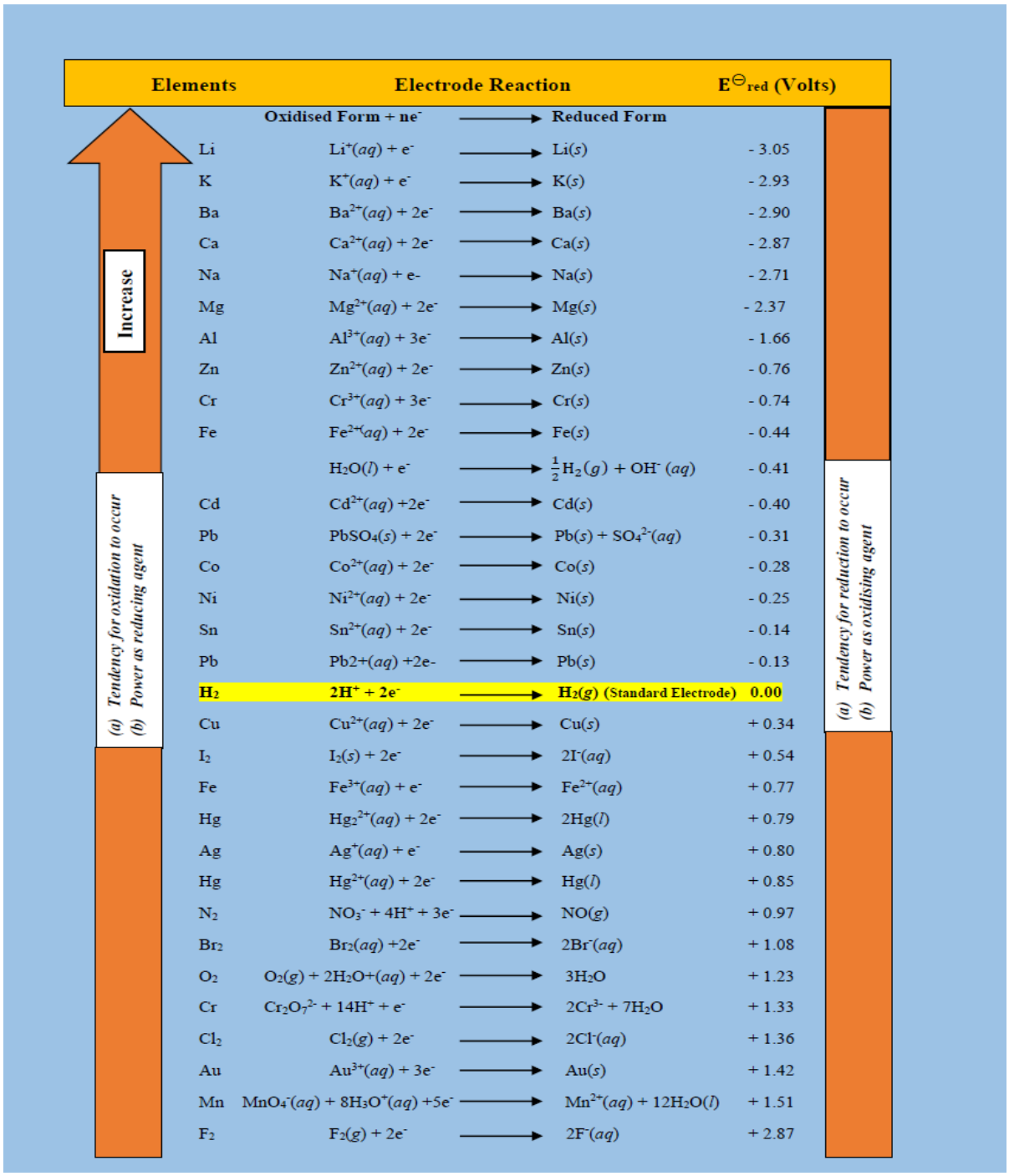

Figure 2.10: Standard potential of some common metals and non-metals

2.12 Electrode Reaction

Electrochemical reactions happening at the interface between the electrode and its electrolyte are fundamental in electrochemistry, with the application of electrode potential. These chemical reactions resulted from the heterogeneous migration of electrons between the electrode and the electroactive species in solution (Marcus, 1993). Hence, a standard electrode reaction requires electron(s) to be transferred between an electrode and the bulk electroactive species. It is not only a single electron-transfer step that is involved in electrode reactions, a sequence of two or more steps may also occur. Electrode reaction may produce positive or negative currents depending on the type of half-reaction occurring at the surface of the electrode. Electrochemical half-reaction can be referred to as anodic half-reaction or cathodic half-reactions and both are called redox reaction as expressed in Equation 2.37.

$$O + ne - \underset{OXIDATION}{\overset{REDUCTION}{\rightleftharpoons}} R \qquad (2.37)$$

O.A R.A

Reduced Oxidized

Where: O (Reactant) gains an electron and becomes reduced (GER), R (Product) losses electron, and becomes oxidized (LEO). Oxidation is the loss of electron/increase in oxidation number and reduction in the gain of electron/decrease in oxidation number. The reducing agent (R.A) loses an electron and it is said to be oxidized, while Oxidizing Agent (O.A) gains an electron and it is said to be reduced. By controlling the applied potential on the working electrode, the electrode reaction can be observed to follow the pathway shown in Figure 2.11. The steps include,

transportation of reactant electroactive species (O) to the electrode surface and this is termed mass transport, adsorption of the electroactive species onto the surface of the electrode, electrode reaction occurs which involves the exchange of electron through quantum mechanical tunnelling between the electrode and the electroactive species (Guo and McKenzie, 2017), the formation of products-R on the electrode surface, desorption of R from the electrode surface and transport of R-product away from the electrode surface to allow fresh reactant to accumulate on the electrode. Electron exchange between the electrode and the chemical species at the interface enables the interface to be electrified (i.e. current flows around) with the formation of a double layer, called an electric double layer (EDL). It was reported that EDL can only be explained using Helmholtz compact layer model, the Gouy-Chapman diffuse layer model, and the Stern model as depicted in Figure 2.12 (Gongadze *et al.,* 2009).

Helmholtz model proposed the existence of three regions, the inner Helmholtz plane (IHP) which passes through the centers of all species specifically adsorbed on the electrode surface as they have lost their solvation shell partially or completely. The second is the outer Helmholtz plane (OHP) which passes through the center of solvated ions located closest to the electrode surface, but not specifically adsorbed, only bounded by electrostatic forces. Ions in the OHP are hydrated with their solvation shell intact. The third region is the diffuse layer which is beyond the OHP. On the other hand, the Gouy-Chapman model assumes an outer "diffusion layer" containing an excess of cations or anions extending from the OHP to the bulk solution through a certain thickness, which is determined by the ion concentration. Stern model is a combination of both the Helmholtz and the Gouy-Chapman models, and he suggested that ions have finite size and consequently an ion's closest approach to the electrode is on the order of the ionic radius (Bard and Faulkner, 2001).

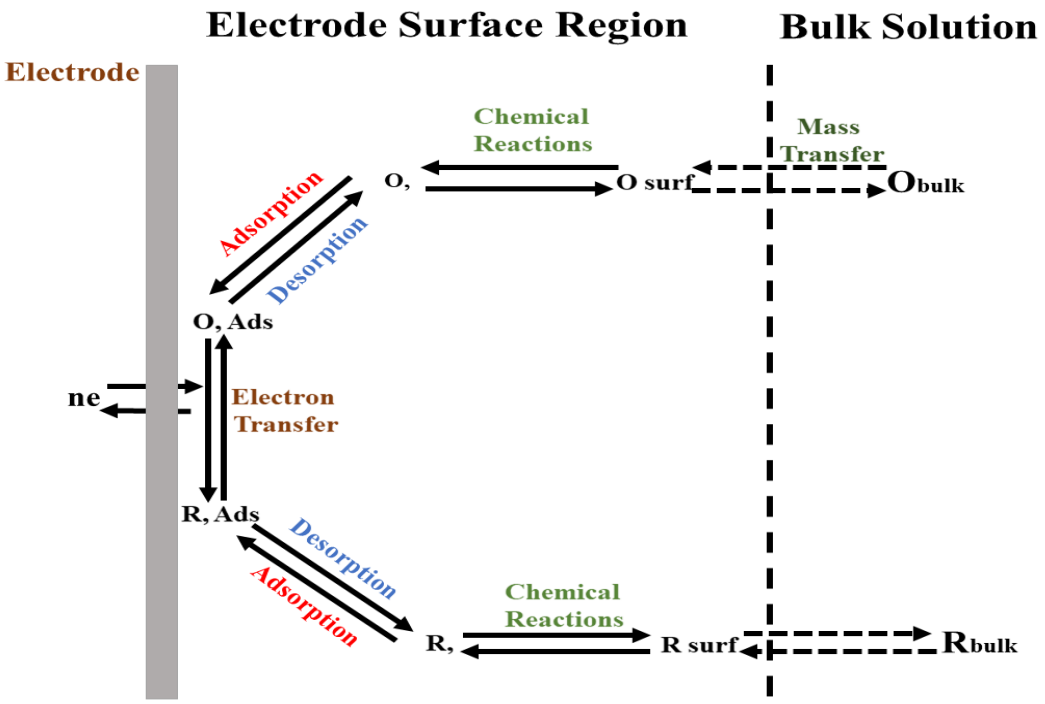

Figure 2.11: Pathway of a general electrode reaction

In the bulk of the ionic liquid, cations and anions are considered as a solid round object, of the same radius r, with its polarity situated at the center of the round object (Gongadze *et al.*, 2009). In another development, from Equation 37, the relationship linking the oxidized (R) and the reduced (O) species in terms of concentration and free energy ($Jmol^{-1}$) is given by Equation 2.38. However, the authentic cell potential is related to the change in Gibbs free energy with the maximum work done in a cell, which can be related to standard conditions (Equation 2.39). Therefore, the expression relating the potential and concentration of electroactive species taken part in any cell reaction at equilibrium is known as the Nernst Equation (Equation 2.40).

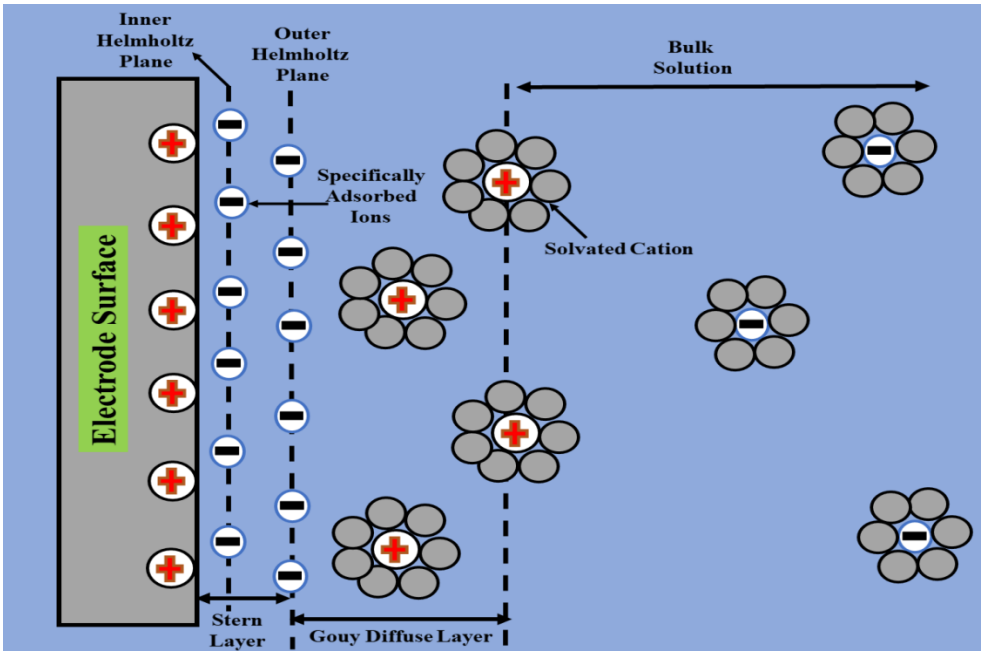

Figure 2.12: Electric Double Layer (EDL) showing Helmholtz compact layer, Gouy-Chapman diffuse layer, and Stern model

Hence, the Nernst Equation is derived from the Gibbs free energy under standard conditions. Under standard conditions, all concentrations are equivalent to 1 m or 1 atm from the Nernst equation.

$$\Delta G = \Delta G^{o} + RT\ln(Q) = \Delta G^{o} + RT \ln \frac{[R]}{[O]} \quad (2.38)$$

$$\Delta G = -nFE = -nFE^{o} \quad (2.39)$$

$$-nFE = -n\,FE^{o} + RT\ln(\frac{[R]}{[O]}), \text{ therefore } E = E^{o} - \frac{RT}{nF}\ln \frac{[R]}{[O]}$$

$$E = E^{o} + \frac{0.059}{n} \ln \frac{[O]}{[R]} \quad (2.40)$$

The expression also indicates that the electrode potential of a cell is dependent on the reaction quotient Q of the reaction. As the reduction and oxidation reaction proceeds, reacting species are

used up, hence, decreasing the concentration of the reactants. Conversely, the concentration of the products formed increases. As this happens, the cell potential slowly decreases until the reaction reaches equilibrium. At equilibrium, $\Delta G = 0$, also $E = 0$. The reaction quotient Q = equilibrium constant, K. then Equation 2.41,

$$\Delta G = \Delta G^o + RT\ln(Q) \equiv \Delta G^o + RT \ln \frac{[R]}{[O]} \quad \text{become}$$

$$0 = \Delta G^o + RT \ln K$$

$$\Delta G^o = - RT \ln K \qquad (2.41)$$

Nernst Equation then gives the standard electrode potential of the cell as,

$$-nFE^o = - RT \ln K,$$

$$\Rightarrow E^O = \frac{RT\ln(K)}{nF}$$

But, when Q equals one, its logarithm gives zero, then the cell potential equals the standard cell potential. Hence:

I.e. When Q = 1, then $\frac{[R]}{[O]} = 1$.

Its logarithm gives: $\ln Q = \ln \frac{[R]}{[O]} = \ln 1 = 0$.

Hence, $E = E^O$

Where Q is the reaction quotient or activity, n represents the number of moles of electrons transported in the reaction (per mole of reactant or product), F represents the Faraday's constant = 96,500 C/Mol. and E is referred to as open circuit potential (OCP) or equilibrium potential.

2.13 Electrochemical Resistance

Electrochemical cells are constructed of various materials, such as the wire, the electrolytic solutions, the electrodes, and the containers. All of these materials together cause the cell to experience some sort of resistance. However, charges are transported in the electrolyte through the motion of ions (positive and negative). As the ions migrate from one point to another in the solution, ionic resistance occurs. The resistance of an ionic solution is therefore determined by the geometry of the area in which current is carried, the ionic concentration and type of ions, temperature. Charge transport can also occur in the electrode through the motion of electrons. Electronic resistance occurs along the electrode and external circuit as an electron is transferred. This type of resistance can be minimized by using electron-conducting materials.

However, over a given cross-sectional area A and length l carrying a uniform current, the resistance is expressed as in Equation 2.42. Expressing ρ (solution resistivity) in terms of κ (solution conductivity), we obtain Equation 2.43. Standard chemical handbooks list conductivity (κ) values of specific solutions as a function of concentration (Weast, 1989). The units for conductivity (κ) are Siemens per meter (S/m). Multiplying Siemens with ohms gives unity by definition, so 1 S = 1/Ω. Generally, theses resistance causes the cell to lose some of its potentials. What remains of the cell's voltage after subtracting the voltage loss due to internal resistance is called the terminal potential difference as expressed in Equation 44. In Equation 2.44, Vt.p.d. is

the terminal potential difference, emf is the electromotive force, or ideal amount of energy (in volts) provided by the cell before there is resistance, I represent current in amperes, and represents the internal resistance in ohms.

$$R = \rho \frac{l}{A} \tag{2.42}$$

$$R = \frac{1}{K}\frac{l}{A} \quad => \quad K = \frac{l}{RA} \tag{2.43}$$

$$V_{t.p.d} = \text{emf} - Ir \tag{2.44}$$

2.14 Faradaic and Non-Faradaic Processes

Redox reaction which involves the migration of electrons occurs at the electrode-solution interface. Such reactions are governed by Faraday's law-which states that the number of moles of the electron, produced or consumed during an electrode process, is proportional to the quantity of electricity passing through the electrode. Therefore electron-transfer process, occurring at the charged interface and obeying faraday law are called Faradaic processes (Bard *et al*., 1980). Under certain given conditions, the electrode-solution interface can exhibit a set of potentials which does not support charge-transfer reactions because such reactions are disadvantaged. Such unit operation includes adsorption, desorption, movement of electrolytic ions, and reorientation of solvent dipoles. Therefore, the non-Faradaic process arises when no charge-transfer processes occur at the interface (Bard *et al.,* 1980). Hence, both Faradaic and non-Faradaic operations occur simultaneously when electrode reactions take place. Generally, Faradaic current which flow at the interface is governed by Faraday's law (Equation 2.45). The transport of a single

electron between two species of (O) and (R) (Equation 2.37) gives the cathodic and anodic current flowing as shown in Equation 2.46. Their corresponding reaction rate constants are predicted in Equation 2.47, which on relating it with free energy give Equation 2.48.

$$\text{Q = Nfn} \qquad \text{then} \quad \frac{dQ}{dt} = i = nF\frac{dN}{dt} \tag{2.45}$$

$$i_{c=-FAK_{red}[O]_o} \qquad \text{And} \quad i_{a=-FAK_{Ox}[R]_o} \tag{2.46}$$

$$K_{RED} = Ze^{\frac{-\Delta G_{RED}}{RT}} \qquad \text{And} \quad K_{OX} = Ze^{\frac{-\Delta G_{OX}}{RT}} \tag{2.47}$$

$$K_{RED} = Ze^{\frac{-\Delta G_{rednovoltage-\propto FV}}{RT} \quad RT} \quad \text{And} \quad K_{OX} = Ze^{\frac{-\Delta G_{oxnovoltage(1-\propto)FV}}{RT} \quad RT} \tag{2.48}$$

Where (Q) represents the total charge or quantity of electricity in the experiment, N is the number of molecules electrolyzed and n is the number of electrons transferred. Also, "i" is the Faradaic current, with i_c and i_a the reduction (cathodic) and oxidation (anodic) current, K_{RED} and K_{OX} are the rate constants of the electron transfer,

2.15 Mass transport processes in an electrochemical cell

Whenever there is a charge transfer process at the surface of the electrode, the reacting species are used-up as they are consumed, setting up a concentration gradient within the solution. Under diffusion-controlled conditions, more reacting species from bulk solution moves in the direction of the electrode as a formed product moves into the bulk solution from the electrode surface. Therefore, mass transport of electroactive species in electrochemistry demonstrates the motion of species from one area to another in the solution due to the species concentration gradient in the

solution mixture. Elgrishi et al. 2017, reported that the three fundamental modes of mass transport are (1) diffusion, (2) migration, (3) convection.

2.15.1 Diffusion

Diffusion is the transport of particles as a result of the local difference in the chemical potential (Baierlein, 2001). In another word, diffusion is simply the random motion of a species from an area of higher concentration to another area of lower concentration and it must occur whenever bonds are broken or formed at the electrode surface. Diffusion-controlled electrode reaction arises when the molecular species close to the surface of the electrode are used-up, thereby reducing its amount near the electrode surface, hence more species diffuses in from the bulk solution to replenish it. Similarly, when a species is continually generated at an electrode, it begins to diffuse away from the electrode, where its concentration is zero. The rate of diffusion depends upon, the solution concentration gradient, and on the diffusion coefficient, D, of electroactive species fixed temperature.

Therefore, the movement of intermolecular species as effected by concentration gradient is described by Fick's first law which states that the flux JA(x,t) of substance A, moving from higher concentration region to lower concentration region, has a magnitude which is proportional to the concentration gradient ΆCA(x,t)/ΆAx as shown in Equation 2.49. If the diffusion coefficient is self-sufficient and does not depend on position, then Fick's Second Law (Equation 2.50) may clarify the situation.

$$J_A(x,t) = -D_A \frac{\partial C_A(x,t)}{\partial x} \tag{2.49}$$

$$\frac{\partial C_o}{\partial t} = D_o \left\{\frac{\partial^2 C_o}{\partial x^2}\right\} \quad (2.50)$$

The diffusion of reactants and products in electrolytes should be considered in many types of interfacial processes. Diffusion of atoms on the electrodes may control the rate on the deposition and the value of the diffusion coefficient would, of course, vary from system to system.

2.15.2 Migration

The movement of charged particles in response to a local electric field is called migration (Yu *et al.,* 2014). This electrostatic phenomenon emerged due to the application of voltage on the electrodes. Therefore, electroactive species near this electrified interface will moreover be attracted or repelled from the electrode surface by electrostatic forces. However, ion solvation effects make intermolecular movement within real solution very difficult to determine correctly. As a result, it has become unavoidably essential to add inert electrolyte in large quantities to the cell solution to shield the molecular species of any interest from migratory effect. The inert electrolyte commonly called the supporting electrolyte offsets the effect of intermolecular forces linking the working electrode and the molecular species by subduing the transported quantity of the reactants. This electrolyte can also act as a conductive solution to assist in the movement of the current.

2.15.3 Convention

Convection is the movement of solution species due to externally controlled forces. Forced movement of bulk electroactive species by rotation or vibration or automated stirring give rise to

forced convection. On the other hand, natural convection arises in solution due to changes in temperature and density. Fluid involved in forced convection can constantly be replaced and treated mathematically while natural convection cannot be reproduced or duplicated. Because the natural convention is not consistent, it is known to complicate the electrode process and therefore should be eliminated. This can be successfully reached by carrying out electrolysis in a thermostat-controlled system, in the absence of vibration.

REFERENCE

ABD EL-GHAFFAR, M.A. AND TIEAMA, H. A. 2017. A review of membranes classifications, configurations, surface modifications, characteristics and Its applications in water purification., *Chemical and Biomolecular Engineering Journal*, 2 (2) : 57.

ABDALLA, K.Z. AND HAMMAM, G. 2014. Correlation between biochemical oxygen demand and chemical oxygen demand for various wastewater treatment plants in Egypt to obtain the biodegradability indices, *International Journal of Sciences: Basic and Applied Research*, 13 (1) : 42–48.

ALZAHRANI, T., KAY, D., ALQAHTANI, S.A., MAKKE, Y., LESKY, L. AND KOUBEISSAOUBEISSI, M. Z. 2015. Levetiracetam-induced pancytopenia, *Epilepsy and Behavior Case Reports*, 4 : 45–47.

BAIERLEIN, R. 2001. The elusive chemical potential, *American Journal of Physics*, 69 (4) : 423–434.

BANUELOS, J.A., GARCÍA-RODRÍGUEZ, O., RODRÍGUEZ-VALADEZ, F.J. AND GODÍNEZ, L. A. 2015. Electrochemically prepared iron-modified activated carbon electrodes for their application in electro-Fenton and photoelectron-Fenton processes, *Journal of The Electrochemical Society*, 162 (9) : E154–E159.

BARD, A.J., FAULKNER, L.R., LEDDY, J. AND ZOSKI, C. G. 1980. *Electrochemical Methods: Fundamentals and Applications*. Wiley New York.

BARD, A.J. AND FAULKNER, L. R. 2001. *No Title Electrochemical Methods: Fundamentals and*

Applications. 2nd edn. Wiley, New York.

BHATT, P.M., AZIM, Y., THAKUR, T.S. AND DESIRAJU, G. R. 2009. Co-crystals of the anti-HIV drugs lamivudine and zidovudine, *Journal of Crystal Growth and Design*, 9 (2) : 951–957.

BHOPALE G. M. 2012. Emerging drugs for the treatment of human immunodeficiency virus, *Journals of recent patents on anti-infective drug discovery*, 7 (1) : 45–52.

BRILLAS, E., SIRES, I. AND OTURAN, M. A. 2009. Electro-Fenton process and related electrochemical technologies based on Fenton's reaction chemistry, *Journal of Chemical Reviews*, 109 (12) : 6570–6631.

BROWN, G.W. 1985. Forestry and water quality: College of Forestry, Oregon State University Publisher, OSU Bookstore. Inc., Corvallis, OR., 142p.

BUTANDA-OCHOA, A., HERNANDEZ-ESPINOSA, D.R., OLGUIN-MARTINEZ, M., SANCHEZ-SEVILLA, L., RODRIGUEZ, M.R., CHAVEZ-RENTERIA, B., ARANDA-FRAUSTRO, A. AND HERNANDEZ-MUNOZ, R. 2017. A single zidovudine (AZT) administration delays hepatic cell proliferation by altering oxidative state in the regenerating rat liver, *Journal of Oxidative Medicine and Cellular Longevity*.

CAMPOS-MARTIN, J.M., BLANCO-BRIEVA, G. AND FIERRO, J. L. 2006. Hydrogen peroxide synthesis: an outlook beyond the anthraquinone process, *Angewandte Chemie International Edition*, 45 (42) : 6962–6984

CARSON, P. AND MUMFORD, C. J. 2002. *Hazardous Chemicals Handbook*. Elsevier Butterworth.

CARSON, P. AND MUMFORD, C. 2002. *Toxic Chemicals. Hazardous Chemicals Handbook.*

CHANDRA, U., GILBERT, O., SWAMY, B.K., BODKE, Y.D. AND SHERIGARA, B. S. 2008. Electrochemical studies of Eriochrome Black T at carbon paste electrode and immobilized by SDS surfactant: A cyclic voltammetric study, *International Journal of Electrochemical Science*, 3 (9) : 1044–1054

CIARDELLI, G. AND RANIERI, N. 2001. The treatment and reuse of wastewater in the textile industry by means of ozonation and electrofloculation, *Water Research Journal*, 35 (2) : 567–572.

CLESCERI, L.S., GREENBERG, A.E., AND EATON, A.D., Eds. 1998. Standard Methods for the Examination of Water and Wastewater (20th Ed.). Washington, D.C.:American Public Health Association, American Water Works Association and the Water Environment Federation

COHEN, M.S. AND GAY, C. L. 2010. Treatment to prevent transmission of HIV-1; Clinical Infectious Diseases', *Clinical Infectious Diseases*, 50 : S85–S95.

CUERDA-CORREA, E.M., ALEXANDRE-FRANCO, M.F. AND FERNANDEZ-GONZALEZ, C. 2020. Advanced Oxidation Processes for the Removal of Antibiotics from Water. An Overview., *Water Journal*, 12 (1) : 102

DAHAMSHEH, A. AND WEDYAN, M. 2017. Evaluation and assessment of performance of Al-Hussein bin Talal University (AHU) wastewater treatment plants., *International Journal of Advanced and Applied Sciences*, 4 (1) : 84–89.

DANTAS, R.F., CANTERINO, M., MAROTTA, R., SANS, C., ESPLUGAS, S. AND ANDREOZZI, R. 2007. Bezafibrate removal by means of ozonation: primary intermediates, kinetics, and toxicity assessment., *Journal of Water Research*, 41 (12) : 2525–2532.

DAVID, S. AND HAMILTON, J.P., 2010. Drug-induced liver injury. US Gastroenterology & Hepatology review, 6 : 73.

DHOTE, J., INGOLE, S. AND CHAVHAN, A. 2012. Review on wastewater treatment technologies., *The International Journal of Engineering Research and Technology*, 1 : 1–10.

DRIOLI, E., CURCIO, E. & FONTANANOVA, E. 2006. *Mass Transfer Operation–Membrane Separations.* Eolss Publishers: Oxford, UK..

DURST, R. A. 1997. Chemically modified electrodes: recommended terminology and definitions (IUPAC Recommendations), *Journal of Pure and Applied Chemistry*, 69 (6) : 1317–1324.

EMEJI, I.C., AMA, O.M., OSIFO, O., RAY, S.S., GARCIA-RODRIGUEZ, O. AND LEFEBVRE, O. 2019. Electrochemical Preparation of Iron-Supported Carbon-Cloth Electrode and Its Application in the In-Situ Production of Hydrogen Peroxide, *International Journal of Electrochemical Science,* 14 : 9355–9368.

EIS03, A. A. N. (2011) 'Electrochemical Impedance Spectroscopy (EIS) Part 3–Data Analysis', *Metrohm Autolab BV.*

ELGRISHI, N., ROUNTREE, K. J., MCCARTHY, B. D., ROUNTREE, E. S., EISENHART, T. T., AND DEMPSEY, J. L. 2017. A 544 practical beginner's guide to cyclic voltammetry, *Journal of Chemical Education,* 95 (2) : 197–206.

FOWOWE, T. 2011. *Development of a 3-electrode system for Gas Phase Dynamic Electrochemistry*. University College London.

FICK, J., LINDBERG, R.H., TYSKLIND, M., HAEMIG, P.D., WALDENSTROM, J., WALLENSTEN, A. AND OLSEN, B. 2007. Antiviral oseltamivir is not removed or degraded in

normal sewage water treatment: implications for development of resistance by influenza A virus, *Plos One Journal*, 2 (10) : e986.

FISCHL, M.A., RICHMAN, D.D., GRIECO, M.H., GOTTLIEB, M.S., VOLBERDING, P.A., LASKIN, O.L., LEEDOM, J.M., GROOPMAN, J.E., MILDVAN, D., SCHOOLEY, R.T. AND JACKSON, G. G. 1987. The efficacy of azidothymidine (AZT) in the treatment of patients with AIDS and AIDS-related complex., *New England Journal of Medicine*, 317 (4) : 185–191.

INZELT, G. 2015. Crossing the bridge between thermodynamics and electrochemistry, From the 542 potential of the cell reaction to the electrode potential, *The Textbook Journal of Chemistrys*, 1 (1) : 2.

GONGADZE, E., PETERSEN, S., BECK, U. AND VAN RIENEN, U. 2009. Classical Models of the Interface between an Electrode and an Electrolyte, in *In COMSOL Conference*,: 14–16.

GUO, E. AND MCKENZIE, D. R. 2017. A post Gurney quantum mechanical perspective on the electrolysis of water: ion neutralization in solution.', in *Proceedings of the Royal Society A: Mathematical, Physical and Engineering Sciences*, 0371.

GRAY, F.N. 2002. Water Technology: An Introduction for Environmental Scientists and Engineers, *Butterworth-Heinemann. Oxford*, : 35–80.

GUNTHARD, H.F., SAAG, M.S., BENSON, C.A., DEL RIO, C., ERON, J.J., GALLANT, J.E., HOY, J.F., MUGAVERO, M.J., SAX, P.E., THOMPSON, M.A. AND GANDHI, R. T. 2016. Antiretroviral drugs for treatment and prevention of HIV infection in adults: 2016 recommendations of the International Antiviral Society–USA panel, *Journal of the American Medical Association*, 316 (2) : 191–210.

GÜNTHARD, H.F., SAAG, M.S., BENSON, C.A., DEL RIO, C., ERON, J.J., GALLANT, J.E., HOY, J.F., MUGAVERO, M.J., SAX, P.E., THOMPSON, M.A. AND GANDHI, R. T. 2016. Antiretroviral drugs for treatment and prevention of HIV infection in adults, *Journal of the American Medical Association*, 316 (2) : 191–210.

GUPTA, N., JANA, N. AND MAJUMDER, C. B. 2008. Submerged membrane bioreactor system for municipal wastewater treatment process: An overview, *Indian Journal of Chemical Technology,* 15 (6) : 604 – 612.

HAQUE, F., RAHMAN, M.S., AHMED, E., BAKSHI, P.K. AND SHAIKH, A. A. 2013. A cyclic voltammetric study of the redox reaction of Cu (II) in presence of ascorbic acid in different pH media, *Dhaka University Journal of Science*, 61 (2) : 161–166.

HISAINDEE, S., MEETANI, M.A. AND RAUF, M. A. 2013. Application of LC-MS to the analysis of advanced oxidation process (AOP) degradation of dye products and reaction mechanisms, *TrAC - Trends in Analytical Chemistry Journal*, 49 : 31 – 44.

HOLZE R. 2012. *Daniell cell, in Electrochemical dictionary*. 2nd edn. Edited by F. 540 A.J. Bard, G. Inzelt. Springer, Berlin.

KAZORA, A.S. AND MOURAD, K. A. 2018. Assessing the sustainability of decentralized wastewater treatment systems in Rwanda, *Sustainability Journal*, 10 (12) : 4617.

KOSAKA, K., YAMADA, H., SHISHIDA, K., ECHIGO, S., MINEAR, R.A., TSUNO, H. AND MATSUI, S. 2001. Evaluation of the treatment performance of a multistage ozone/hydrogen peroxide process by decomposition by-products, *Water Research Journal,* 35 (15).

KRISHNAN, S., RAWINDRAN, H., SINNATHAMBI, C.M. AND LIM, J. W. 2017. Comparison

of various advanced oxidation processes used in the remediation of industrial wastewater laden with recalcitrant pollutants. In IOP Conference Series, *Materials Science and Engineering*, 206 (1) : 012089.

KUMMERER, K. 2008. *Pharmaceuticals in the environment: sources, fate, effects and risks.* Springer Science & Business Media.

LAROSA, D.F. AND ORANGE, J. S. 2008. Lymphocytes, *Journal of Allergy and Clinical Immunology*, 121 (2) : S364–S369.

Lee, J. 2014. Electrochemical sensing of oxygen gas in ionic liquids on screen printed electrodes (Doctoral dissertation, Curtin University).

MARCUS, R. A. 1993. Electron transfer reactions in chemistry, Theory and experiment, *Reviews of Modern Physics*, 65 : 599–610.

MARTINSON, C.A., VAN SCHOOR, G., UREN, K.R. AND BESSARABOV, D. 2014. Characterisation of a PEM electrolyser using the current interrupt method, *International Journal of Hydrogen Energy*, 39 (36) : 20865–20878.

MOHAMMADA, S.G., ABULYAZIEDB, D.E. AND AHMEDB, S. M. 2019. Application of polyaniline/activated carbon nanocomposites derived from different agriculture wastes for the removal of Pb (II) from aqueous media, *Desalination and Water Treatment*, 170 : 199–210.

MANN, J. M. 1989. *AIDS: A worldwide pandemic, Current Topics in AIDS*. Edited by M. et al. Gottlieb. John Wiley & Sons.

MERT, B.K., OZENGIN, N., DOGAN, E.C. AND AYDINER, C. 2018. Efficient removal approach of micropollutants in Wastewater Using Membrane Bioreactor, *Wastewater and Water*

Quality,: 41-70.

MOMBA, M.N.B., OSODE, A.N. AND SIBEWU, M. 2006, The impact of inadequate wastewater treatment on the receiving water bodies–Case study: Buffalo City and Nkokonbe Municipalities of the Eastern Cape Province, *Water S.A. Journal*, 32 (5).

NAIMI, I. & B. N. 2012. Removal of 17β-Estradiol by Electro-Fenton Process, *Journal of Materials Sciences and Applications*, 3 : 880–886.

NICHOLSON, R.S. 1965. Theory and application of cyclic voltammetry for measurement of electrode reaction kinetics, *Journal of Analytical Chemistry*, 37 (11) : 1351–1355.

NICHOLSON, R.S. AND SHAIN, I. 1965.Theory of Stationary Electrode Polarography for a Chemical Reaction Coupled between Two Charge Transfers, *Journal of Analytical Chemistry*, 37 (2) : 178–190.

OON, H. L. 2007. *A simple electric cell, Chemistry Expression: An Inquiry Approach. Panpac Education Pte Ltd: Singapore,*.

PATEL, P.S., BANDRE, N., SARAF, A. AND RUPARELIA, J. P. 2013. Electro-catalytic materials (electrode materials) in electrochemical wastewater treatment, *Procedia Engineering*, 51 : 430–435.

PANIZZA, M. AND OTURAN, M. A. 2011. Degradation of Alizarin Red by electro-Fenton process using a graphite-felt cathode, *Electrochimica Acta*, 56 (20) : 7084–7087.

PERALTA-HERNANDEZ, J.M. AND GODINEZ, L. A. 2014. Electrochemical hydrogen peroxide production in acidic medium using a tubular photo-reactor: Application in advanced oxidation processes., *Journal of The Mexican Chemical Society*, 58 (3) : 348–355.

PERALTA, E., NATIVIDAD, R., ROA, G., MARIN, R., ROMERO, R., AND PAVON, T. 2013. A comparative study on the electrochemical production of H_2O_2 between BDD and graphite cathodes., *Sustainable Environment Research Journal*, 23 (4) : 259–66.

PEREIRA, B.G., FONTE-BOA, F.D., RESENDE, J.A., PINHEIRO, C.B., FERNANDES, N.G., YOSHIDA, M.I. AND VIANNA-SOARES, C. D. 2007. Pseudopolymorphs and intrinsic dissolution of nevirapine., *Journal of Crystal Growth and Design*, 7 (10) : 2016–2023.

PRASSE, C., SCHLUSENER, M.P., SCHULZ, R. AND TERNES, T. A. 2010. Antiviral drugs in wastewater and surface waters: a new pharmaceutical class of environmental relevance., *Journal of Environmental Science and Technology*, 44 (5) : 1728–1735.

PENG, H., YAO, B., WEI, X., LIU, T., KOU, T., XIAO, P., ZHANG, Y. AND LI, Y. 2019. Pore and heteroatom engineered carbon foams for supercapacitors, *Advanced Energy Materials*, 9 (19) : 1803665.

PLETCHER, D., GREEN, R.A. AND BROWN, R. C. 2017. Flow electrolysis cells for the synthetic organic chemistry laboratory., *Journal of Chemical Reviews*, 118 (9) : 4573–4591.

QUERCIA, R., PRNO, C.F., KOTEFF, J., MOORE, K., MCCOIG, C., CLAIR, M.S. AND KURITZKES, D. 1999. Twenty-Five Years of Lamivudine: Current and Future Use for the Treatment of HIV-1 Infection., *Journal of Acquired Immune Deficiency Syndromes*, 78 (2) : 125.

RAJASULOCHANA, P. AND PREETHY, V. 2016. Comparison on efficiency of various techniques in treatment of waste and sewage water–A comprehensive review., *Resource-Efficient Technologies Journal*, 2 (4) : 175–184.

RANGANATHAN, S. AND SIEBER, V. 2018. Recent Advances in the Direct Synthesis of

Hydrogen Peroxide Using Chemical Catalysis—A Review., *Catalysts Journal*, 8 (9) : 379.

ROSALES, E., PAZOS, M. AND SANROMAN, M.A. 2012. Advances in the electro-Fenton process for remediation of recalcitrant organic compounds., *Journal of Chemical Engineering & Technology*, 35 (4) : 609–617.

SABER, S., HOSSEINI NAROUEI, F., NOROOZIFAR, M. AND SABBAGHI, N. (2016) 'Detection of Ascorbic Acid in Biological Samples by a New Modified Glassy Carbon Electrode., *Biomacromolecular Journal*, 2 (2) : 108–117.

SCHOEMAN, C., MASHIANE, M., DLAMINI, M. AND OKONKWO, O. J. 2015. Quantification of selected antiretroviral drugs in a wastewater treatment works in South Africa using GC-TOFMS., *Journal of Chromatography & Separation Techniques*, 6 (4) : 1.

SIDDIQUI, W.A. AND WASEEM, M. 2012. A comparative study of sugar mill treated and untreated effluent—a case study', *Oriental Journal of Chemistry*, 28 (4) : 1899–1904.

SWAIN, G. 1994. The Use of CVD Diamond Thin-Films in Electrochemical Systems, *Advanced Materials*, 6 : 388–392.

TIAN, M., COUSINS, C., BEAUCHEMIN, D., FURUYA, Y., OHMA, A. AND JERKIEWICZ, G. 2016. Influence of the working and counter electrode surface area ratios on the dissolution of platinum under electrochemical conditions., *ACS Catalysis*, 6 (8) : 5108–5116.

TANG, S., LU, N., SHANG, K., LI, J. AND WU, Y. 2013. Detection of hydroxyl radicals during regeneration of granular activated carbon in dielectric barrier discharge plasma system., *Journal of Physics: Conference Series*, 418 (1) : 012104.

TCHOBANOGLUS, G., BURTON, F. AND STENSEL, H. D. 2003. Wastewater engineering:

Treatment and reuse., *Journal of the American Water Works Association*, 95 (5) : 201.

TONWE-GOLD, B., EKOUEVI, D.K., VIHO, I., AMANI-BOSSE, C., TOURE, S., COFFIE, P.A., ROUET, F., BECQUET, R., LEROY, V., EL-SADR, W.M. AND ABRAMS, E. J. (2007). Antiretroviral treatment and prevention of peripartum and postnatal HIV transmission in West Africa: evaluation of a two-tiered approach., *Plos Medicine Journal*, 4 (8) : e257.

TRO, N.J., 2018. Chemistry in focus: A molecular view of our world. Cengage Learning.

UNAIDS DATA. 2018. Global HIV & AIDS statistics — Fact sheet

VANKOVA, M. 2010. *Biodegradability analysis of pharmaceuticals used in developing countries; screening with OxiTop C-110*. Tampere University of Technology, Finland.

WANG, D., ZHANG, Y., LU, X., MA, Z., XIE, C. AND ZHENG, Z. 2018. Chemical formation of soft metal electrodes for flexible and wearable electronics., *Journal of Chemical Society Reviews*, 47 (12) : 4611–4641.

WOOD, T.P., DUVENAGE, C.S. AND ROHWER, E. 2015. The occurrence of anti-retroviral compounds used for HIV treatment in South African surface water., *Environmental Pollution Journal*, 199 : 235–243.

WATTS, K., BAKER, A. AND WIRTH, T. 2015. Electrochemical synthesis in microreactors., *Journal of Flow Chemistry*, 4 (1) : 2–11.

WEAST, R. C. (1989) *Handbook of chemical physics*.

YANG, Y., CHIANG, K. AND BURKE, N. 2011. Porous carbon-supported catalysts for energy and environmental applications: A short review., *Catalysis Today*, 178 (1) : 197–205.

YING, R., GRANICH, R.M., GUPTA, S. AND WILLIAMS, B. G. 2016. CD4 cell count: declining value for antiretroviral therapy eligibility., *Journal of clinical infectious diseases*, 62 (8) : 1022–1028.

YU, X., ZHOU, M., HU, Y., SERRANO, K.G. AND YU, F. 2014. Recent updates on electrochemical degradation of bio-refractory organic pollutants using BDD anode: a mini review., *Environmental Science and Pollution Research*, 21 : 8417–8431.

Chapter 3: Materials and Methods

Materials and methods used during the preparation of the supported CC electrode and the testing of the synthesized iron-supported carbon-cloth electrode on industrial wastewater with a focus on antiretroviral wastewater are discussed in this chapter. The material section highlighted sources of all reagents and equipment used for the electro-Fenton treatment process. On the other hand, the methodology gave an insight on electrode preparation and shows exactly how the active iron salts precursor was impregnated to the CC electrode to acquire the desired modified electrode. The procedure of electrode tested, sample collection, and characterization was also reported.

3.1 Materials and Apparatus

Materials used in this research are:

- Potassium sulfate (K_2SO_4)
- Sulphuric acid (H_2SO_4)
- Iron (II) sulfate heptahydrate ($FeSO_4 \cdot 7H_2O$)
- Titanium (IV) oxy-sulfate ($TiOSO_4$, 15 wt. % in dilute sulphuric acid and purity of 99.99% trace metals basis)
- All chemicals were purchased from Sigma-Aldrich, South Africa, and are used as they were received without further purification. All reagents used were prepared with high purity water (Millipore Milli-Q, 18 Mcm).

- Stainless steel wire was purchased from Nemtek, South Africa. AGA, South Africa supplied oxygen and nitrogen gasses. Hailea ACO-2204 air-pump, HM8040-3 triple-power supplier, and beakers were also purchased in South Africa.
- The Carbon-cloth electrode was purchased from Fuel Cell Earth, Massachusetts, United States. Boron doped diamond (BDD) electrode was purchased from CONDIAS GmbH, Germany. Platinum electrode and Silver/silver chloride (Ag/AgCl) electrode was purchased from china.
- UV–vis spectrophotometer (Perkin Elmer model Lambda 35) was used to measure the absorbance. An Autolab potentiostat galvanostatic (PGSTAT) was employed during electrode conductivity text, iron reduction potential experiment, electrodeposition, and degradation process.
- The characterizations of the bare and modified CC electrode were carried out using the following techniques: scanning electron microscopy (SEM), energy-dispersive x-ray spectroscopy (EDX), and x-ray photoelectron spectroscopy (XPS) microanalysis.

3.2 Methods

3.2.1 Conductivity measurement using Linear Sweep Voltammetry (LSV)

A conductivity experiment for the carbonaceous electrode was done in a typical three-electrode electrochemical cell consisting of bare CC electrode (12.5 cm^2) as the working electrode (WE), platinum wire and Ag/AgCl as the counter electrode (CE) and a reference electrode (RE), respectively. Cell-connecting cables with crocodile clips were used to clip the heads of the

electrodes (WE, CE, and RE) and the other side connected to the Autolab PGSTAT. LSV measurement was carried out at room temperature in 50 mM K_2SO_4 electrolytic solution at a pH of 3.The first LSV scan was carried out in electrolyte enriched with O_2/air for 35 minutes; the second linear sweep was carried in deoxygenated electrolyte achieved by pumping N_2 gas into the solution for 35 minutes. This was very necessary to confirm if the material has large surface area with high porosity for surface adsorption of micro-pollutant. The LSV scan tested the electrode for 300 seconds (5minutes), using an electrochemical potential range of -1.5 V ≦ E≦ 1.00 V at a scan rate of 0.05 V/s.

3.2.2 Iron Reduction Potential measurement using Cyclic Voltammetry (CV)

The iron reduction potential experiment was also performed using a typical three-electrode electrochemical cell (Figure 3.1) consisting of bare CC electrode (12.5 cm^2) as the working electrode (WE), platinum wire, and Ag/AgCl as the counter electrode (CE) and a reference electrode (RE), respectively. Through the Teflon-cap of the cell cover, two tiny stainless-steel wires were used to hold the CC-working electrode and the platinum counter electrode firmly. Connecting cell cables with three crocodile clip heads were used to hold the heads of WE, CE, and RE with the other end connected to the Autolab PGSTAT. CV measurements were performed at room temperature in 50mM K_2SO_4 solution at a pH of 3 containing 0.1 M 100 ml $FeSO_4.7H_2O$. The electrolyte was only enriched with N_2 gas for 35 min before the experiment.

Iron electrodeposition on CC electrode was optimsed using the following CV potential ranges -0.8 V ≦ E≦ 1.00 V; -1.3 V ≦ E ≦1.00 V and -1.8 V to 1 V; for 180 seconds and a scan rate of

0.05 V/S. When adding the electrolyte into the cell, it was done utilizing a thistle funnel, in such a way that the WE was completely immersed in the solution.

3.2.3 Preparation of Iron-Supported CC Electrode by Electrodeposition

Reagent grade iron (II) sulfate heptahydrate ($FeSO_4.7H_2O$) was used to prepare 0.1 M 100 mL iron (II) sulfate solution using 50 mM, N_2-gas enriched K_2SO_4 electrolyte at a pH of 3.0. The electrochemical setup for electrodeposition was a standard three-electrode cell (Figure 3.1) with 12.5 cm^2 carbon cloth as the working electrode, platinum as the counter electrode, and silver-silver chloride as the reference electrode. Two stainless steel wires passing through two separate smallest holes on the cell cover were used to hold WE and the CE externally. Through another hole on the cell cover, closer to the WE, Ag/AgCl reference electrode (RE) was inserted, and utilizing a thistle funnel, about 10 ml of the prepared iron (II) solutions were poured into the cell. The electrodeposition of iron on the surface of the electrode was performed using chronoamperometry techniques of Autolab PGSTAT 302F. Iron particles were deposited by cyclic sweeping from -1.8 to 1 V and back at 0.05V/s for 90 cycles in an N_2-enriched working solution containing 0.1M $FeSO_4.7H_2O$ and 50 mM (millimole) of K_2SO_4 at a pH of 3. To load different amount of iron on the electrode surface, 0.01M, 0.001M and 0.0001M of Iron (II) sulfate heptahydrate in 100ml of solution were prepared using 50 mM, N_2-gas enriched K_2SO_4 electrolyte at a pH of 3.0.

The modified electrodes were rinsed with high purity water and air-dried, after which they were characterized using SEM analysis, EDX analysis, and XPS analysis.

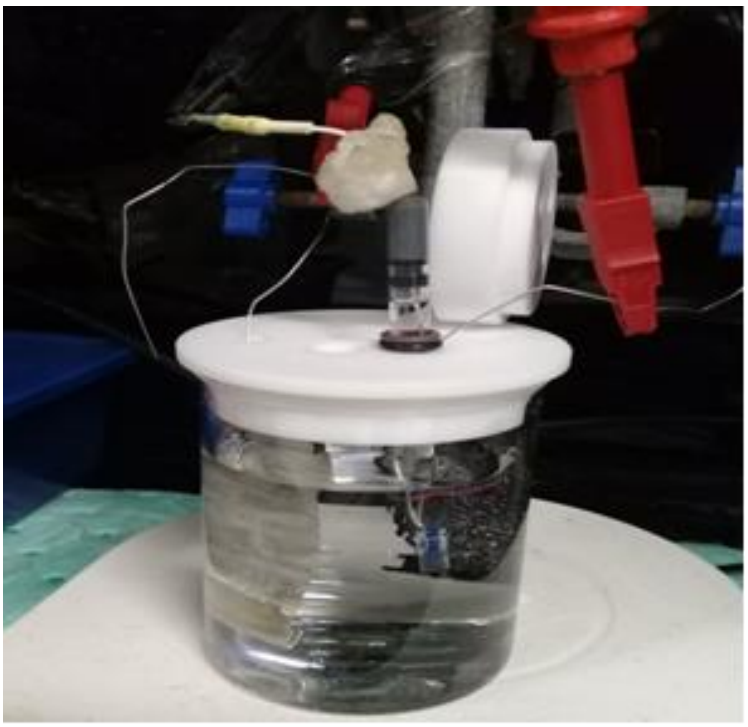

Figure 3.1: Standard three-electrode electrochemical cell containing 2.78g $FeSO_4.7H_2O$ in 50 mM, N_2-gas enriched K_2SO_4 electrolyte at a pH of 3.0

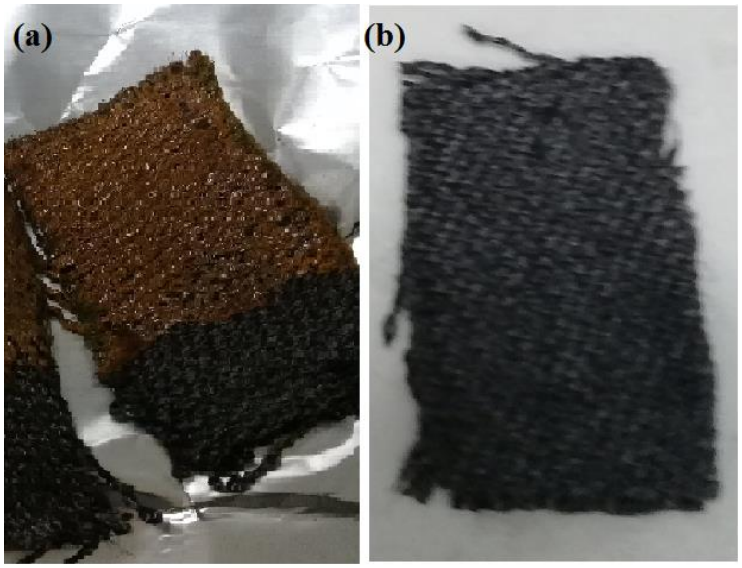

Figure 3.2: Photo image of (a) modified iron-supported carbon-cloth electrode (b) bare carbon-cloth electrode

3.3 Characterization of the electrode

Figure 3.2 presents the image of the synthesized iron-supported carbon cloth electrode and bare carbon cloth electrode. These electrodes were characterized using methods presented in the subsection of 4.3 below.

3.3.1 SEM, EDX, XPS analysis, and electrochemical measurements.

To depict the surface morphology of the material after iron electrodeposition, the electrodes were characterized. Scanning electron microscopy (SEM) and energy-dispersive X-ray spectroscopy (EDX) analyses were done on a gold plate with an application of 20 KV electron acceleration voltages using JEOL-733 super probe equipment. The X-ray photoelectron spectroscopy (XPS) spectrum was obtained on a Thermo ESCALAB system which uses AXIS SUPRA for data acquisition (Shimadzu Inc., Kyoto, Japan). Further characterization was evaluated using electrochemical experiments with Autolab PGSTAT-307, in a typical three-electrode system, with silver-silver chloride (Ag/AgCl) serving as the reference electrode, BDD as the counter electrode and bare or modified CC electrode as the working electrode. The electrochemical techniques used for characterization were cyclic Voltammetry (CV) and Electrochemical impedance spectroscopy (EIS) with a working electrolytic solution of 50 mM

(millimole) of K_2SO_4 at a pH of 3 enriched with O_2-gas for 35 min before the experiment at room temperature

3.4 Evaluation of "*in-situ*" generated H_2O_2 using the electrolysis method

The electrolysis experiment enables the determination of the maximum concentration of H_2O_2 electro-generation within the system. It also enables current to be optimized at maximum peroxide concentration. The H_2O_2 electro-generation experiment was performed in an undivided glass cell of 250 ml capacity using an air pump and HM8040-3 triple-power supply. The modified iron-supported CC electrode (2.5 cm x 5 cm) was selected as the cathode and a platinum wire was employed as the anode. Using stainless-steel wire, the electrodes were held firmly in such a manner that they were 2 cm from the bottom of the glass cell and 2 cm from one another. Before the electrolysis experiment, compressed air (oxygen) was used to saturate 0.05M K_2SO_4 aqueous electrolyte using the air pump for about 35 minutes. By transferring the aeration-tube near the cathodic surface, an essential amount of oxygen was supplied for the electrochemical reactions; electrolyte oxygenation was maintained with a constant magnetic stirrer of 400 rpm. Oxygen was reduced by applying a constant electric current (I) of 0.1A on the surface of the working electrode for 60 minutes. Sampling was done every 10 minutes utilizing an Eppendorf micro-pipette. The concentration of H_2O_2 electro-generated during the process (C) was quantified by photoelectric measurement, measuring the absorbance of the color complex intensity of hydrogen peroxide solution treated with titanium oxy-sulfate at a wavelength of 405 nm using a UV-Vis spectrophotometer (García-Rodríguez *et al.*, 2016; Eisenberg, 1943). Hence,

0.5 ml of working solution was introduced into a sample bottle where 0.5 ml $TiOSO_4$ and 4 ml of deionized water were added to obtain a total of 5 ml sampling solution whose absorbance was obtained at a wavelength of 405 nm. Different synthesized CC electrode with different iron concentration were used to generate in-situ H_2O_2, for optimum performance

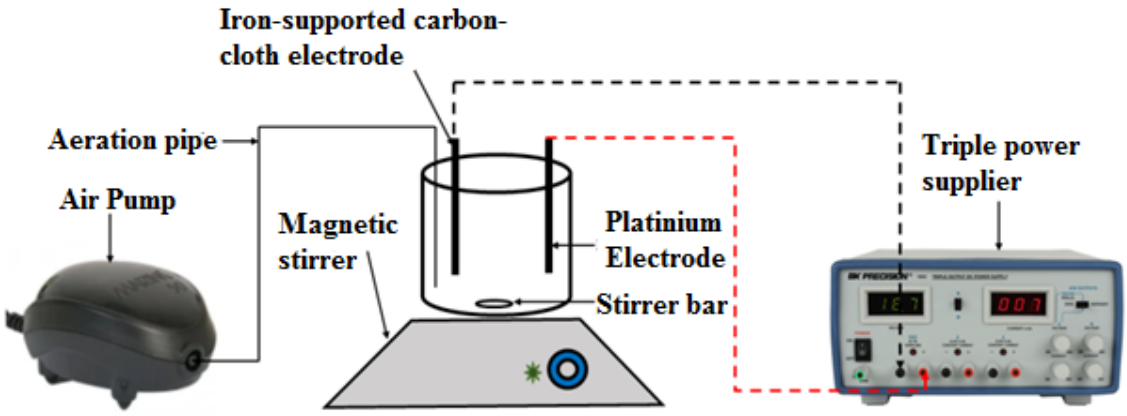

Figure 3.3: Setup used for the "*in-situ*" generation of hydrogen peroxide (H_2O_2).

3.5 Preparation of standard stock solution

A standard stock solution of nevirapine (NVP), lamivudine (LVD), and zidovudine (ZVD) were prepared by transferring 100 mg (0.1 g) of accurately weighed powdered pure samples into 100ml volumetric flask. 60 ml of methanol was poured into the flask and manually shaken for 5 minutes to dissolve the powder. The volumetric flask was made up to the mark with 40 ml of deionized water to obtain a final strength of 1mg/ml (1000 µg/ml = 1000 mg/L) of Nevirapine, lamivudine, and zidovudine separately.

3.5.1 Selection of sample wavelength

Sample wavelength for NVP, LVD, and ZVD were determined by scanning two milliliters (2 ml) of stock solutions from 50 – 300 nm range using UV-vis spectrophotometer and their obtained UV spectra recorded. From this stock solution, working standard solutions were prepared for calibration by the dilution process. This involves adding defined volumes of the stock standard solutions into 100 ml flask and toping-up the volume mark with deionized water to obtain concentrations of 5.0, 10.0, 15.0, 18.0, 20.0 $\mu g \cdot mL^{-1}$ respectively for NVP, LVD, and ZVD.

3.5.2 Preparation of Synthetic Wastewater for degradation.

The working solution for the degradation process was prepared using the appropriate dilution process. Two milliliters (2 ml) of the stock solution was transferred into a 100 ml volumetric flask containing 0.8713 g of K_2SO_4 supporting electrolyte (50 mM). The volumetric flask was then made up to the mark with deionized water and sonicated for 30 minutes. Supporting electrolytes was used in all experiments to increase the conductivity of the antiretroviral solution. Concentrated sulfuric acid was then added to reduce the pH of the resulting solution to 3.0.

3.6 Electrochemical degradation experiments.

The degradation experiments were carried out at room temperature in an undivided, magnetically stirred electrochemical glass cell with a working volume of 100 ml. The prepared synthetic ARVDs wastewater solution of 20 mg/L at a pH of 3, was transferred into the electrochemical

cell containing iron supported or bare CC electrode as the cathode electrode, and a 24 cm^2 thin-film BDD as the anode. The BDD-anode was clamped in the middle of the cell, and a distance 2 cm from the cathode. The crocodile clips were used to clip the head of the cathode and anode while connecting the other end to Autolab PGSTAT-204. For two-electrode setup using PGSTAT, CE, and RE are joined together to serves as an anode, while sense (S) and WE joined together became the cathode (EC08, 2011). The air pump was used to saturate the electrolyte with oxygen (O_2) for about 35 minutes before the experiment and continue thereafter during the electrolysis process. Oxygenation is maintained throughout to ensure continuous saturation of the wastewater with oxygen. A magnetic stirrer apparatus with an agitation speed of 400 rpm was used to completely ensure homogenous conditions in the reactor. Degradation reaction was initiated by selecting a chronoamperometric method for 3 and a half hour, with a voltage range of -0.5 to 0.5 V and a constant current condition of 0.025A. All the experiments were repeated three times, as aliquot is taken every 40 minutes. Antiretroviral drug residues were analyzed using UV-vis spectrophotometer according to the method recently reported by Kumar *et al.* (Kumar *et al.,* 2014). Also according to Youssef *et al*. 2016, the degradation removal efficiency was calculated using:

$$\text{Removal efficiency \%} = \left(1 - \frac{C_t}{C_0}\right) X\ 100 \qquad (3.1)$$

Where C_t and C_0 are the concentration of the antiretrovirals at reaction time = t and time = 0, respectively.

3.7 Electrochemical Regeneration.

For reusability and stability study, the catalytic efficiency of the synthesized electrode was measured for five cycles using the same protocol as in the degradation experiment of section 3.6. After initially using the Fe/CC electrode in the electrochemical cell filled with the micro-pollutant, the first degradation cycle was initiated for 210 minutes. After the first degradation cycle, the spent electrode was separated, rinsed with high purity water and oven dry for 70 ^{O}C. It was then used for the next degradation cycle consecutively until five cycles.

REFERENCES

EC08, A. A. N. 2011. Basic overview of the working principle of a potentiostat/galvanostat (PGSTAT)–Electrochemical cell setup, *Metrohm Autolab. BV*, : 1–3

EISENBERG, G. M. 1943. Colorimetric determination of hydrogen peroxide., *Industrial & Engineering Chemistry Analytical Edition*, 15 (5) : 327-328

GARCÍA-RODRÍGUEZ, O., BAÑUELOS, J.A., RICO-ZAVALA, A., GODÍNEZ, L.A., AND RODRÍGUEZ-VALADEZ, F. J. 2016. Electrocatalytic activity of three carbon materials for the in-situ production of hydrogen peroxide and its application to the electro-fenton heterogeneous process, *International Journal of Chemical Reactor Engineering*, 14 (4) : 843–850.

KUMAR, P.P., SHIVA, P.V., KUMAR, K.S., AND KULKARNI, R. M. 2014. The fate of Zidovudine through Water Treatment with Chlorine: A Kinetic Study, *International Research Journal of Environment Sciences*, 3 (9) : 50–55

YOUSSEF, N.A., SHABAN, S.A., IBRAHIM, F.A. AND MAHMOUD, A.S. 2016. Degradation of methyl orange using Fenton catalytic reaction. *Egyptian Journal of Petroleum*, 25 (3) : 317-321

Chapter 4: Electrochemical Preparation of Iron-Supported Carbon-Cloth Electrode and Its Application in the In-Situ Production of Hydrogen Peroxide

4.1 Introduction

Hydrogen peroxide (H_2O_2) is an ecologically benign oxidant and one of those chemicals used in advanced oxidation processes (AOPs) for water and sewage decontamination (Čolić *et al.*, 2018). The use of H_2O_2 has offered an efficient alternative for the obliteration of organic and inorganic contaminants in aqueous media. Although hydrogen peroxide is profitably produced on a commercial scale by anthraquinone process, the process is rigorous and generates a significant volume of liquid wastes. Besides, the product must be handled and transported to the worksite, posing a safety risk. Therefore, hydrogen peroxide produced using this technique, encompasses a significant environmental influence, which is in contrast to green chemistry principles (Goti and Cardona, 2018). As a result, a replacement for H_2O_2 production follows the pathway of two-electron oxygen reduction reaction (ORR) in acidic, basic, or neutral media as shown in Equation 4.1 and 4.2 (Jiao-jiao *et al.*, 2018; Zhou *et al.*, 2018). ORR can also occur by a direct process called 4e− process as depicted in Equations 5.3 and 5.4 (Zhou *et al.*, 2018). Hence, the on-site generation of sustainable hydrogen peroxide requires the operations of air (oxygen), water, and electricity, which could be provided from renewable sources.

Generally, the use of Fenton's reagent in recent times, as an oxidative degradation tool is very attractive because iron is a non-toxic element and easily available. Besides, H_2O_2 breaks down to environmentally harmless products of hydrogen and water (equation 5.5) (Foustoukos *et al.*, 2011; Pouran *et al.*, 2015). However, homogeneous Fenton technology has its limitations, in the massive ferric-hydroxide sludge formation (Pouran *et al.*, 2015) at pH greater than 4.0 and the complication arising from the transportation, handling, and storage of H_2O_2 (Qiu *et al.*, 2015). To overcome these limitations to some extent, heterogeneous catalysts are used. Hence, in a heterogeneous Fenton process, iron is fixed or immobilized within the catalyst structure and reaction occurs on the surface interfaces of the solid catalyst-electrode and the conducting solution. Therefore, an apparent adsorption and diffusion process of H_2O_2 on the surface of the electrode enhances catalytic reaction (Zhang *et al.*, 2015). Punzi and co-workers, in 2012, also reported that the slower step of the heterogeneous catalytic system, as compared to their homogeneous counterpart, could be as a result of an electrodeposited small fraction of iron on the surface of the catalyst.

$$O_2\,(g) + 2H^+ + 2e^- \longrightarrow H_2O_2\ (\text{acidic}) \qquad (4.1)$$

$$O_2\,(g) + 2H_2O + 2e^- \longrightarrow H_2O_2 + 2OH^{\bullet}\ (\text{basic}) \qquad (4.2)$$

$$O_2\,(g) + 4H^+ + 4e^- \longrightarrow 2H_2O\ (\text{acidic}) \qquad (4.3)$$

$$2O_2\,(g) + 4H^+ + 4e^- \longrightarrow 4\,OH^{\bullet}\ (\text{basic}) \qquad (4.4)$$

$$2H_2O_2 \longrightarrow O_2 + 2H_2O \qquad (4.5)$$

$$Fe^{2+} + H_2O_2 \longrightarrow Fe^{3+} + OH^- + OH^{\bullet} \qquad (4.6)$$

$$\text{Organics} + OH^{\bullet} \longrightarrow \text{Oxidation intermediates} + CO_2 + H_2O \qquad (4.7)$$

Several authors such as Peralta-Hernández *et al.* 2008, Martínez-Huitle and Brillas 2009, and others, have demonstrated that "*in-situ"* electro-generated H_2O_2 can be used successfully to separate micro-pollutants from water effluents contaminated with different organic compounds in an aqueous or a non-aqueous medium.

The principle of decontamination, however, is initiated through Fenton reaction (Equation 4.6) (Pouran *et al.,* 2015; Heidari *et al.,* 2015), as "*in-situ"* electrochemical generated peroxide reacts with ferrous ions (Fe^{2+}) to produce hydroxyl radicals ($OH^{\bullet}$) which can efficiently mineralize recalcitrant organic micro-pollutants contained in wastewater as shown by Equation 4.7 (Zhang, 2021). This technique, frequently called electro-Fenton (EF) is an advanced oxidation process (AOP) because of the creation of active hydroxyl radicals ($OH^{\bullet}$) a very strong reactive oxidant with high oxidation potentials of 2.8 V. The use of carbonaceous materials as electrode materials are found to catalyze oxygen reduction reaction (ORR) selectively by two electrons using appropriate cathodic potential, in an electrolytic solution enriched with oxygen forming hydrogen peroxide. Apart from electrode materials, another inhibiting consideration in the capability of hydrogen peroxide production through ORR is the high insolubility of oxygen in water at room temperature. Hence, the use of gas diffusion electrode (GDE) overcomes the high insolubility of oxygen, which causes mass transfer limitations at the cathode surface. Carbon-based materials such as glassy carbon modified with palladium nanoparticles (Kitte *et al.,* 2013), activated carbon (Zhou *et al.,* 2019), carbon nanotubes (CNTs) (Lu *et al.,* 2018), and nitrogen-doped mesoporous carbon (Sun *et al.,* 2018), have shown great promise as alternative catalysts for the electrochemical production of hydrogen peroxide. Despite progress in the synthesis of carbon-based electrodes, there is still room for improvement in modifying and

developing carbon-based substances for "*in-situ"* production of hydrogen peroxide. In this study, we analyzed the electrocatalytic activity and selectivity of carbon-cloth and iron supported carbon-cloth electrode toward *"in-situ"* production of H_2O_2 using surface oxidation.

4.2 Materials and Methods

4.3 Materials and Apparatus

The described materials and apparatus under section 3.1 of chapter 3 were also used in this chapter.

4.3.1 Linear Sweep Voltammetry (LSV) Measurement for ORR

The linear sweep voltammetry measurement was achieved by following the same procedure as described under section 3.2.1.

4.3.2 Evaluation of Iron Reduction Potential through Cyclic Voltammetry (CV) Measurement

The procedure to determine the iron reduction potential measurement through cyclic voltammetry follows that described under section 3.2.2

4.3.3 Preparation of Iron-Supported CC Electrode by Electrodeposition

A similar approach as explained under section 3.2.3 above were followed for the preparation of composite Fe-supported-CC electrode through chronoamperometry method

4.3.4 "*In-situ"* electrochemical generation of H_2O_2

Using the same procedural method given under section 3.2.3, "in-situ" electrochemical generation of H_2O_2 was quantified.

The current efficiency (CE) for H_2O_2 generation was calculated with the formula depicted in Equation 4.8 (Qiang *et al.*, 2002; Yu *et al.*, 2015).

$$CE = \frac{2FCV}{\int_0^t Idt} \times 100\% \quad (4.8)$$

Where F is the Faraday constant, equal to 96500 C/mol, C is the concentration of H_2O_2 in mol/L, V is the solution volume (L), I is the applied current (A), and t is the production time (s). The electric energy consumption (EEC) (kWh/m^3) was calculated using the expression in Equation 4.9 (Yu *et al*., 2015).

$$EEC = \frac{UIt}{V} \tag{4.9}$$

Where U represents the applied voltage (V), I the current (A), t the treatment time (h) and V is the solution volume (m^3)

4.4 Result and Discussion

4.4.1 Characterization Result

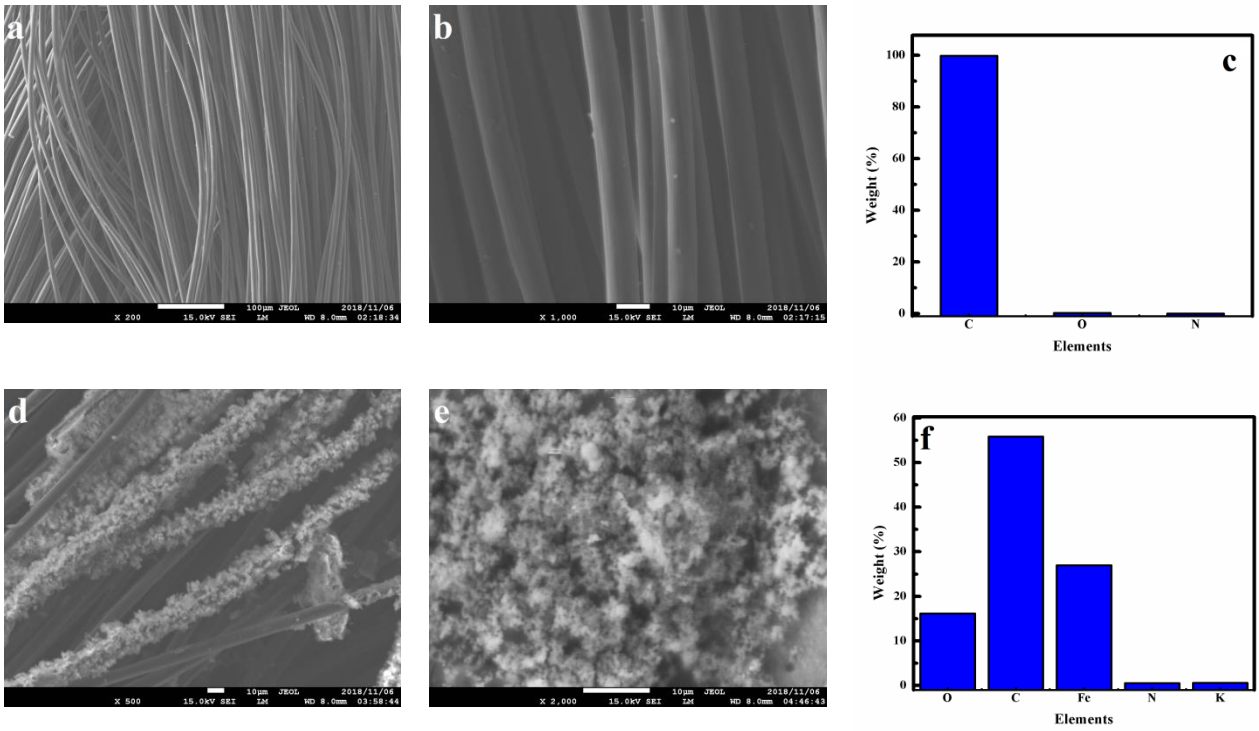

Figure 4.1: (a) SEM of bare-CC electrode, (b) SEM of bare-CC electrode showing lumps as impurities, (c) EDX of bare-CC electrode, (d) SEM of iron-supported CC electrode, not completely covered, (e) SEM of iron-supported CC electrode, uniformly covered, and (f) EDX of iron-supported CC electrode

Iron deposition on the surface of the electrode was performed by applying a constant potential of -1.8 V to 1 V vs Ag/AgCl for 40 minutes. During this process, some bubbles were observed moving from the platinum electrode toward the carbon cloth electrode. After sometime, the

solution changes its color to yellow colouration. Once electrodeposition stops, the CC working electrode was removed, rinsed inside a beaker of distilled water to remove any surface impurities, oven dried at 70 ^{o}C for 2 hours and stored for characterisation. Using SEM analysis, the morphological characteristics of the electrode prepared using 0.1M $FeSO_4.7H_2O$; 50 mM (millimole) of K_2SO_4 at a pH of 3 and the bare electrode were inspected as depicted in Figure 4.1 (a, b, d, and e). This is because the electrode prepared by 0.1M $FeSO_4.7H_2O$, were found to give higher organics removal efficiency as expressed in section 5.4.9. Figure 4.1a shows that the untreated bare-CC electrode had a porous structure with overlapping carbon fibers. The carbon fibers have a very smooth surface with irregular small lumps attached to it, as shown in Figure 4.1b.

These attachments may have been some contaminant and could be removed through pre-treatment with acid and alkali. Figures 4.1d and 4.1e shows that after electrodeposition, iron particles were deposited and well dispersed on the surface of the CC electrode, making their surface rough. This means that the CC electrode has high porosity and consequently, good adsorption capacity. As shown in Figure 4.1d, the iron deposit was not completely uniform as observed in some places of the bare carbon-cloth electrode. However, in Figure 4.1e, the coverage was uniform over the carbon cloth lattice. This structure was expected to help enhance electrochemical activity and the mass-transfer process of ORR by $2e^-$, leading to the *"in-situ"* generation of H_2O_2. The EDX result as shown in Figure 4.1(c & f) and Table 4.1, confirms the elemental composition of the electrode surface. Based on the result, the presence of C, O, and N was confirmed on the bare CC electrode. Besides, the presence of different weight % of Fe was confirmed in the structure of the modified electrode.

Table 4.1: EDX result of bare and iron-supported CC electrode

Samples	Weight %				
	Carbon	Oxygen	Nitrogen	Potassium	Iron
Fe / CC Electrode	55.79	16.14	0.53	0.58	26.96
Bare Electrode	99.74	0.22	0.04		

Based on the EDX results, the magnitudes of nitrogen-to-carbon (N/C) and oxygen-to-carbon (O/C) ratios were calculated to be 0.009% and 0.29% after electrodeposition on the surface of the electrode. The calculated result shows that the resultant modified electrode has high oxygen content as compared to nitrogen, which confirmed the adsorption of iron onto the CC electrode surface after electrodeposition.

Another surface analysis that determines the atomic composition of the electrode was X-ray photoelectron spectroscopy (XPS) analysis as shown in Figure 4.2. It can be seen from Figure 4.2a, that the bare-CC electrode has three detectable peaks: one at 284.3 eV, which corresponds to carbon C1s, another at 532.1 eV corresponding to oxygen O1s and the last at 400.7 eV corresponding to nitrogen N1s. The modified electrode presented an extra peak at 711.3 eV, corresponding to the iron Fe2p3 particles and 377.8 eV corresponding to the potassium K2s. For the coated CC electrode, a high-resolution XPS spectrum of O1s shows the presence of an additional functional group of O1s (metal oxide) (530.1 eV) and O1s (organic C-

O) (531.6 eV). However, oxygen-based functional groups in carbon materials serves as an active sites for adsorbing dissolved oxygen molecules and converting them to hydrogen peroxide via a two-electron oxygen reduction process (ORR).

Therefore, the existence of these oxygen-containing functional groups in the carbon-cloth electrode provided more active sites, which enhances the catalytic activity for the promotion and generation of H_2O_2. This result agrees with Zhong *et al.* 2018, who demonstrated that the surface reduction/modification of carbon support produces more active and anchor sites for the enhancement of ORR catalytic activities. Also, agreeing with this assertion is Ananth and co-workers (2009), who reported that the protection of crystalline structures and the presence of additional surface oxygen-containing functional groups improve ORR activity. On the other hand, bare cc electrode contains very low oxygen functional group (Figure 4.2a) which cannot generate sufficiently needed in-situ hydrogen peroxide for catalytic Fenton reaction.

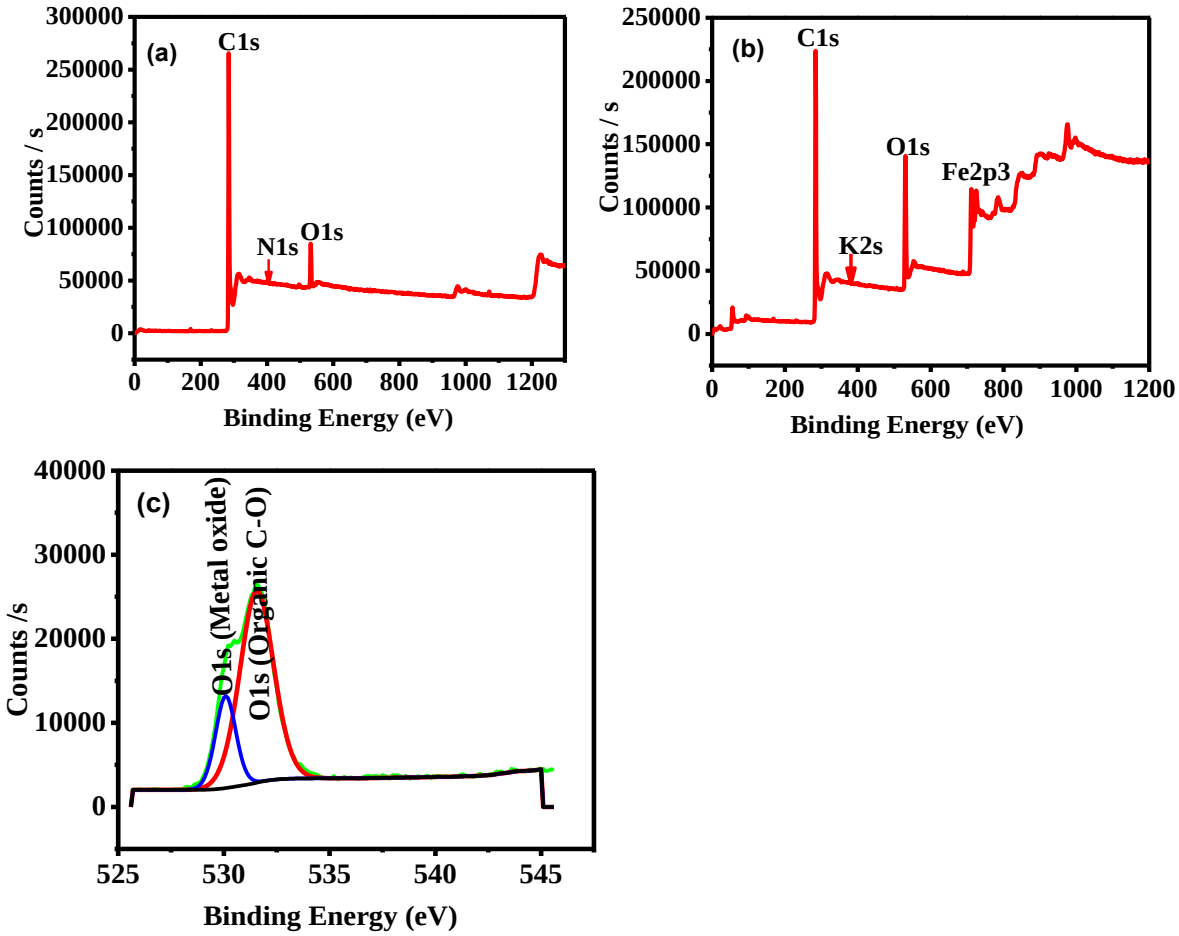

Figure 4.2: XPS analysis of (a) Bare-CC electrode, (b) Iron-supported CC electrode and (c) High-resolution spectra of iron-supported CC electrode

4.4.2 *"In-situ"* electrochemical generation of H_2O_2 in the electrochemical Cell

The Linear sweep voltammetry (LSV) study was performed at a scan rate of 0.05 mV/s and electrochemical potential range of -1.5 V ≦ E ≦ 1.00 V. The experiments were carried out to examine the ability of the CC electrode to create H_2O_2 through the cathodic reduction of diffused

O_2 in a 50 mM solution of K_2SO_4 electrolyte altered to a pH of 3 with H_2SO_4. LSV curves for the CC electrode are presented in Figure 4.3.

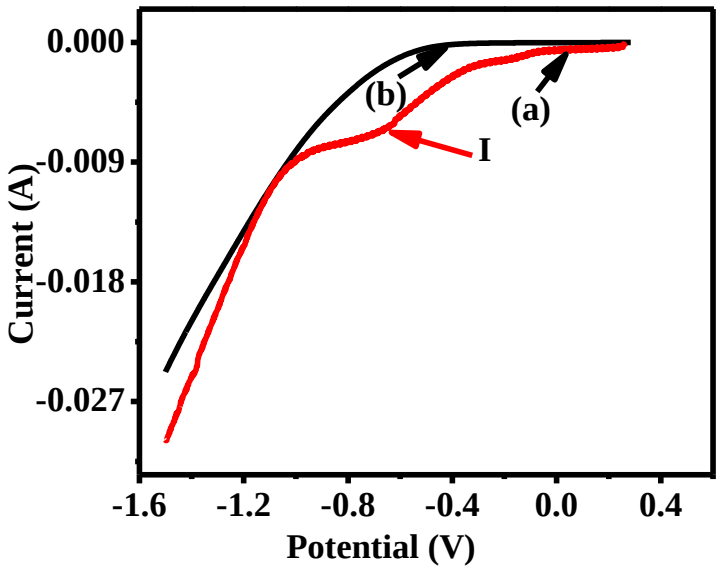

Figure 4.3: LSV response of CC electrode immersed in (a) O_2-saturated (b) N_2-saturated, 50 mM K_2SO_4 solution, Scan rate = 0.05V/s

The CC electrode discloses good ORR activity in the oxygen-enriched electrolyte (curve a), and relatively poor activity in the nitrogen-enriched electrolyte (curve b). The oxygen reduction reaction (ORR) occurs within the depressed region (I), generating hydrogen peroxide. The oxygen reduction potentials for the CC electrode were therefore detected at -0.65V. Although oxygen reduction reaction is recognized to progress through two and four-electron pathways, as presented in Equation 4.1, 4.2, 4.3 and 4.4, the use of carbonaceous material, selectively enables the two-electron pathway thus favoring the production of "*in-situ*" generated H_2O_2 (Reid, 2017). However, the route of oxygen reduction is firmly based on the type of electrode material. The surface chemistry and the majority of the electrode's crystalline structure are responsible for the

perceived excellent oxygen reduction capabilities. The LSV results have, therefore, demonstrated that the CC electrode are conductive (conducts electricity), highly porous with has larger surface area, hence can rapidly adsorbed dissolved oxygen on its surface for ORR producing H_2O_2.

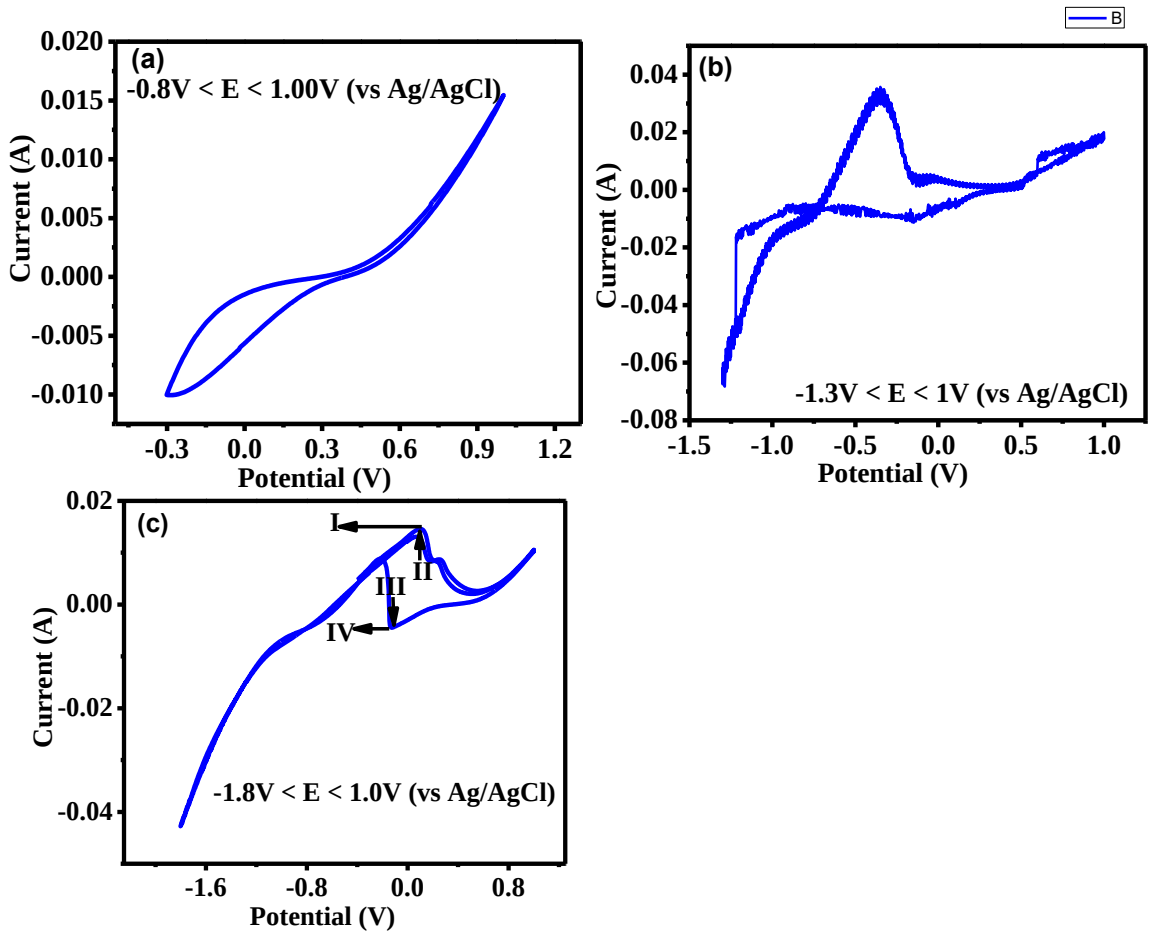

Figure 4.4: CV measurement of CC electrode in N_2-saturated 50 mM K_2SO_4 solution, at a pH of 3 containing 0.1M 100ml $FeSO_4.7H_2O$. Scan rate = 0.05V/s

On another development, Figure 4.4 (a-c) depicts the CV measurement within the range 0.8 V ≦ E≦ 1.00 V; -1.3 V ≦ E ≦1.00 V and -1.8 V≦ E ≦1.00 V which was carried out to optimize iron reduction potentials for successful electrodeposition. Figure 4.4a reveals that during the potential

sweep of -0.8V < E < 1 (vs Ag/AgCl), there was no observable peak for the oxidation and reduction reaction in the electrochemical cell. This is an indication that the electrode needs a wider potential window within which to operate. The rapid increase in current as shown by arrow-I was attributed to the electrochemical decomposition of the electrolyte (K_2SO_4). As iron species are initially present in the solution competing with potassium ions for active sites, a further negative potential sweep (-1.3 V vs Ag/AgCl) results in a cathodic reduction process on the electrode surface. This results in the desire of the system to set-up an equilibrium directed by the applied voltage. Hence, in Figure 4.4b, it was observed that the shape of the forward reduction peak is not identical to the shape of the oxidation peak for the reverse sweep.

This indicates that iron reduction and oxidation rates are not equal, indicating successful electrodeposition at this potential. Improved electrodeposition was observed in Figure 4.4c at a potential sweep of -1.8 V to 1 V vs Ag/AgCl. The voltammograms resulting from this potential scan show similarity in shape between cathodic and anodic waves. The cathodic peak current and voltage were located at IV = - 4 mA and III = - 124 mV while the anodic peak current and voltage correspond to I = 15 mA and II = 102 mV. However, peak-to-peak potential difference greater than 200 mV ($\mathbf{\Delta E_p} > 200mV$) indicates irreversibility (Brookes and Inman, 1986). The redox peak potential difference ($\mathbf{\Delta E_p} = E_p^c - E_p^a$) was 226 mV indicating that the process is not reversible. Hence at the applied potentials of -1.8V < E < 1 (vs Ag/AgCl) and 1 V to -1.5 V (vs Ag/AgCl), the cyclic voltammetry (CV) measurement obtained with CC electrode indicates better morphological structure, as corroborated by the diagram in Figure 4.4. Therefore, -1.8V < E < 1 is the optimized iron reduction potential for effective and uniform electrodepoition of iron on the electrode surface. However, the irreversibility of the process may probably be responsible for the successful iron electrodeposition on the surface of the electrode.

4.4.3 Effect of current density on *"in-situ"* electro-generated H_2O_2

The effect of current density on H_2O_2 production, based on the study conducted using a UV-vis spectrophotometer is shown in Figure 4.5. The yield of H_2O_2 with the bare-CC electrode in 60 min at different current densities of 1, 2, 4, and 8 mA/cm^2 was 3.796, 3.983, 3.924, and 4.011 mg/L, respectively. For current densities of 1, 2, 4, and 8 mA/cm^2, it was observed that generated H_2O_2 concentration is directly related to the current density furnished to the system. Hence, the optimal current density was 8 mA/cm^2 which resulted with the application of 0.1 A. This result conforms to previously reported results (García-Rodríguez *et al.* 2016). In the case of 4 mA/cm^2 current density application, the H_2O_2 concentration obtained was 3.924 mg/L (Figure 4.5a), a value lower than what was obtained when a current density of 2 mA/cm^2 was applied for 60 minutes. A tenable clarification for this phenomenon lies in the mass transfer coefficient of H_2O_2 formation in the system, as explained by Peralta-Hernández and Godínez 2014.

However, increased current density accelerates electron transfer on the CC electrode, promoting the oxygen reduction reaction. As a result, the higher current density can produce more "*in-situ"* generated H_2O_2 as depicted in Figure 4.5b. Petrucci and co-workers in 2016 reported a decrease in the generation of "*in-situ"* generated H_2O_2 when the current density is increased by a few milliamps per square centimeter (mAcm^{-2}) in plain carbonaceous materials.

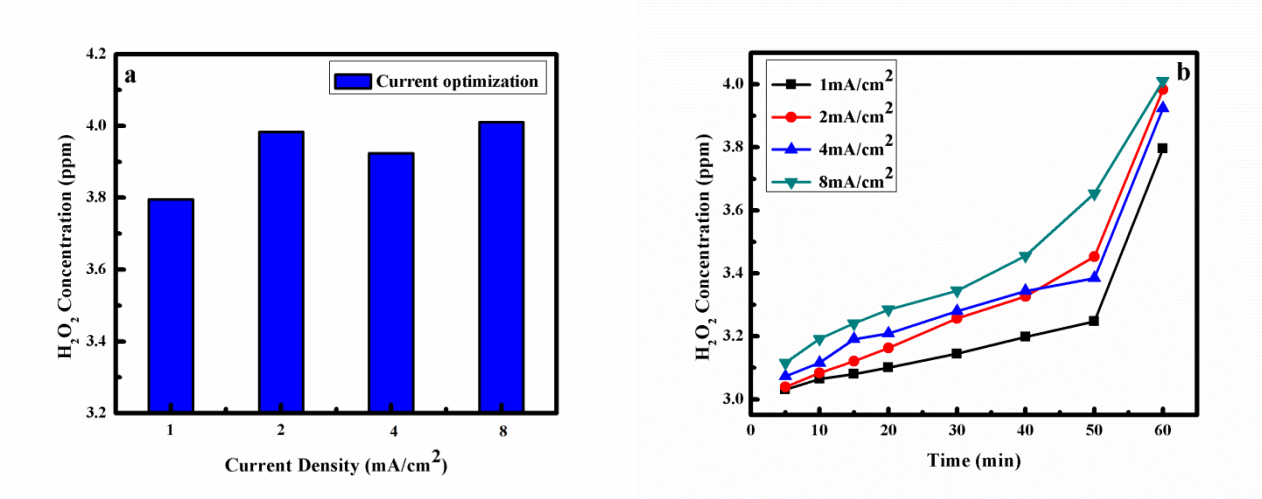

Figure 4.5: H_2O_2 production during electrolysis using triple power supplier in an O_2-saturated 50 mM K_2SO_4 solution, at a pH of 3 (a) at different current densities (b) at different reaction time.

Pérez *et al.* 2017, suggested in his report that the application of current density higher than the limiting current density, could lead to the advancement of some side reactions, which compete with the generation and accumulation of H_2O_2, like $4e^-$ reduction of O_2 to H_2O (Equation 4.3) and peroxide decomposition (Vázquez *et al.*, 2018) leading to oxygen evolution (Equation 4.5). Some researchers such as Barros *et al.* 2015, Kolyagin and Kornienko 2014, etc. have previously applied higher current density in the electrochemical generation of hydrogen peroxide with an excellent outcome. However, those results show that more research is needed for the advancement of hydrogen peroxide production using carbonaceous materials. It was reported that at high current density, current efficiency decreases, and at low current density, current

efficiency increases (Petrucci *et al.*, 2016). This is in agreement with the results obtained in this study, with the modified CC electrode given higher current efficiency.

4.4.4 Evaluation of the catalytic activity of CC electrode

The catalytic activity in the oxygen reduction reaction of the CC electrode was carried out during the production of "*in-situ"* generated H_2O_2. Bare-CC electrode accumulated 4.011 mg/L of H_2O_2 in the electrochemical cell, as shown in Figure 4.5. The accumulated H_2O_2 in the cell is low, as compared to 8 mg/L results obtained by García-Rodríguez *et al.* 2016. Though, the "*in-situ*" generation of H_2O_2 was achieved by the bare-CC electrode, instability, and self-decomposition of the resulting H_2O_2 molecule (equation 4.5) may be responsible for the low value of result obtained. The limitation of oxygen reduction reaction (ORR) on carbonaceous material may be another reason for the low generation of hydrogen peroxide in the electrochemical cell or lack of availability of an active site on the electrode surface for a surface reaction as proposed by (Bañuelos *et al.*, 2015).

After the analysis of the bare-CC electrode, an iron-supported CC electrode prepared by electrodeposition was used to determine the response of iron-metal to the amount of H_2O_2 accumulated in the electrochemical cell. As shown in Figure 4.6b, the H_2O_2 concentration increases linearly in the system with electrolysis time up to 60 minutes. The enhanced value of 36.939 mg/L of H_2O_2 was accumulated in the electrochemical cell for 60 minutes. Therefore the modified CC-electrode generated an outstanding amount of "*in-situ"* generated H_2O_2 of 36.939 mg/L as compared to the 4.011 mg/L generated by the bare CC electrode. However, the generated amount of H_2O_2 in the electrochemical cell could be much higher than the spectrophotometrically measured amount. It has been reported that after iron electrodeposition

on the surface of the carbon-based electrode, zero-valent iron(ZVI)(Fe^0) was found to be electrodeposited on the material, which, through time, oxidizes and generates Fenton reagent (Equation 4.10), which, in turn, reduces the accumulated amount of hydrogen peroxide as indicated by Equation 4.6 (Banuelos *et al.*, 2015). Also, having a greater amount of iron present on the electrode surface (26.96 wt. %) as depicted by EDX analysis (Table 4.1) means that iron was interfering with the generated H_2O_2 to produce hydroxyl free radicals as indicated in equation 4.6, so the electrogenerated H_2O_2 was consumed as quickly as it was produced (Banuelos *et al.*, 2015).

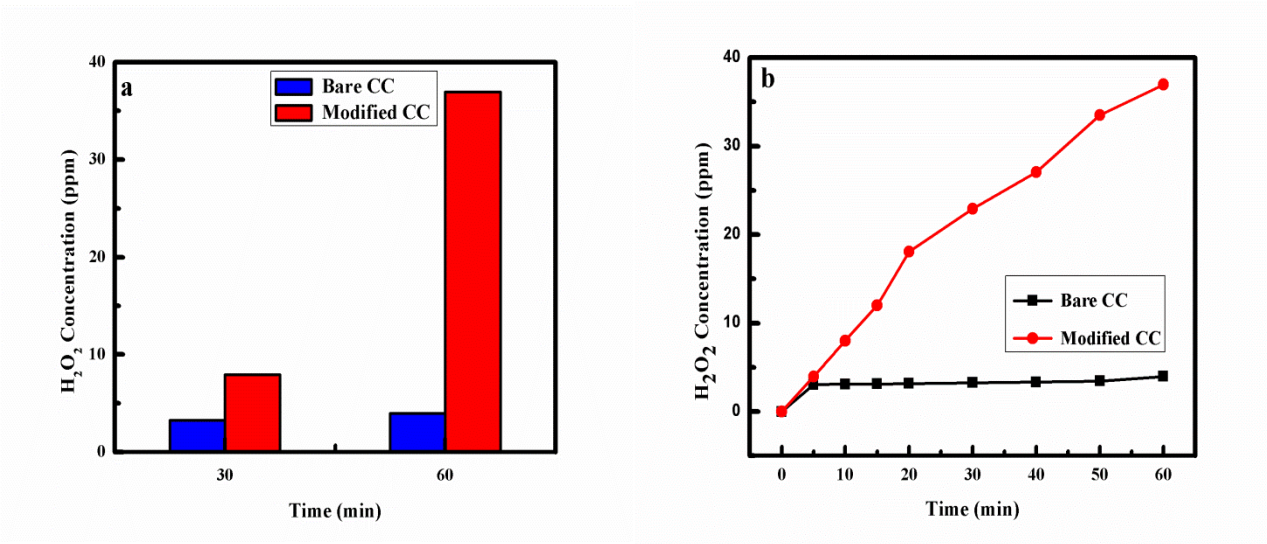

Figure 4.6: Performance of bare and iron-supported CC electrode for H_2O_2 accumulation by electrolysis using triple power supplier (a) at 30 and 60 minutes (b) against electrolysis time Vs Ag/AgCl

Therefore, it is evident that the iron-supported CC electrode exhibits higher catalytic activity and reaches a larger accumulation of H_2O_2 after electrodeposition than bare CC electrode. On a general note, oxygen-containing functional groups introduced on the surface of the electrode as corroborated by XPS analysis (Figure 4.2), could be responsible for higher catalytic activity for H_2O_2 enhancement. In comparison with other previously reported (Table 4.2), the modified CC electrode was found to be superior, and this implies that the iron-supported CC electrode used herein can be considered as an effective catalyst for "*in-situ"* generation of hydrogen peroxide

$$Fe^0 + O_2 + 2H^+ \longrightarrow Fe^{2+} + H_2O_2 \qquad (4.10)$$

Table 4.2: Performance of various supported CC electrode

Catalyst	Electrolyte		Reference
1. Carbon cloth modified with anthraquinone derivatives	KOH in Milli-Q water, saturated with O_2	Unreported data. Very low con. of H_2O_2 generated	Lobyntseva *et al.*, 2017
2. carbon cloth modified with Pd/C and Ni/C	Formic acid with deionized water	Unreported data. Much smaller con. of H_2O_2 generated	Fan *et al.*, 2017
3. carbon cloth	Na_2SO_4 enriched with	7.6	

	modified with mesoporous carbon black	oxygen		Papagiannis *et al.*, 2019
4.	Carbon cloth modified with iron particles	K_2SO_4 enriched with oxygen.	36.7	[This work].

4.5 Conclusion

In this study, the CC electrode was found to be electrically conductive with a stronger ORR activity in the oxygen-enriched electrolyte for H_2O_2 production. Iron was used to modify the CC electrode by electrodeposition, after using CV measurement to determine iron deposition potential. Hence, the application of negative potential on electrode material promotes oxygen reduction reaction (ORR) via 2e- as verified by EDX analysis. After modification, characterization analysis confirms a successful iron electrodeposited process on the surface of the carbon cloth electrode. More active and anchor sites were found to be present on the iron-supported CC electrode for ORR enhancement leading to higher catalytic activity for the generation and accumulation of H_2O_2. On quantification, the concentrations of "*in-situ*" generated H_2O_2 were found to be related to the current density furnished to the system. Although accumulated H_2O_2 concentration appears to be low, it could be that the generated amount of H_2O_2 was depleted by side reactions. Hence, modified iron supported CC electrode has a higher

electrocatalytic activity of oxygen reduction reaction (ORR) via 2e- than bare CC electrode, thus providing an improvement in the initial production of H_2O_2.

REFERENCES

ANANTH, M.V., GIRIDHAR, V.V., AND RENUGA, K. 2009. Linear sweep voltametry studies on oxygen reduction of some oxides in alkaline electrolytes, *International Journal of Hydrogen Energy*, 34 (2) : 658–664.

BANUELOS, J.A., GARCÍA-RODRÍGUEZ, O., RODRÍGUEZ-VALADEZ, F.J., MANRÍQUEZ, J., BUSTOS, E., RODRÍGUEZ, A. AND GODÍNEZ, L. A. 2015. Cathodic polarization effect on the electro-Fenton regeneration of activated carbon, *Journal of Applied Electrochemistry*, 45 (5) : 523–531.

BARROS, W.R., ERENO, T., TAVARES, A.C. AND LANZA, M. R. 2015. In situ electrochemical generation of hydrogen peroxide in alkaline aqueous solution by using an unmodified gas diffusion electrode, *ChemElectroChem*, 2 (5) : 714–719.

BROOKES, H.C. AND INMAN, D. 1986. An Electrochemical Study of Oxyspecies in Calcium Chloride based Melts, *Proceedings of the Fifth International Symposium on Molten Salts*, 1986 (1) : 128–148.

ČOLIC, V., YANG, S., REVAY, Z., STEPHENS, I.E. AND CHORKENDORFF, I. 2018. Carbon catalysts for electrochemical hydrogen peroxide production in acidic media, *Electrochimica Acta*, 272 : 192-202.

EISENBERG, G. 1943. Colorimetric determination of hydrogen peroxide, *Industrial & Engineering Chemistry Analytical Edition*, 15 (5) : 327–328.

FAN, Z., KWON, Y.H., YANG, X., XU, W., AND WU, Z. 2017. In-situ production of hydrogen peroxide as oxidant for direct urea fuel cell, *Energy Procedia*, 105 : 1858–1863.

FOUSTOUKOS, D.I., HOUGHTON, J.L., SEYFRIED JR, W.E., SIEVERT, S.M. AND CODY, G. D. 2011. Kinetics of H_2–O_2–H_2O redox equilibria and formation of metastable H_2O_2 under low temperature hydrothermal conditions, *Geochimica et Cosmochimica Acta*, 75 (6) : 1594–1607.

GARCÍA-RODRÍGUEZ, O., BAÑUELOS, J.A., RICO-ZAVALA, A., GODÍNEZ, L.A. AND RODRÍGUEZ-VALADEZ, F. 2016. Electrocatalytic activity of three carbon materials for the in-situ production of hydrogen peroxide and its application to the electro-fenton heterogeneous process, *International Journal of Chemical Reactor Engineering*, 14 (14) : 843–850.

GOTI, A. AND CARDONA, F. 2018. Hydrogen peroxide in green oxidation reactions: recent catalytic processes. In *Green Chemical Reactions*: 191–212.

HEIDARI, Z., MOTEVASEL, M. AND JAAFARZADEH, N. 2015. Application of Electro-Fenton (EF) process to the removal of pentachlorophenol from aqueous solutions, *Iranian Journal of Oil & Gas Science and Technology*, 4 (4) : 76–87.

KITTE, A.S., ASSRESAHEGN, D.B. AND SORETA, R. T. 2013. Electrochemical determination of hydrogen peroxide at glassy carbon electrode modified with palladium nanoparticles, *Journal of the Serbian Chemical Society*, 78 (5) : 701–711.

KOLYAGIN, G.A. AND KORNIENKO, V. 2014. Electrosynthesis of hydrogen peroxide in solutions of salts that form molecular addition products (peroxo solvates) with it, *Russian Journal of Electrochemistry*, 50 (8) : 798–803.

LOBYNTSEVA, E., KALLIO, T., ALEXEYEVA, N., TAMMEVESKI, K. AND KONTTURI, K. 2007. Electrochemical synthesis of hydrogen peroxide: Rotating disk electrode and fuel cell studies. Electrochimica Acta, 52 (25) : 7262-7269.

LI, J.J., WEI, J., CAI, J. AND CHEN, Y. X. 2018. pH effect on oxidation of hydrogen peroxide on Au (111) electrode in alkaline solutions, *Chinese Journal of Chemical Physics,* 31 (6) : 779–783.

MARTÍNEZ-HUITLE, C.A. AND BRILLAS, E. 2009. Decontamination of wastewaters containing synthetic organic dyes by electrochemical methods: a general review, *Applied Catalysis B: Environmental*, 87 (3–4) : 105–145.

PAPAGIANNIS, I., DOUKAS, E., KALARAKIS, A., AVGOUROPOULOS, G. AND LIANOS, P. 2019. Photoelectrocatalytic H_2 and H_2O_2 production using visible-light-absorbing photoanodes, *Catalysts*, 9 (3) : 243.

PERALTA-HERNÁNDEZ, J.M., MEAS-VONG, Y., RODRÍGUEZ, F.J., CHAPMAN, T.W., MALDONADO, M.I. AND GODÍNEZ, L. 2008. Comparison of hydrogen peroxide-based processes for treating dye-containing wastewater: decolorization and destruction of Orange II azo dye in dilute solution, *Dyes and Pigments*, 76 (3) : 656–662.

PERALTA-HERNÁNDEZ, J.M. AND GODÍNEZ, L. A. 2014. Electrochemical hydrogen peroxide production in acidic medium using a tubular photo-reactor: Application in Advanced oxidation processes, *Journal of the Mexican Chemical Society,* 58 (3) : 348–355.

PÉREZ, J.F., SÁEZ, C., LLANOS, J., CAÑIZARES, P., LÓPEZ, C. AND RODRIGO, M. A. 2017. Improving the efficiency of carbon cloth for the electrogeneration of H_2O_2: role of polytetrafluoroethylene and carbon black loading, *Industrial & Engineering Chemistry Research*, 56 (44) : 12588–12595.

PETRUCCI, E., DA POZZO, A. AND DI PALMA, L. 2016. On the ability to electrogenerate hydrogen peroxide and to regenerate ferrous ions of three selected carbon-based cathodes for electro-

Fenton processes, *Chemical Engineering Journal*, 283 : 750–758.

POURAN, S.R., AZIZ, A.A. AND DAUD, W. M. A. W. 2015. Review on the main advances in photo-Fenton oxidation system for recalcitrant wastewaters., *Journal of Industrial and Engineering Chemistry*, 21 : 53–69.

PUNZI, M., MATTIASSON, B. AND JONSTRUP, M. 2012. Treatment of synthetic textile wastewater by homogeneous and heterogeneous photo-Fenton oxidation, *Journal of Photochemistry and Photobiology A: Chemistry*, 248 : 30–35.

QIANG, Z., CHANG, J.H. AND HUANG, C. P. 2002. Electrochemical generation of hydrogen peroxide from dissolved oxygen in acidic solutions, *Water Research*, 36 (1) : 85–94.

SUN, Y., LI, S., JOVANOV, Z.P., BERNSMEIER, D., WANG, H., PAUL, B., WANG, X., KÜHL, S. AND STRASSER, P. 2018. Structure, Activity, and Faradaic Efficiency of Nitrogen-Doped Porous Carbon Catalysts for Direct Electrochemical Hydrogen Peroxide Production, *ChemSusChem*, 11(19) : 3388–3395.

VÁZQUEZ, A., ALVARADO, L., LÁZARO, I., CRUZ, R., NAVA, J.L., AND RODRÍGUEZ-TORRES, I. 2018. A Comparative Analysis of 2-(Thiocyanomethylthio)-Benzothiazole Degradation Using Electro-Fenton and Anodic Oxidation on a Boron-Doped Diamond Electrode, *International Journal of Photoenergy*, 2018.

YU, F., ZHOU, M. AND YU, X. 2015. Cost-effective electro-Fenton using modified graphite felt that dramatically enhanced on H_2O_2 electro-generation without external aeration, *Electrochimica Acta*, 163 : 182–189.

ZHANG, C., ZHOU, M., REN, G., YU, X., MA, L., YANG, J. AND YU, F. 2015. Heterogeneous

electro-Fenton using modified iron–carbon as catalyst for 2, 4-dichlorophenol degradation: influence factors, mechanism and degradation pathway, *Water Research*, 70 : 414–424.

ZHANG, W., CHEN, J., WANG, J., CUI, C.X., WANG, B. AND ZHANG, Y. 2021. Impact of Active Chlorines and •OH Radicals on Degradation of Quinoline Using the Bipolar Electro-Fenton Process. *Water*, 13 (2) : 128.

ZHONG, H., CAMPOS-ROLDÁN, C.A., ZHAO, Y., ZHANG, S., FENG, Y. AND ALONSO-VANTE, N. 2018. Recent advances of cobalt-based electrocatalysts for oxygen electrode reactions and hydrogen evolution reaction, *Catalysts*, 8 (11) : 559.

ZHOU, W., RAJIC, L., CHEN, L., KOU, K., DING, Y., MENG, X., WANG, Y., MULAW, B., GAO, J., QIN, Y. AND ALSHAWABKEH, A. N. 2019. Activated carbon as effective cathode material in iron-free Electro-Fenton process: Integrated H_2O_2 electrogeneration, activation, and pollutants adsorption, *Electrochimica Acta*, 296 : 317–326.

ZHOU, Z., CHEN, A., KONG, A., FAN, X., ZHANG, X. AND SHAN, Y. 2018. Low-Cost Sulfonated Phthalocyanines-Derived Hierarchical Porous Co-Cu-NS-Doped Carbons for Efficient Oxygen Electroreduction, *Journal of The Electrochemical Society*, 165 (10) : H658.

Chapter 5: Electro-Fenton degradation of selected antiretroviral drugs using a low-cost iron-modified carbon-cloth electrode

5.1 Introduction

Ever since the discovery of the human immunodeficiency virus (HIV) around 1981 (Sharp and Hahn 2011), its eventual prevalence was found to be causative of acquired immune deficiency syndrome (AIDS). Recently, it has globally been estimated that about 36.7 million of people are living with HIV (Klaas *et al.,* 2018). From developing countries, South Africa has the largest HIV epidemic in the world, with an estimated 7.1 million people living with HIV by the end of 2016 (Gutreuter *et al.,* 2019). The collapse of the body's immune defense system (IDS) provides a route to AIDS. Due to its negatively causative impact on people, AIDS has been a subject of great concern to researchers, governments, countries, individuals, etc. In treating HIV from positive patients, antiretroviral drugs (ARVDs) are used. South Africa had the largest antiretroviral therapy program in the world (Evans, 2013). Indisputably, ARVDs are very important for human survival in the 21st century. When consumed, some go through biotransformation while other antiretrovirals are excreted from the body unchanged (*Galasso et al.,* 2002).

Hence, anti-HIV compounds often used to treat HIV/AIDS are classified into Nucleoside reverse transcriptase inhibitors (NRTIs) (e.g. Lamivudine), non-nucleoside reverse transcriptase inhibitors (NNRTIs) (e.g. Nevirapine), protease inhibitors (PIs) (e.g. atazanavir), HIV integrase inhibitors (INSTIs) (e.g. raltegravir), fusion inhibitors (FIs) (e.g. enfuvirtide) and C-C chemokine receptor type five (CCR5) (e.g. maraviroc) (Swanepoel *et al.,* 2015; Shi *et al.,* 2016; De Clercq and Li 2016).

Since South Africa uses more of these compounds than any other nation in the world, a larger amount of ARVDs is potentially discharged into the South African wastewater system. Although ARVDs enter the environment through the myriad of scattered points, the major source is through, excretion of unmetabolized ARVDs via feces or urine, domestic and sewage wastes (septic tanks) (Bound and Voulvoulis 2005), direct disposal of medicine into the environment (Bound and Voulvoulis 2005), and wastewater generated from pharmaceutical industries and hospitals (Khetan and Collins 2007; Lillenberg *et al.*, 2010). In water, these micropollutants form recalcitrant non-biodegradable metabolites (Mascolo *et al.,* 2010; Prasse *et al.*, 2010), which persist and bioaccumulates (Badmus *et al.,* 2018). They are also deemed extremely hazardous due to their toxicity (Sanderson *et al.,* 2004), causing adverse effects on humans and the ecosystem. ARVDs in water are responsible for reproductive disorders, cancer and immune abnormalities. These dilemmas of discharging untreated wastewater into the ecosystem, therefore, threaten humans, animals and plant's health, hence purification is needed. In another development, it has been shown that conventional wastewater treatment systems (a system which removes solids, organic matter and sometimes nutrients with the combination of physical, chemical and biological processes) cannot sufficiently remove these micro-pollutants; hence other treatment methods such as secondary and tertiary treatment methods were employed

(Clouzot *et al.,* 2013). Since conventional treatment processes are problematic, the use of activated carbon adsorption, membrane bioreactor and electrochemical processes (such as AOPs) have been reported as a successful alternative for treating wastewater containing compounds such as ARVD and persistent organic pollutants (POP) (Badmus *et al.,* 2018). Advanced oxidation processes (AOPs) are chemical treatment processes which predominately generates hydroxyl radicals ($OH^{\bullet}$) for the degradation of recalcitrant micropollutants.

The $OH^{\bullet}$ radicals effectively destroy soluble organic contaminants into biodegradable forms (Badmus *et al.,* 2018). The mechanism of destruction is such that the end product of the chemical oxidation is the mineralization of the contaminant to form water, carbon dioxide, nitrogen and other non-toxic minerals**.** These processes usually employ ozone, hydrogen peroxide and/or UV light. Mokhbi et al. 2019, gave a detailed classification of AOPs, in which among various classified AOP technologies, electrochemical advanced oxidation processes (EAOPs) have attracted much interest because of their usage of electric current as the main reagent without the use of harmful chemicals to produce hydroxyl ($OH^{\bullet}$) radical's in solution "*in situ"*. Garcia-Segura et al. reported that electrochemical advanced oxidation processes (EAOPs) have been effectively and extensively employed to degrade recalcitrant and/or toxic pollutants in wastewater and they includes anodic oxidation (AO), electro-Fenton (EF) and photoelectron-Fenton (PEF) (Garcia-Segura *et al.,* 2016). While AO process destroys organics at the anode surface by electron transfer, electrochemical "in situ" generation hydrogen peroxide (H_2O_2), with the addition of iron (II) in the bulk, originates EF process, which produces hydroxyl ions ($OH^{\bullet}$) from Fenton's reaction of Equation 5.1 (Garcia-Segura *et al.,* 2016). Fenton's reaction can be effectively applied in an acidic pH of 2.8–3.0 (Sirés *et al.,* 2014). However, in a Fenton-like

reaction, the Fe^{3+} produced can react with hydrogen peroxide and hydroperoxyl radical to regenerate Fe^{2+} as indicated in Equations 5.2 and 5.3 (Mortazavi *et al.,* 2005; Vasquez-Medrano *et al.,* 2018).

To achieve high generation of "in situ" H_2O_2, the contact between cathode, oxygen, and water must be maximized. In another development, it has been reported that the utilization of carbonaceous materials in EAOPs as the cathodic electrode selectively catalyze oxygen reduction reaction (ORR) by two electron transfer thus generating H_2O_2 continuously (Equation 5.4) (Emeji *et al.,* 2019).

$$Fe^{2+} + H_2O_2 \longrightarrow Fe^{3+} + OH^{\bullet} + OH^{-} \quad (5.1)$$

$$Fe^{3+} + H_2O_2 \longrightarrow Fe^{2+} + HO_2^{*} + H^{+} \quad (5.2)$$

$$Fe^{3+} + HO_2^{*} \longrightarrow Fe^{2+} + O_2 + H^{+} \quad (5.3)$$

$$O_2 + 2H^{+} + 2e^{-} \longrightarrow H_2O_2 \text{ (acidic)} \quad (5.4)$$

$$M + H_2O \longrightarrow M(OH^{\bullet}) + H^{+} + e^{-} \quad (5.5)$$

Some of the cathodic electrodes used by researchers are carbon-cloth modified with iron (Emeji *et al.,* 2019), activated carbon fiber (Wang *et al.,* 2008), and carbon nanotubes (Khataee *et al.,* 2014). In the same manner, anode materials are also very important in EAOPs, hence Boron-doped diamond (BDD) thin-film electrodes are regarded as the best anode used for EAOP due to their higher oxidation ability producing "in situ" $BDD(OH^{\bullet})$ and their larger O_2-overpotential

(Garcia-Segura *et al.,* 2016). Equation 5.5 indicates how the radicals are being formed chemically (Garcia-Segura *et al.,* 2016).

However, some of these electrodes exhibit much more complex behavior in solution with the application of a small AC potential perturbation over a range of frequencies. The input voltage signal as expressed in Equation 5.6 resulted to a response current signal through the electrochemical cell (Equation 5.7) (Lvovich, 2012). With the application of an expression analogous to Ohm's law, the impedance response of the system was obtained and measured as indicated in Equation 5.8 and 5.9 (Lvovich, 2012). While Nyquist plot details processes taking part at the electrode surface, combined electrical circuit elements called equivalent circuits are used to fit the Nyquist data obtained as a model (Pandey *et al.,* 2017).

$$E_t = E_o \sin \omega t \tag{5.6}$$

$$I_t = I_o \sin(\omega t + \emptyset) \tag{5.7}$$

$$Z = \frac{E_t}{I_t} = Z_o \frac{\sin(\omega t)}{\sin(\omega t + \emptyset)} \tag{5.8}$$

$$Z(\omega) = Z_o(cos\emptyset + jsin\emptyset) \tag{5.9}$$

In this study, the carbon-cloth electrode was modified with iron particles. The simulated pharmaceutical, antiretroviral wastewater of NVR, ZDV, and LVD were chosen as a good example of micro-pollutant because of their high toxicity and persistence in South African environs. The redox behavior of the electrode in terms of electron charge transfer kinetics and impedance at the interface with this selected antiretroviral wastewater was measured using electrical impedance spectroscopy (EIS) and cyclic Voltammetry.

5.2 Experimental

5.2.1 Materials and Apparatus

Potassium sulphate (K_2SO_4), Sulfuric acid (H_2SO_4), Iron (II) sulfate heptahydrate ($FeSO_4 \cdot 7H_2O$), Nevirapine (NVR), Zidovudine (ZDV), Lamivudine (LVD), methanol and titanium (IV) oxy-sulphate ($TiOSO_4.xH_2O$, 15 wt. % in dilute sulphuric acid and purity of 99.99% trace metals basis), were all purchased from Sigma-Aldrich, South Africa. All reagents used were prepared with double-distilled water (DDW). Nevirapine (NVR), zidovudine (ZDV) and lamivudine (LVD) chemical structures were depicted in Figure 5.1 and other properties specified in Table 5.1. They were simulated in this study as ARVDs wastewater when combined with potassium sulphate supporting electrolyte. A carbon-cloth electrode was purchased from Fuel Cell Earth, Massachusetts, United States. Nitrogen and oxygen gasses were supplied by AGA, South Africa. The characterizations of the CC electrode were carried out using scanning electron microscopy (SEM) to determine the surface morphology after electrodeposition and energy-dispersive x-ray spectroscopy (EDX) for elemental composition of the synthesized electrode. X-ray photoelectron spectroscopy (XPS) microanalysis further confirms the atomic composition of the synthesized electrode. 100 mL undivided electrochemical cell equipped with 2 electrodes, simulated ARVDs wastewater and 50 mM (millimole) K_2SO_4 aqueous electrolyte at a pH of 3, was used to conduct the degradation experiment. While oxygenation of the system was done using Hailea air-pump, an Auto lab potentiostat/galvanostat (PGSTAT) was employed during degradation electrolysis method, electrode conductivity text, iron reduction potential experiment and electrodeposition. The decay of ARVDs wastewater and the absorbance of pertitanic acid complexes formed by the

reaction between hydrogen peroxide and titanium (IV) oxy-sulphate, was studied using a UV–vis spectrophotometer (PerkinElmer model Lambda 35).

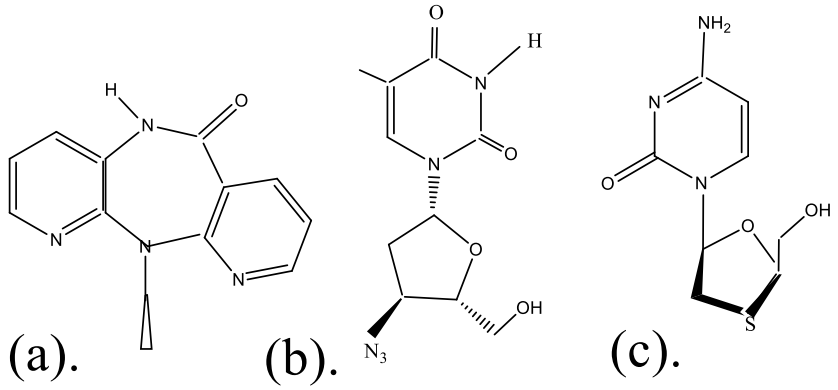

Figure 5.1: Structures of (a) nevirapine, (b) zidovudine and (c) lamivudine

Table 5.1: Properties of Nevirapine, lamivudine, and Zidovudine

	Nevirapine	Lamivudine	Zidovudine
Class	NNRTIs	NRTIs	NRTIs
Molecular Formula	$C_{15}H_{14}N_4O$	$C_8H_{11}N_3O_3S$	$C_{10}H_{13}N_5O_4$
Molar Mass (g/mol)	266.8	229.3	267.3
CAS No.	129618-40-2	134678-17-4	30516-87-1
UV/Vis.-λmax (nm)	213, 233, 284	203, 233, 271	209, 266
Soluble in	methanol	water	water

5.3 Methods

5.3.1 Preparation of standard stock solution

The method for the preparation of standard stock solution was followed as explained under section 3.5 of chapter 3.

5.3.2 Selection of sample wavelength

Also, the determination of wavelength for NVP, LVD, and ZVD sample solution was strictly followed as explained under section 3.5.1.

5.3.3 Preparation of modified iron-supported carbon-cloth electrode.

A similar method as explained under section 3.2.3 above were followed for the preparation of composite Fe-supported-CC electrode through chronoamperometry method

5.3.4 Preparation of Synthetic Wastewater for degradation

Synthetic wastewater of the ARVDs was prepared following the same method as under section 3.5.2

5.3.5 Electrochemical degradation experiments

The electrochemical degradation method followed for the degradation of sample ARVDs was performed under section 3.6

5.3.6 Electrochemical Measurements

The techniques involved under electrochemical measurements were electrochemical impedance spectroscopy (EIS) and cyclic voltammetry (CV). For all engaged electrochemical measurements, standard three-electrode configured system and Autolab PGSTAT-204 were employed. The bare or modified carbon-cloth electrode was engaged as the working electrodes, while BDD and Ag/AgCl were used as the counter (CE) and reference electrodes (RE). CV and EIS measurement was carried out using 100 mL electrochemical cell containing 50 mM of K_2SO_4 supporting electrolyte at a pH of 3. The electrolytic solution was enriched with O_2 gas for 35 min prior to the experiment at room temperature. Open circuit potential (OCP) with a frequency range from 0.1 Hz to 100000 Hz was then applied.

5.3.7 Chromatographic conditions

The degradation of antiretroviral solution, with samples taken at specific time intervals of 30 minutes were further analysed on a high performance liquid chromatography (HPLC) with photodiode array detector (UltiMate 3000 series) set at a wavelength of 254 nm. A gradient LC

method was used to achieve the elution of samples at a flow rate of 0.2 mL/min on a LUNA 5 mm C 18 reversed phase column (150 x 4.6 mm) maintained at room temperature. Initial elution of the sample was carried out for 6 minutes using acetonitrile: water ratio of (30:70, v/v). This ratio was then increased to 90:10 within 2 minutes and held for 1 minute. For the next 8 minutes the ratio was reverted back to the initial value of (30:70) ratio and held constant for 3 minutes. Separation of intermediate products was achieved using LC-20Ad XR model liquid chromatography (LC) with column and mobile phase same as those used in HPLC analysis. However, in all cases, the identification of intermediate products was made by comparison of the HPLC retention times (t_R) of all peaks in the degradation solution with the peak of the pure standard solutions.

5.4 Results and discussion

5.4.1 Characterization

The morphological structure of the carbon-cloth electrode before and after electrodeposition was investigated using scanning electron microscopy (SEM) analysis. The micrograph of the bare CC electrode shows naturally overlapping tube-like carbon fibers with a porous texture as depicted in Figure 5.2a. Also shown in Figure 5.2b is bare CC electrode contaminated with small lumps attached to the stem of the carbon-fiber and this contaminant can be removed by pretreatment with alkali or acid. Figure 5.2c shows a typical rough structure of iron particles deposited on the surface of the CC electrode, and the SEM image of Figure 5.2d indicates well-dispersed iron

particles on the surface of the CC electrode. This dispersion was completely uniform over the crystal lattice of the carbon-cloth structure. The depicted structure of the modified CC electrode by SEM analysis was expected to help improve the electrochemical activity of the electrode toward the "*in situ"* generation of hydrogen peroxide (H_2O_2). On the other hand, the EDX result which is shown in Table 5.2 confirms C, O, N, K and Fe as the elemental components of the synthesized modified Fe/CC electrode. The availability of these elements in the lattice structure of the carbon support indicates the successful fabrication of the intended Fe/CC electrode.

From the EDX result shown in Table 5.2, 0.26% and 0.06% was obtained as the values of oxygen-to-carbon (O/C) ratio and nitrogen-to-carbon (N/C) ratio. This result indicates higher oxygen content as compared to nitrogen in the modified electrode and this confirmed the adsorption of iron particles onto the surface of carbon support after electrodeposition. Higher resolution O 1s XPS spectra in Figure 5.2e, shows a few additional oxygen functional group of O 1s (metal oxide) at 531.0 eV and O 1s (organic C-O) at 532.7 eV. The introduction of this oxygen functional group in the structural matrix of carbon-cloth electrode provides more active sites for catalyzed oxygen reduction reaction (ORR) activity which promotes "*in situ"* hydrogen peroxide generation. The obtained, therefore, agrees with Wang and coworkers in 2012, indicated that surface functionality of carbon support generates active and anchor sites for the improvement of ORR catalytic activities.

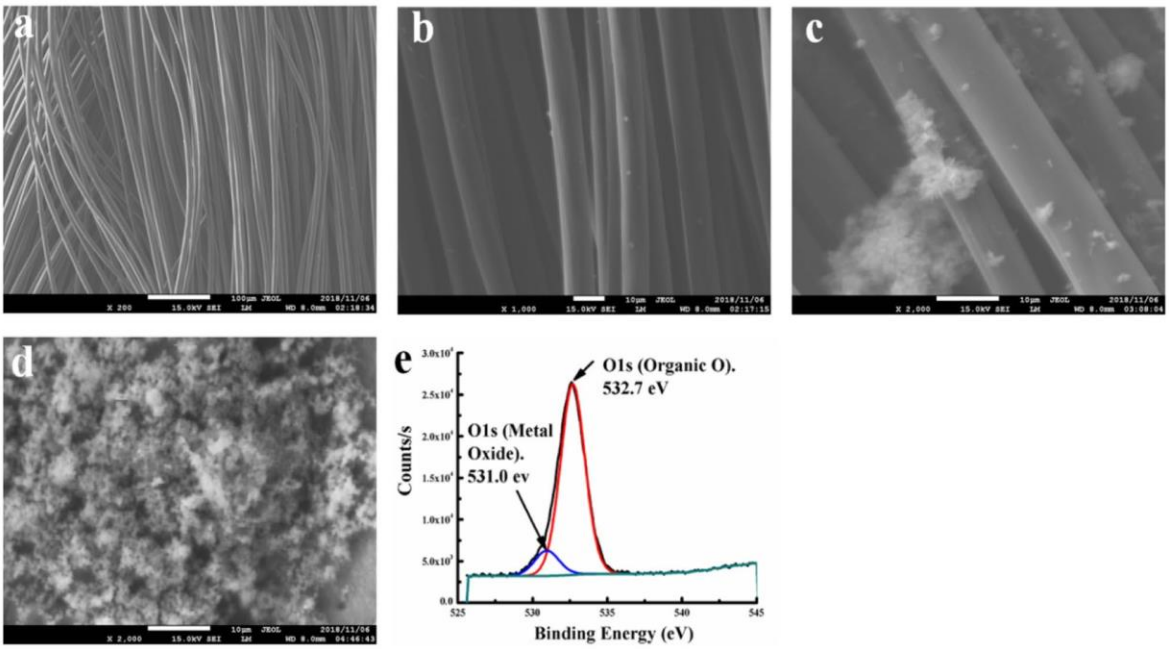

Figure 5.2: (a). SEM image of bare carbon-cloth electrode, (b) SEM image of bare carbon-cloth electrode showing impurities, (c) SEM image of iron-supported CC electrode, not completely covered, (d) SEM image of iron-supported CC electrode, uniformly covered, (e) High-resolution O 1s XPS spectrum of modified Fe/CC electrode showing relatively few types of oxygen functional groups

Table 5.2: EDX result obtained from the circuit fitting for bare CC and modified CC electrode

Samples	Weight %				
	C	O	N	K	Fe
Bare CC electrode	99.74	0.24	0.02		
Modified (Fe/CC) electrode	57.09	14.70	0.36	0.41	27.44

5.4.2 Electrochemical study using CV and electrical impedance spectroscopy (EIS)

The electrochemical characterization of bare CC and modified Fe/CC electrodes were performed in a 100 mL electrochemical cell containing 50 mM potassium sulphate (K_2SO_4) electrolyte at a pH of 3. Back and forth application of a potential sweep to the WE at a scan rate of 50 mV for a definite number of cycles produces a CV voltammogram which was represented in Figure 5.3 (a, and b). About 50% of enhancements in current signals were observed after using a modified carbon-cloth electrode with iron (II). This enhancement may be attributed to the improvement in the conductivity and the surface area of the modified Fe/CC electrode due to the presence of nanoscale iron (II) nanoparticles in their morphological matrix. Hence, this quality appends to the electrochemical application of the synthesized electrode.

On another development, the EIS analysis denotes the measurement of the impedance at the surface of the electrode occurring at the solution-electrode interface which resulted when there is an application of a small alternating (AC) sinusoidal voltage (~10 mV peak-to-peak). In this study, EIS testing was also used to estimate the conductivity and diffusivity of bare CC and iron-modified CC (Fe/CC) electrode. Obtained results were shown in the Nyquist complex plots of real impedance (Z') vs. imaginary impedance (Z'') of Figure 5.3c.

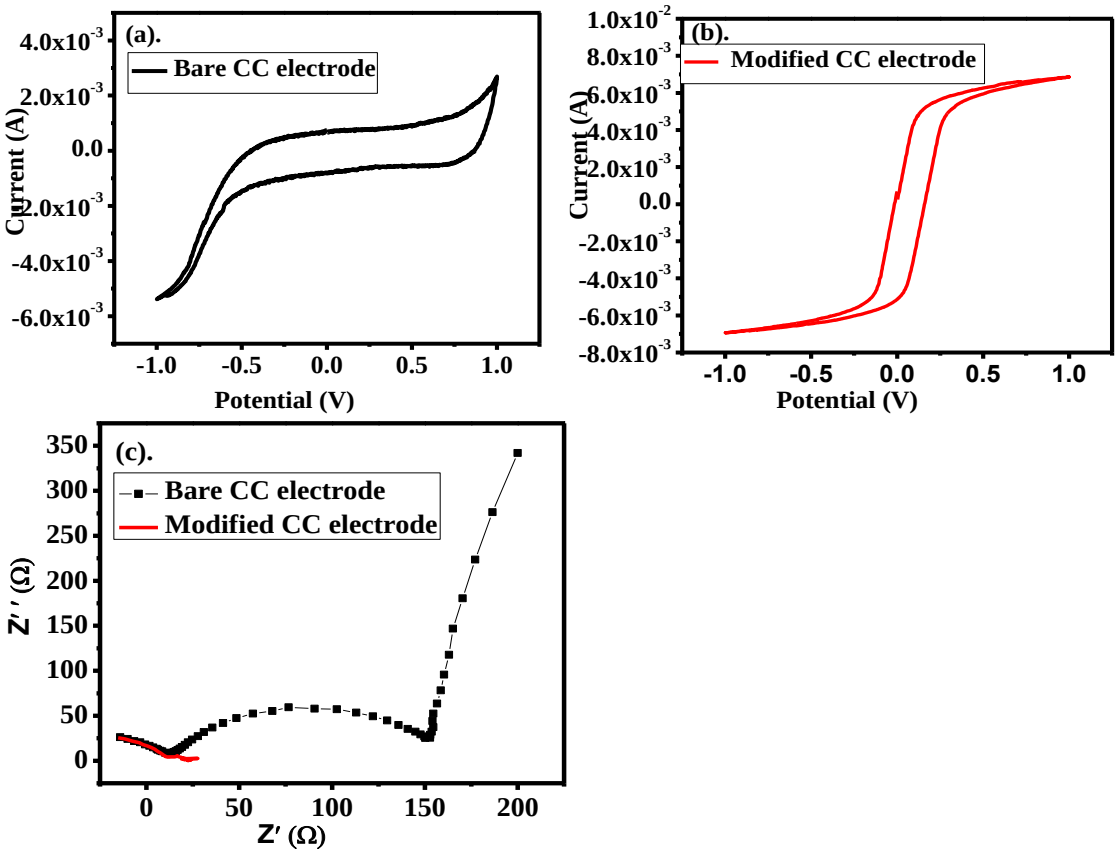

Figure 5.3: (a). Cyclic Voltammogram of bare CC electrode (b) Cyclic Voltammogram of modified Fe/CC electrode (c) EIS of bare CC and modified Fe/CC electrodes; in 50 mM K_2SO_4 at 50 mV/s and a pH of 3

From Figure 5.3c, it was observed that the EIS spectrum of the bare electrode is composed of a well-defined large semicircle at the high-frequency region and a straight line at lower frequency region as indicated by the black curve. On the other hand, the red modified electrodes under all conditions show very compressed semicircles than the black bare ones. The formed semicircle may be ascribed to the electron (charge) transfer process at the interface and its diameter is equivalent to charge transfer resistance (Rct) (Dhillon and Kant 2017). The larger the diameter of the semicircle the higher the resistance (Dhillon and Kant 2017); hence smaller diameter shows

faster charge transfer kinetics at the interface (Wang *et al.*, 2012), between the heterogeneous electrode and the electrolyte. Obtained results are in line with that suggested by Dhillon and Kant 2017. Fitting the EIS data of the bare and modified electrode using the Randle–Sevcik model, Table 5.3 is obtained. The EIS results presented by Nyquist plots of Figure 5.3c and Table 5.3 concur with the CV of Figure 5.3a, b. It is therefore imperative to pinpoint that an increment in current indicates smaller charge transfer resistance or lower resistance to current flow. Therefore, the lowest charge transfer resistance was established from the modified Fe/CC electrode (Table 5.3), which was in agreement with the highest peak current obtained from the CV measurement (Figure 5.3). Hence, smaller semicircle narrows down predominantly charge transfer regions with an increase in ionic conduction at the interface while the raised arm region of the curve corresponds to the diffusion-limited process.

Table 5.3: Obtained result from circuit fitting for bare CC and modified CC electrode

Circuit Element	Bare CC electrode	Modified (Fe/CC) electrode
Rs (Ω)	9.5187	7.6209
Rct (Ω)	184.9824	14.0625

5.4.3 Catalytic activity of the synthesized Fe/CC electrode

The amount of hydrogen peroxide generated “in situ” was measured in order to determine the catalytic activity in oxygen reduction reaction (ORR) of the electrode. Iron-supported carbon-

cloth (Fe/CC) electrode was used to evaluate the iron response to the accumulated H_2O_2 in the electrochemical cell. As depicted in Figure 5.4a, the concentration of "in situ" H_2O_2 electrogenerated in the cell increases linearly with electrolysis time up to 60 minutes. The modified Fe/CC electrode generated an enhanced H_2O_2 value of 39 mg/L for 60 minutes as indicatively shown, while the bare electrode accumulated a smaller concentration of about 3 mg/L of H_2O_2. In comparison, it can be deduced that 89% more H_2O_2 was reached with the modified Fe/CC electrode and this is favorable to the EF process. Hence, the enhanced "in situ" peroxide may be attributed to the oxygenated functional groups within the structural matrix of the CC electrode as stipulated by XPs analysis.

On the other hand, the EDX result which was presented in Table 5.2, shows that C, Fe and O, are predominantly the elemental component of the synthesized electrode which indicatively suggested successful electrodeposition. This means that zero valence iron (ZVI) is most likely present on the freshly coated electrode surface after electrodepositon. The production of iron oxide was unavoidable during drying and exposure to the atmosphere. This then helps us to infer that the carbon-cloth support has been electrodeposited with iron oxides. However, it has previously been reported that in the presence of dissolved oxygen, zero valence iron (ZVI) (Fe^0) can degrade and oxidize organic compounds by transferring two electrons to O_2 to generate H_2O_2 at shown in Equation 5.10 (Bañuelos *et al.,* 2015; Fu *et al.,* 2014; Shahwan *et al.,* 2011). However, the true amount of maximum peroxide produced in the electrochemical cell may not exactly be the measured value of 39 mg/L as spectrophotometrically presented. This suggestion occurs because of the iron oxides present on the surface of the electrode which interferes with the created H_2O_2 in order to generate free hydroxyl radicals as shown in equation 5.1. The "in situ"

H_2O_2 was consumed as quickly as it was generated (Bañuelos *et al.,* 2014), thus reducing them as obviously observed in the spectrophotometric concentration reported.

$$Fe^0 + O_2 + 2H^+ \longrightarrow Fe^{2+} + H_2O_2 \qquad (5.10)$$

5.4.4 Electrochemical degradation study of ARVDs (LVD, ZVD, and NVP) in a solution using the electro-Fenton process

The UV spectra of Figure 5.4b - d stipulates the antiretroviral detection wavelengths that gave a good peak response at 289 nm, 274 nm and 271 nm for nevirapine, lamivudine and zidovudine. Therefore, in studying ARVDs degradability using a uv-spectrophotometer, NVP, LVD and ZVD micropollutants show maximum absorbance at 289, 274 and 281 nm respectively; hence their wavelengths were used to construct a calibration curve of absorbance vs. concentration so as to find their absorbance linear range. The obtained calibration curves as shown in Figure 5.5a - c were acquired with 5 standard samples of each drug solution. Their correlation coefficients (R^2) were greater than 0.98 and this indicates good adjustment for all calibration curves. However, with the application of the modified electrode, degradation process was observed as electrolysis time increases (Figure 5.5d). The iron (II) particles electrodeposited on the carbon-cloth (CC) electrode was observed to play an important role as Electro-Fenton reaction occurs given an increased production of "in situ" hydrogen peroxide as shown by Equation 5.4.

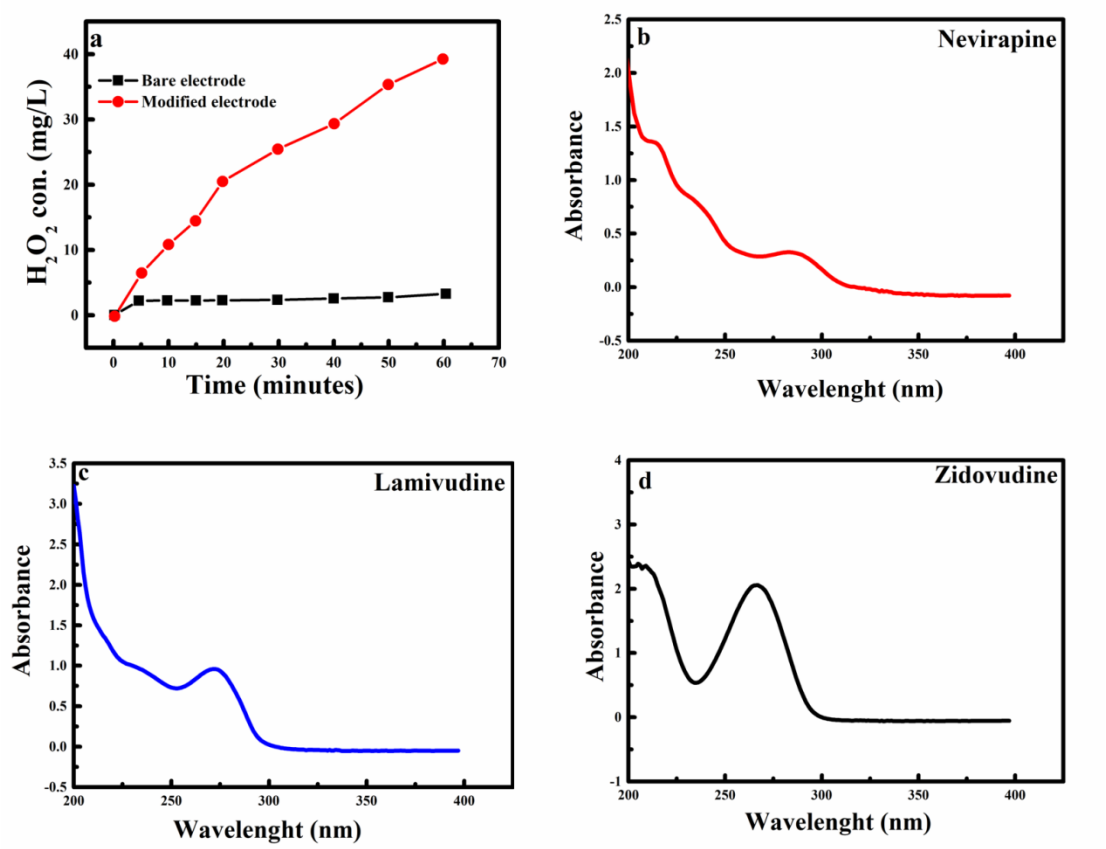

Figure 5.4: (a) H_2O_2 accumulation by electrolysis of bare and iron-modified CC electrode; UV spectra of (b). Nevirapine, λ_{max} = 289 nm (c). Lamivudine, λ_{max} = 274 nm (d). Zidovudine, λ_{max} = 271 nm

Increasing the electro-generation of hydrogen peroxide ($OH^{\bullet}$) results in the attack of the micropollutants, and this causes a gradual decrease in the absorbance of the antiretroviral drug solutions. Decrease in absorbance was used to measure the extent of degradability at a pH of 3. The degradation profile of lamivudine, nevirapine, and zidovudine with modified CC electrode was shown in Figure 5.5d. Indicated was the normalized concentration (C_t/C_o) of ZVD which decreases to 0.688 as electrolysis time increases to 210 minutes. Also shown in the same manner is the normalized concentration (C_t/C_o) for NVP and LVD which decreases to 0.753 and 0.763

respectively. Deductions of obtained data shows that ZVD degrades faster with a removal efficiency of 31% as compared to 25% removal efficiency recorded for NVD and LVD respectively. In comparison with previously reported, Gouthami et al. 2013, obtained a lower removal efficiency of 20% when 10 mg/L of lamivudine solution were degraded against 0.1 N HCl in India.

On another instance, Pottabathini and co-workers in 2016 recorded a lower removal efficiency of 20.91% in acid degradation of nevirapine at 80 ^{o}C for 8 hr. Degradation product formation may be responsible for the low removal efficiency recorded in most antiretroviral degradation processes (Boix *et al.,* 2013). Although removal of microorganics from ARVDs in wastewater has been scarcely reported, the removal efficiency obtained in this study represent good and superior on comparison with others as indicated in Table 5.4. In another development, the kinetics of Figure (5.4d) shows that the decrease in ARVDs concentration with time indicates an exponential relationship which follows a pseudo-first-order dynamics (Asenjo *et al.,* 2013; Turabik *et al.,* 2014). The organics attack by short lifetime hydroxyl radicals ($OH^{\bullet}$) as shown in Equation 5.11, were described by Langmuir-Hinshelwood model in Equation 5.12 which on integration can be written as either Equations 5.13 or 5.14 (Ahmed *et al.,* 2016).

$$\text{ARVDs} + OH^{\bullet} \longrightarrow \text{oxidation products} \tag{5.11}$$

$$-\frac{dC}{dt} = K_{abs}[OH\bullet][ARVDs] = K_{app}[ARVDs] \tag{5.12}$$

$$\ln\left(\frac{C_o}{C_t}\right) = K_{app}.t \tag{5.13}$$

$$\ln\left(\frac{C_t}{C_o}\right) = -K_{app}.t \tag{5.14}$$

Where, C_o represents the initial concentration of the selected ARVDs to be degraded at time of degradation = 0 min. C_t is the concentration of the same ARVDs at time t of degradation.

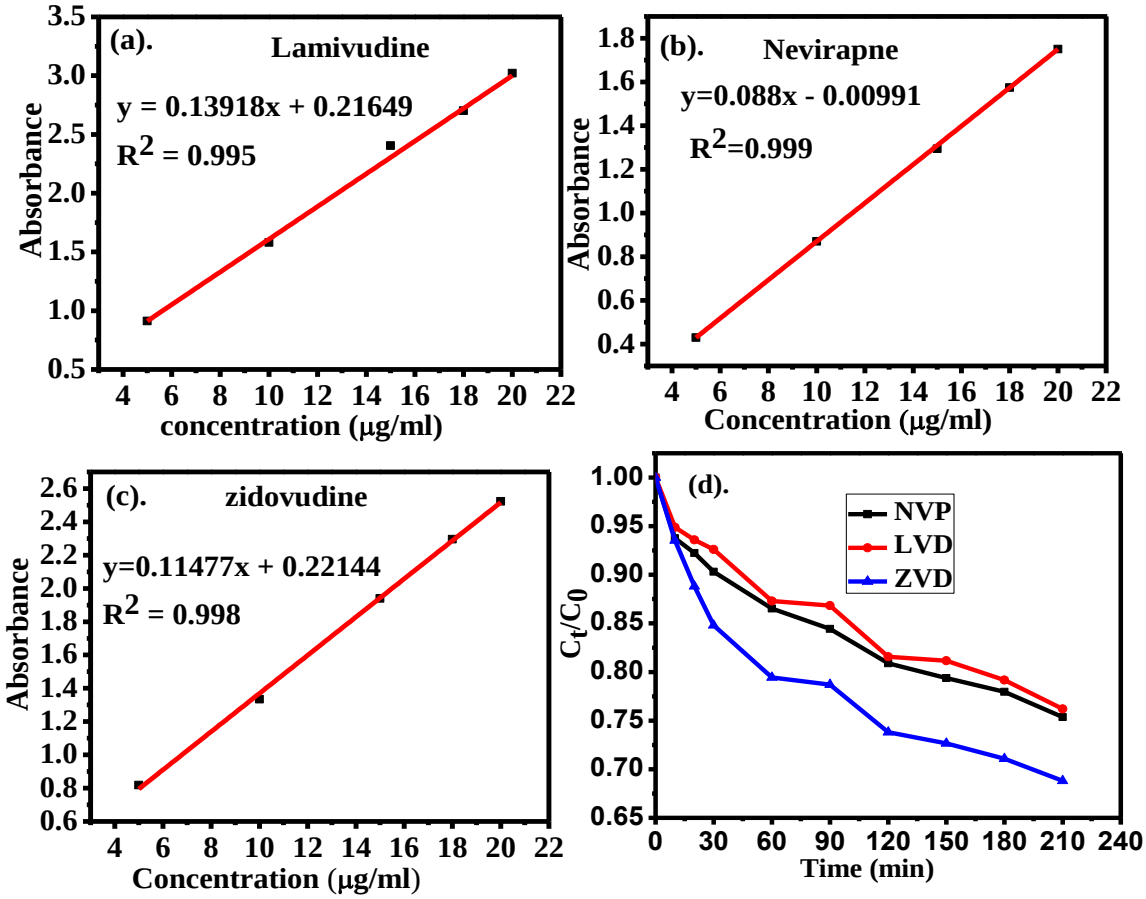

Figure 5.5: Calibration curve of (a) Lamivudine, (b) Nevirapine, (c) Zidovudine, and (d) Degradation profile of modified electrode on LVD, NVP, and ZVD all at a pH 3

The apparent degradable rate constants (K_{app}) for the different sampled ARVDs solution were determined from the slope of the straight lines of the graphs in Figure 5.5d, according to Equation 5.12. Their values were 1.52 x 10^{-3} mol^{-1} min^{-1} for ZVD, 1.20 x 10^{-3} mol^{-1} min^{-1} for NVP and 1.18 x 10^{-3} mol^{-1} min^{-1} for LVD. Hence, degradability of antiretroviral micropollutants was observed using the EF process and a couple of "in situ" generated oxidant species at the

surface of the electrode was responsible for the degradation process. On the other hand, the result of Figure 5.6 demonstrated that with increasing electrolysis time, the normalized concentration (Ct/Co) of ZDV, LVD, and NVP using bare electrode only decreases marginally to 0.9303, 0.9811, and 0.981.

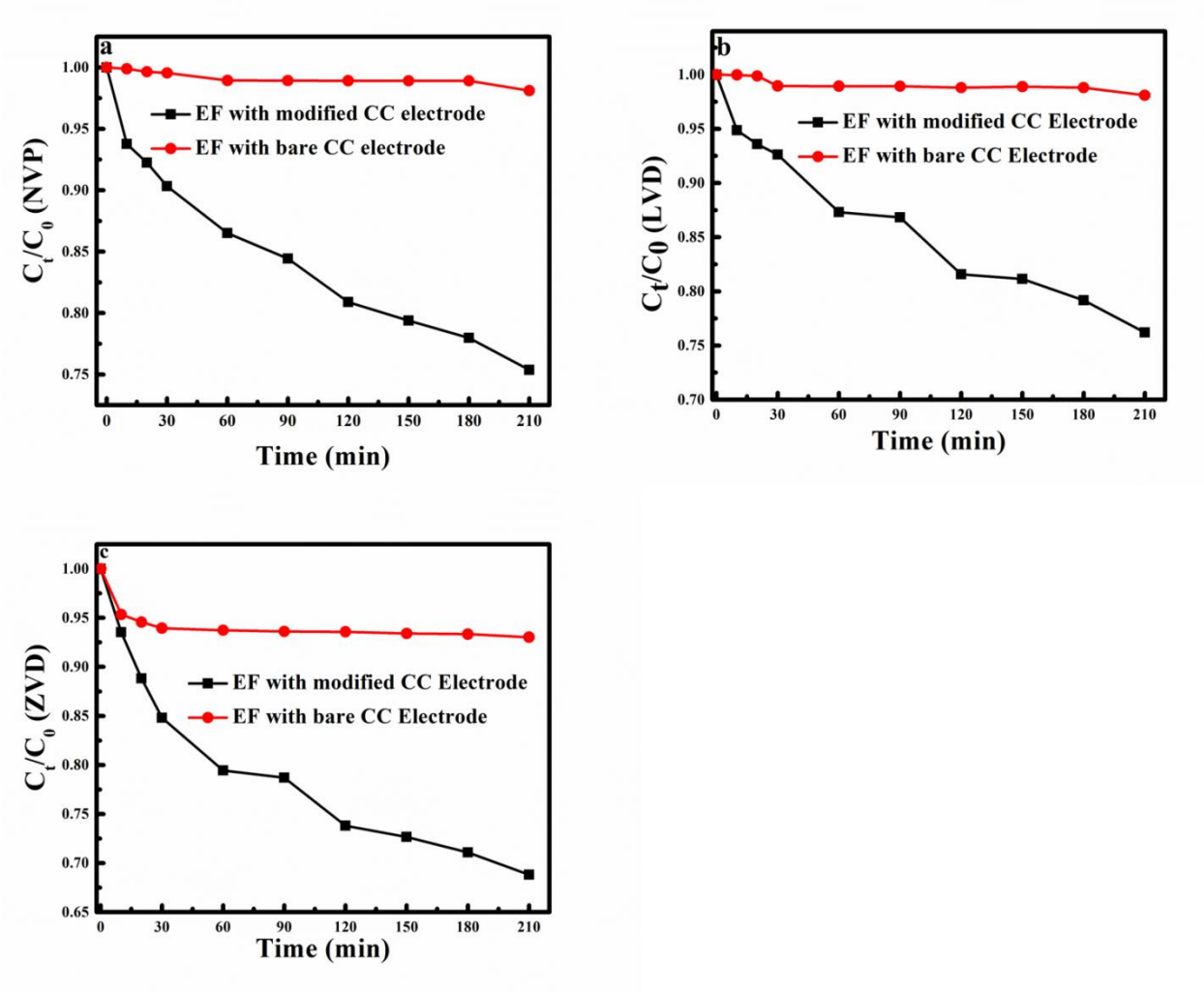

Figure 5.6: Degradation of (a) NVP, (b) LVD, and (c) ZDV, in electro-Fenton (EF) process with iron modified CC and bare CC electrode

This slight decrease was attributed to the lower quantity of "in situ" H_2O_2 and hydroxyl ions ($OH^{\bullet}$) generated in the solution as shown in Equation 5.1 and 5.4, which was quite insufficient to degrade the organics catalytically. This is consistent with the literature which under acidic conditions produces protons for 2-electron ORR to generate "in situ" H_2O_2 (Sirés *et al.,* 2014; Zhang *et al.,* 2009; Qiang *et al.,* 2002). The outcome has therefore portrays that the EF process using iron modified CC electrode is more efficient than bare CC electrode for ZDV, NVP and LVD degradation. This is also verified by the results presented in Figure 5.4a, in which modified CC electrode and bare CC electrode obtained higher and lower H_2O_2 output.

Table 5.4: Comparison with other removal methods Degradation processes Drugs degraded Equipment used and Removal efficiency Reference

Degradation processes	Drugs degraded	Equipment used and Removal efficiency	Reference
1. Acid degradation, Base degradation, Oxidative degradation, Thermal	Nevirapine (NVP) degraded significantly in acid and thermal degradation	High-Resolution Mass Spectrometry (HRMS). 20.9%	*Gouthami et al., 2013*

	degradation, and Photolytic degradation was carried out			
2.	Oxidative degradation was done against 0.3% H_2O_2	Lamivudine (LVD) degraded more in alkaline condition than in acidic hydrolysis	UV-Vis Spectrophotometer. 20%	Pottabathini *et al.*, 2016
3.	EF process using iron modified carbon-cloth electrode	Zidovudine, Lamivudine, and Nevirapine was degraded using EF Process	UV-Vis Spectrophotometer. 31%, 25% and 25%.	This work

5.4.5 Effect of initial pH on the degradation of NVP, LVD and ZVD pharmaceuticals

The pH value has been shown to have a considerable impact on the performance of electro - Fenton reactions (Badawy *et al.*, 2006). The pH value of 3 has long been thought to be the best for wastewater treatment (Zhou *et al.*, 2012). As a result, the influence of pH on the degradation efficiency of antiretroviral pharmaceuticals by electro-Fenton process was investigated, with the results given in Fig. 3. The findings revealed that the degradation of ARVDs pharmaceuticals was accelerated in acidic environments. After 210 minutes at pH 3, the degradation removal efficiency of NVD, LVD, and ZVD was 25%, 25% and 31%. At increased pH, the degradation removal efficiency dropped to 20%, 21% and 25% at pH 5 for NVD, LVD, and ZVD and 17%, 18% and 20% at pH of 7. As a result, increasing the pH of the ARVDs pharmaceutical solution reduces the efficiency of breakdown. Based on these findings, the ideal pH is thought to be 3. This tendency could be explained by the slow rate of breakdown of H_2O_2 at pH levels over 3.0, which results in a decrease in hydroxyl ions ($OH^{\bullet}$) production (Li *et al.*, 2009). Previous studies on electro-Fenton degradation of several types of organics (Ravina *et al.*, 2002; Yang *et al.*, 2009) similarly found pH of 3 as the optimized pH.

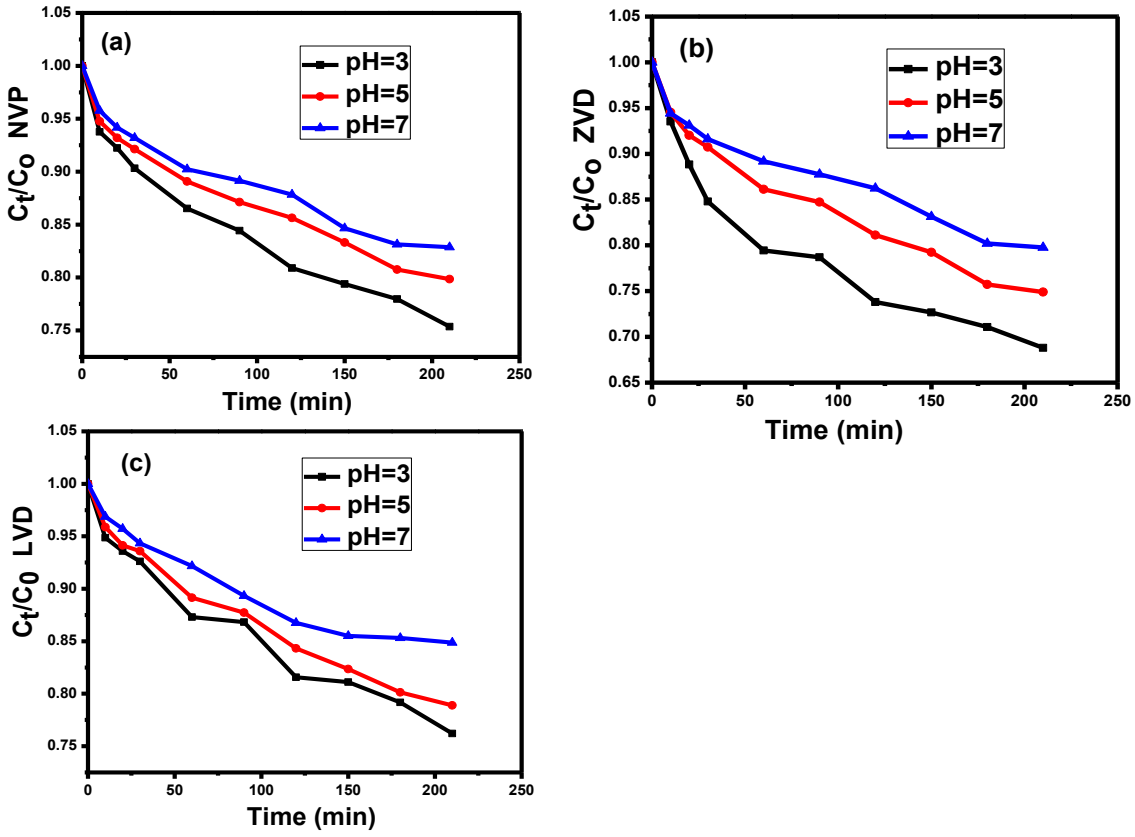

Figure 5.7: Effect of initial pH on the degradation of organics from NVP, LVD and ZVD by Fenton oxidation.

5.4.6 Effect of different pollutant concentration on the degradation of organics from ARVDs

The degradation of simulated antiretroviral pharmaceutical wastewater at various doses was investigated; the findings were given in Fig. 3. It can be seen that as the concentration of ARVDs was increased, the efficiency of its decomposition reduced. The degrading efficiency of NVP

concentration within 210 minutes of reaction fell from 25% to 12% and then 8% as its concentration was increased from 20mg/L to 40mg/L and then 60mg/L. Similarly, the degrading efficiency of ZVD concentration also decreases from 31% to 16% and then 10% as the concentration increases from 20mg/L to 40mg/L and then 60mg/L. LVD on the other hand has its degradation efficiency decreases from 25% to 21% and then 15%. This is because with the application of same current density, the same number of iron ions and hydroxyl radicals move to the solution at different ARVDs concentrations. Hence, lower concentration of hydroxyl ions resulted from increasing the concentration of ARVDs within the solution. Researchers who observed same trend includes Rahmani et al. 2015, Babuponnusami and Muthukumar 2011, Zazouli and Taghavi 2012, etc.

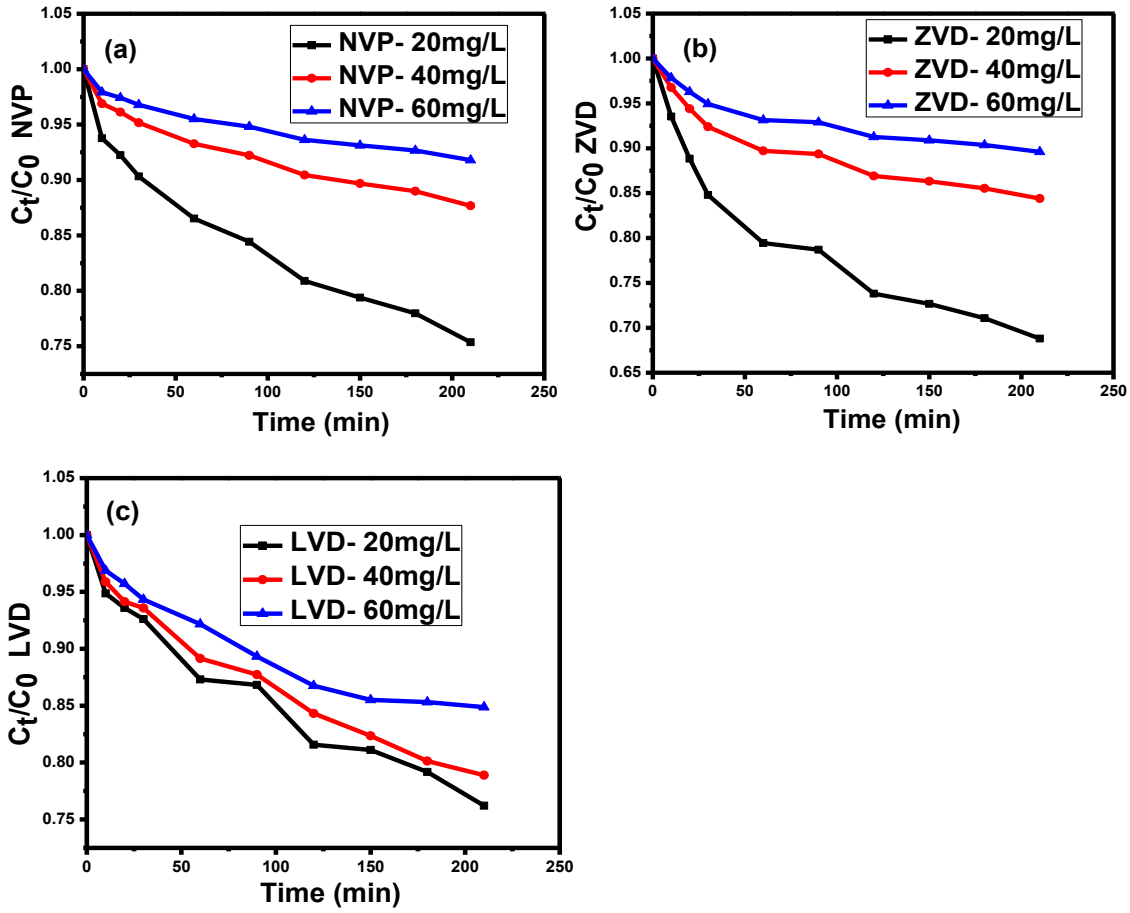

Figure 5.8: Effect of initial NVP, LVD and ZVD concentration on NVP, LVD and ZVD removal by electro-Fenton process (operation condition: applied current 8 mA/cm^2, K_2SO_4 100 mg and pH 3)

5.4.7 HPLC analysis

HPLC analysis was performed to identify the oxidation by-products formed during the electro-Fenton treatment of aqueous lamivudine, nevirapine and Zidovudine antiretroviral samples mediated by iron-supported carbon-cloth electrode. As shown by UV-Vis analysis of Figure

5.5d, the concentration of the ARVD samples decreases with increasing time monitored at the specified wavelengths. This decrease was accompanied by the appearance of new peaks as shown in the HPLC chromatogram of Figure 5.10. By comparing the obtained peak's retention time (t_R) with that of injected reference standards in the same chromatographic system, intermediate products were identified. However, unreacted drug solutions showed only one major peak, as depicted in a standard chromatogram of nevirapine (Vijayaraj *et al.,* 2013), lamivudine (Bedse *et al.,* 2009) and zidovudine (Mandloi *et al.,* 2011) of Figure 5.9. As shown in Figure 5.10a, peak I and II with retention time 3.27, 3.78 minutes indicates two degradation product formations on treating nevirapine aqueous solution with Fenton reagent. Peaks assigned to the intermediate products III, IV, V and VI (Figure 5.10 b, c) with retention times of 2.64, 2.98, 1.24 and 3.13 minutes, respectively, were observed from the degradation sample solutions of LVD and ZVD at a pH of 3.

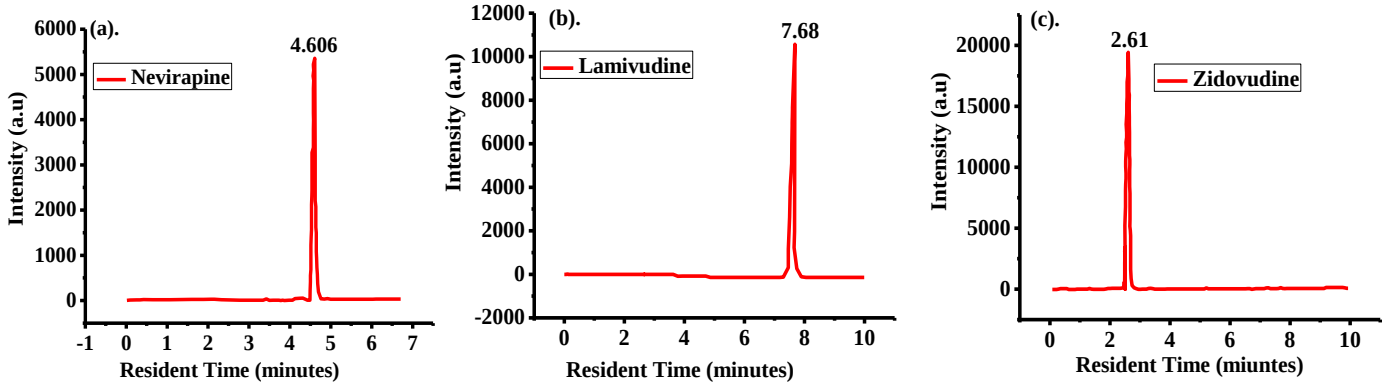

Figure 5.9: Typical Chromatogram of (a) Nevirapine, (b) Lamivudine, and (c) Zidovudine

The existence of these degradation products confirms degradation oxidation reactions of ARVD solutions mediated through iron-supported carbon-cloth electrode during electro-Fenton process. Furthermore, this analysis corroborated the UV–Vis analysis of Figure 5.5d which suggested a decrease in microorganic concentration from the solution of aqueous ARVDs. However, peaks with similar retention times have been previously observed for nevirapine (Vijayaraj *et al.*, 2013), lamivudie (Bedse *et al.*, 2009), and zidovudine (Mandloi *et al.*, 2011).

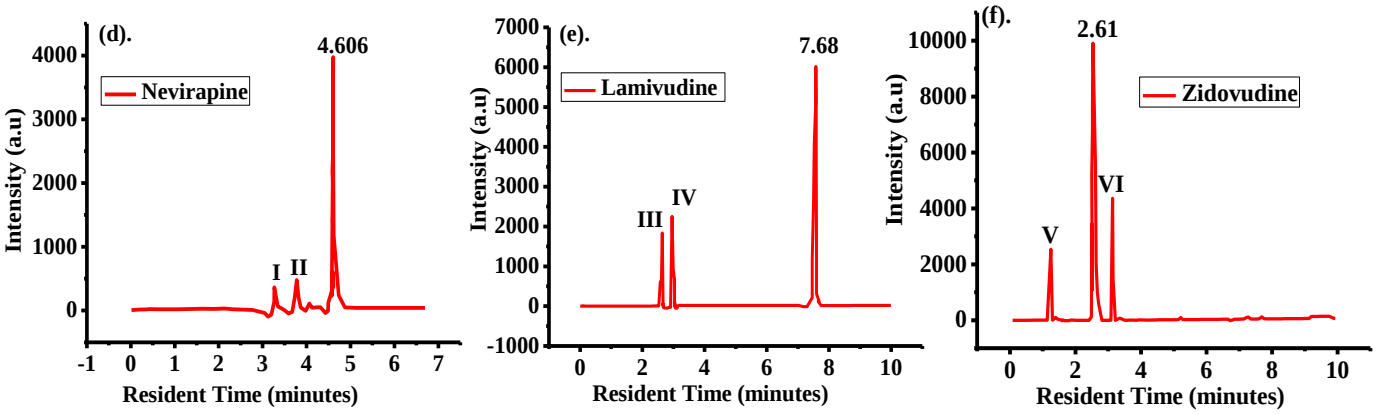

Figure 5.10: Degradation Chromatogram of (a) Nevirapine, (b) Lamivudine, and (c) Zidovudine

5.4.8 Regenerability of Fe/CC electrode

The catalytic performance of Fe/CC electrode on regeneration was examined for five consecutive cycles by washing and drying the same electrode at 70°C after usage in the sample wastewater for degradation. For the five consecutive trials, the Fe/CC electrode exhibited a higher degree of stability and strong catalytic activity towards the destruction of organics from ARVDs, as shown

in Figure 5.11. The removal efficiency of the iron modified electrode in terms of yield was stable, after the first cycle with values 30% for ZVD, 24%, for NVP and LVD. Hence, the stability of the electrode in the second, third, fourth and fifth circle is an indication that it is highly reusable and hence possibly appropriate for low-cost wastewater treatment.

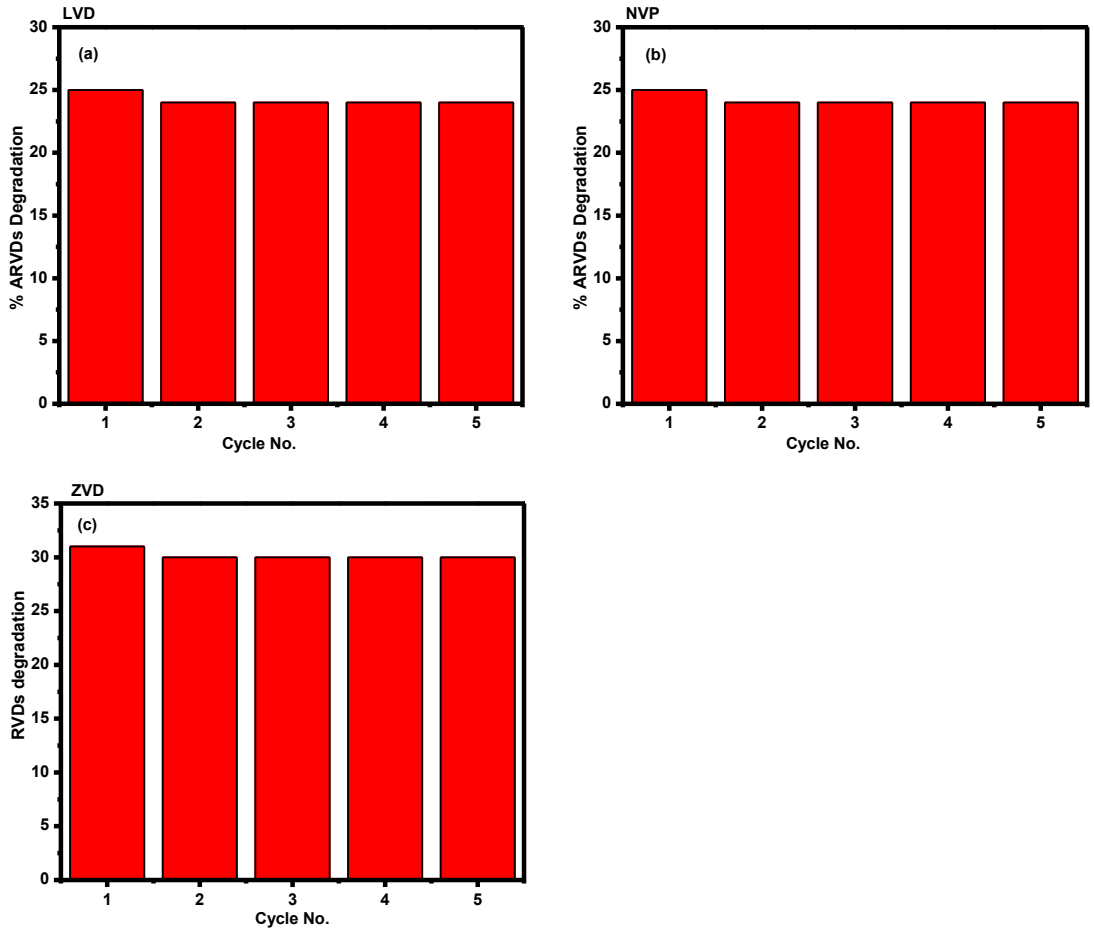

Figure 5.11: Reusability of Fe/CC electrode for five successive cycles for the degradation of ARVDs.

5.4.9 Effect of Fe^{2+} dosage on the degradation of organics from ARVDs

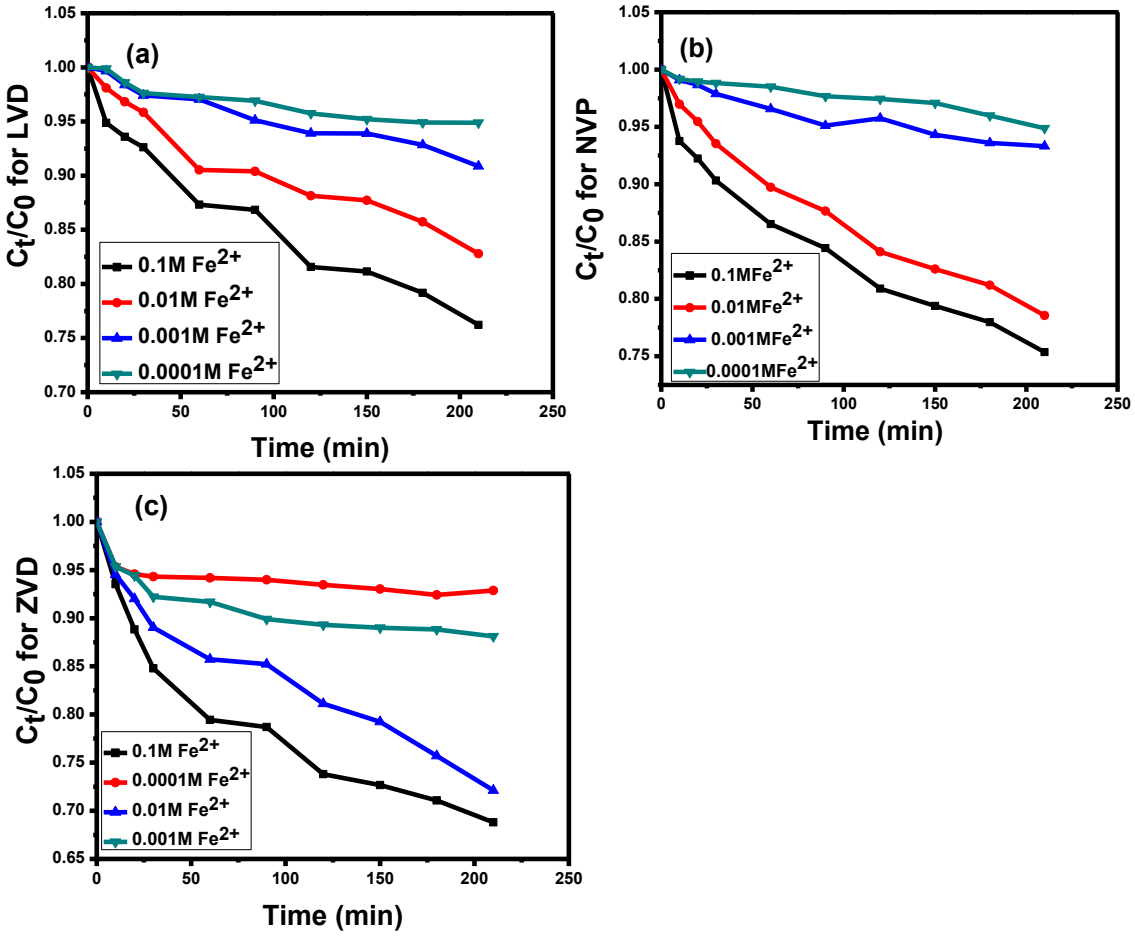

Figure 5.12: Effect of electrodeposited iron concentration of 0.1M, 0.01M, 0.001M and 0.0001M on the degradation of organics from ZVD by Electro Fenton.Experimental Condition: [ZVD] = 20 mg/L , pH = 3

The effect of Fe^{2+} doses on the degradation of ARVDs was investigated by varying its concentration between 0.1 - 0.0001M while maintaining the optimal current density of 8

mA/cm^2. The ZVD concentration was measured against time after the application of current to see if the electro-Fenton reaction would start and aid in the breakdown of the organics from ARVD. It can be seen from the ZVD normalization concentration profile as a function of initial iron concentration and time that at 0.0001 and 0.001M Fe^{+2}, there is only 7 % and 12 % removal efficiency of ZVD within 210 min of reaction. The obtained lower degradation efficiency was attributed to Fe^{2+} concentrations scavenging for more hydroxyl radicals as represented in Equation (5.15), thus reducing the oxidation power of the Fenton system and ZVD removal efficiency (Brillas et al., 2009; Brillas and Martínez-Huitle 2015).

This is a significant inhibitory reaction because hydroxyl radicals are wasted by reacting with Fe^{2+}, thus limiting the amount of organics from ARVDs that can be oxidized. The scavenging role of Fe^{2+} therefore destroys hydroxyl ions and is parasitic, competing with Fenton's reaction. However, a significant improvement in the degradation of organics from ARVDs was found in the presence of 0.01 and 0.1M Fe^{2+}, with degradation efficiencies of 28 % and 31 %, respectively, within 210 minutes of reaction. The increased generation of $OH^{\bullet}$ with high dose of Fe^{2+} in the Fenton reaction was primarily responsible for the enhanced degradation efficiency. As a result, 0.1 M Fe^{2+} was determined to be an appropriate dosage for ARVDs decomposition.

$$Fe^{2+} + OH^{\bullet} \longrightarrow Fe^{3+} + OH^{-} \qquad (5.15)$$

5.5 Conclusions

In this study, iron particles were successfully electrodeposited on a carbon-cloth electrode using the chronoamperometric method. An electrochemical technique was used to investigate its electron charge transfer and redox behavior. Result obtained herein indicates that synthesized iron-supported CC electrode has iron particles embedded in its matrix structure and this enhances the surface area, improve the conductivity and charge transfer properties of the electrode. This was demonstrated by the reduced semicircle diameter and lower Rct values observed from the modified carbon-cloth electrodes. The modified electrodes also show excellent redox behaviour with faster electron transfer kinetics as compared to the bare electrode. This property was evident in the apparently improved oxidation and reduction peak currents of the modified electrode. The application of the synthesized electrode was observed using EF process in the degradation of antiretroviral drugs solution at a pH of 3. While 31% removal efficiency was observed for ZVD, 25% was recorded for NVD and LVD. However, the result obtained is in corroboration with Jain *et al.* 2013, who demonstrated partial degradation for antiretroviral drugs during wastewater treatment. It is therefore anticipated that this work will motivate more interest in the use of modified CC electrode and advanced oxidation process to advance more knowledge for efficient antiretroviral drugs removal from the environment.

REFERENCES

AHMED, L.M., TAWFEEQ, F.T., AL-AMEER, M.H.A., AL-HUSSEIN, K.A. AND ATHAAB, A. R. 2016. Photo-degradation of Reactive Yellow 14 dye (a textile dye) employing ZnO as photocatalyst, *Journal of Geoscience and Environment Protection*, 4 (11) : 34–44.

ASENJO, N.G., SANTAMARIA, R., BLANCO, C., GRANDA, M., ALVAREZ, P. AND MENÉNDEZ, R. 2013. Correct use of the Langmuir–Hinshelwood equation for proving the absence of a synergy effect in the photocatalytic degradation of phenol on a suspended mixture of titania and activated carbon, *Carbon*, 55 : 62 – 69.

BABUPONNUSAMI, A. AND MUTHUKUMAR, K. 2011. Degradation of phenol in aqueous solution by fenton, sono-fenton and sono-photo-fenton methods, *Clean–Soil, Air, Water*, 39 (2) : 142 - 147

BADMUS, K.O., TIJANI, J.O., MASSIMA, E. AND PETRIK, L. 2018. Treatment of persistent organic pollutants in wastewater using hydrodynamic cavitation in synergy with advanced oxidation process, *Environmental Science and Pollution Research*, 25 (8) : 7299 – 7314.

BADAWY, M.I., GHALY, M.Y. AND GAD-ALLAH, T.A. 2006. Advanced oxidation processes for the removal of organophosphorus pesticides from wastewater, *Desalination*, *194* (1-3) : 166-175

BAÑUELOS, C., BEAS, B.S., MCQUAIL, J.A., GILBERT, R.J., FRAZIER, C.J., SETLOW, B. AND BIZON, J. L. 2014. Prefrontal cortical GABAergic dysfunction contributes to age-related working memory impairment, *Journal of Neuroscience*, 34 (10) : 3457 – 3466.

BANUELOS, J.A., GARCÍA-RODRÍGUEZ, O., RODRÍGUEZ-VALADEZ, F.J., MANRÍQUEZ, J., BUSTOS,

E., RODRÍGUEZ, A. AND GODÍNEZ, L. A. 2015. Cathodic polarization effect on the electro-Fenton regeneration of activated carbon, *Journal of Applied Electrochemistry*, 45 (5) : 523–531.

BEDSE, G., KUMAR, V. AND SINGH, S. 2009. Study of forced decomposition behavior of lamivudine using LC, LC–MS/TOF and MSn. *Journal of Pharmaceutical and Biomedical analysis*, 49 (1) : 55 - 63.

BOIX, C., IBÁÑEZ, M., SANCHO, J.V., NIESSEN, W.M.A. AND HERNÁNDEZ, F. 2013. Investigating the presence of omeprazole in waters by liquid chromatography coupled to low and high resolution mass spectrometry: degradation experiments, *Journal of Mass Spectrometry, 48 (10) :* 1091–1100.

BOUND, J AND VOULVOULIS, N. 2005. Household disposal of pharmaceuticals as a pathway for aquatic contamination in the United Kingdom, *Environmental Health Perspectives*, 113 (12) : 1705–1711.

DE CLERCQ, E. AND LI, G. 2016. Approved antiviral drugs over the past 50 years, *Clinical Microbiology Reviews*, 29 (3) : 695–747.

CLOUZOT, L., CHOUBERT, J.M., CLOUTIER, F., GOEL, R., LOVE, N.G., MELCER, H., ORT, C., PATUREAU, D., PLÓSZ, B.G., POMIÈS, M. AND VANROLLEGHEM, P. A. 2013. Perspectives on modelling micropollutants in wastewater treatment plants., *Water Science and Technology*, 68 (2) : 448–461.

DHILLON, S. AND KANT, R. 2017. Theory for electrochemical impedance spectroscopy of heterogeneous electrode with distributed capacitance and charge transfer resistance, *Journal of Chemical Sciences*, 129 (8) : 1277–1292.

EC08, A. A. N. 2011. Basic overview of the working principle of a potentiostat/galvanostat (PGSTAT)–Electrochemical cell setup. MetrohmAutolab, *MetrohmAutolab. BV*, : 1–3.

EMEJI1, I.C., AMA, O.M., OSIFO, P.O., RAY, S.S., GARCÍA-RODRÍGUEZ, O., AND LEFEBVRE, O. 2019. Electrochemical Preparation of Iron-Supported Carbon-Cloth Electrode and Its Application in the In-Situ Production of Hydrogen Peroxide, *International Journal of Electrochemical Science,* 14 : 9355 – 9368.

EVANS, D. 2013. Ten years on ART-where to now? SAMJ, *South African Medical Journal*, 103 (4) : 229–231.

FU, F., DIONYSIOU, D.D. AND LIU, H. 2014. The use of zero-valent iron for groundwater remediation and wastewater treatment: a review, *Journal of hazardous materials*, 267 : 194–205.

GALASSO, G. J., BOUCHER, C. A. B., COOPER, D. A., AND KATZENSTEIN, D. A. 2002. *Practical guidelines in antiviral therapy*. 1st edn. Netherlands: Elsevier Science B.V.

GARCIA-SEGURA, S., LIMA, Á.S., CAVALCANTI, E.B. AND BRILLAS, E. 2016. Anodic oxidation, electro-Fenton and photoelectro-Fenton degradations of pyridinium-and imidazolium-based ionic liquids in waters using a BDD/air-diffusion cell, *Electrochimica Acta*, 198 : 268–279.

GOUTHAMI, K., ANUSHA, P. K., NIKHILA, S.A. AND PUSHPA, L. 2013. Spectrophotometric method for degradation study of lamivudine, *International Journal of Medicinal Chemistry & Analysis*, 3 (2) : 66–69.

GUTREUTER, S., IGUMBOR, E., WABIRI, N., DESAI, M. AND DURAND, L. 2019. Improving estimates of district HIV prevalence and burden in South Africa using small area estimation techniques, *PloS One*, 14(2) : e0212445.

JAIN, S., KUMAR, P., VYAS, R.K., PANDIT, P., AND DALAI, A. K. 2013. Occurrence and removal of antiviral drugs in environment: a review, *Water, Air, & Soil Pollution*, 224 (2) : 1-19.

KHATAEE, A., AKBARPOUR, A. AND VAHID, B. 2014. Photoassisted electrochemical degradation of an azo dye using Ti/RuO2 anode and carbon nanotubes containing gas-diffusion cathode, *Journal of the Taiwan Institute of Chemical Engineers*, 45 (3) : 930–936.

KHETAN, S.K. AND COLLINS, T. J. 2007. Human pharmaceuticals in the aquatic environment: a challenge to green chemistry, *Chemical Reviews*, 107 (6) : 2319–2364.

KLAAS, N.E., THUPAYAGALE, G. AND MAKUA, T. P. 2018. The role of gender in the spread of HIV and AIDS among farm workers in South Africa, *African Journal of Primary Health Care & Family Medicine*, 10 (1) : 1–8.

KUMAR, P.P., SHIVA, P.V., KUMAR, K.S., AND KULKARNI, R. M. 2014. Fate of Zidovudine through Water Treatment with Chlorine: A Kinetic Study, *International Research Journal of Environment Sciences*, 3 (9) : 50–55.

LI, R., YANG, C., CHEN, H., ZENG, G., YU, G., AND GUO, J. 2009. Removal of triazophos pesticide from wastewater with Fenton reagent, *Journal of Hazardous Materials*, *167* (1-3) : 1028-1032

LILLENBERG, M., YURCHENKO, S., KIPPER, K., HERODES, K., PIHL, V., LÕHMUS, R., IVASK, M., KUU, A., KUTTI, S., LITVIN, S.V. AND NEI, L. 2010. Presence of fluoroquinolones and sulfonamides in urban sewage sludge and their degradation as a result of composting, *International Journal of Environmental Science & Technology*, 7 (2) : 307–312.

LVOVICH, V. F. 2012. *Impedance Spectroscopy: Applications to Electrochemical and Dielectric*

Phenomena. John Wiley and Sons.

MANDLOI, D., TRIPATHI, P., MOHANRAJ, P., CHAUHAN, N.S. AND PATEL, J. R. 2011. Development and validation of a stability-indicating hplc method for analysis of zidovudine (zdv) in bulk drug and in vitro release studies of tablets, *Journal of Liquid Chromatography & Related Technologies*, 34 (8) : 601–612.

MASCOLO, G., LOCAPUTO, V. AND MININNI, G. 2010. New perspective on the determination of flame retardants in sewage sludge by using ultrahigh pressure liquid chromatography–tandem mass spectrometry with different ion sources. *Journal of Chromatography A,* 1217 (27) : 4601 - 4611.

MOKHBI, Y., KORICHI, M. AND AKCHICHE, Z. 2019. Combined photocatalytic and Fenton oxidation for oily wastewater treatment, *Applied Water Science*, 9 (2) : 1 - 9.

MORTAZAVI, S.B., SABZALI, A. AND REZAEE, A. 2005. SEQUENCE-FENTON REACTION FOR DECREASING PHENOL FORMATION DURING BENZENE CHEMICAL CONVERSION IN AQUEOUS SOLUTIONS'. *JOURNAL OF ENVIRONMENTAL HEALTH SCIENCE & ENGINEERING*, 2 (2) : 62 - 71

PANDEY, K., ISLAM, S.T., HAPPE, T. AND ARMSTRONG, F. A. 2017. Frequency and potential dependence of reversible electrocatalytic hydrogen interconversion by [FeFe]-hydrogenases, In *Proceedings of the National Academy of Sciences*, : 3843–3848.

POTTABATHINI, V., GUGULOTHU, V., KALIYAPERUMAL, M. AND BATTU, S. 2016. Identification, Isolation and Characterization of Unknown Acid Degradation Product of Nevirapine, *American Journal of Analytical Chemistry, 7 (09) :* 663.

PRASSE, C., SCHLÜSENER M. P., SCHULZ, R., AND TERNES, T. A. 2010. Antiviral Drugs in

Wastewater and Surface Waters: A new Pharmaceutical Class of Environmental Relevance, *Environmental Science & Technology,* 44 (5) : 1728–1735.

QIANG, Z., CHANG, J.H. AND HUANG, C.P. 2002. ELECTROCHEMICAL GENERATION OF HYDROGEN PEROXIDE FROM DISSOLVED OXYGEN IN ACIDIC SOLUTIONS, *WATER RESEARCH,* 36 (1) : 85 - 94.

RAVINA, M., CAMPANELLA, L. AND KIWI, J. 2002. Accelerated mineralization of the drug diclofenac via Fenton reactions in a concentric photo-reactor, *Water Research,* 36 (14) : 3553-3560

RAHMANI, A.R., SHABANLOO, A., MEHRALIPOUR, J., FAZLZADEH, M. AND Poureshgh, Y. 2015. Degradation of Phenol in Aqueous Solutions Using Electro-Fenton Process, *Research Journal of Environmental Sciences,* 9 (7): 332

SANDERSON, H., JOHNSON, D.J., REITSMA, T., BRAIN, R.A., WILSON, C.J. AND SOLOMON, K. R. 2004. Ranking and prioritization of environmental risks of pharmaceuticals in surface waters, *Regulatory Toxicology and Pharmacology,* 39 (2) : 158–183.

SIRES, I., BRILLAS, E., OTURAN, M.A., RODRIGO, M.A. AND PANIZZA, M. 2014. ELECTROCHEMICAL ADVANCED OXIDATION PROCESSES: TODAY AND TOMORROW. A REVIEW, *ENVIRONMENTAL SCIENCE AND POLLUTION RESEARCH,* 21 (14) : 8336 - 8367.

SHAHWAN, T., SIRRIAH, S.A., NAIRAT, M., BOYACI, E., EROĞLU, A.E., SCOTT, T.B. AND HALLAM, K. R. 2011. Green synthesis of iron nanoparticles and their application as a Fenton-like catalyst for the degradation of aqueous cationic and anionic dyes, *Chemical Engineering Journal,* 172 (1) : 258–266.

SHARP, P.M. AND HAHN, B. H. 2011. Origins of HIV and the AIDS pandemic, *Cold Spring Harbor Perspectives in Medicine*, 1 (1) : a006841.

SHI, S., NGUYEN, P.K., CABRAL, H.J., DIEZ-BARROSO, R., DERRY, P.J., KANAHARA, S.M. AND KUMAR, V. A. 2016. Development of peptide inhibitors of HIV transmission. Bioactive materials, *Bioactive Materials*, 1 (2) : 109–121.

SWANEPOEL, C., BOUWMAN, H., PIETERS, R. AND BEZUIDENHOUT, C. 2015. Presence, concentrations and potential implications of HIV-anti-retrovirals in selected water resources in South Africa, *Water Research Commission. WRC Report*, 2144/1 : 14.

TURABIK, M., OTURAN, N., GÖZMEN, B. AND OTURAN, M. 2014. Efficient removal of insecticide "imidacloprid" from water by electrochemical advanced oxidation processes, *Environmental Science and Pollution Research*, 21 (14) : 8387–8397.

VASQUEZ-MEDRANO, R., PRATO-GARCIA, D. AND VEDRENNE, M. 2018. Ferrioxalate-mediated processes. In *Advanced Oxidation Processes for Waste Water Treatment* (pp. 89-113). Academic press.

VIJAYARAJ, S., HARIKA1, T., CHANDRASEKHAR, B., PALLAVI, G., SANGEETHA, V., AND SHANTHI, B. O. 2013. Stability Indicating RP-HPLC Method for Estimation of Nevirapine in Formulations, *Inventi Rapid: Pharm Analysis & Quality Assurance*, 2 : 1–5

WANG, A., QU, J., LIU, H., AND RU, J. 2008. Mineralization of an azo dye Acid Red 14 by photoelectro-Fenton process using an activated carbon fiber cathode, *Applied Catalysis B: Environmental - Journals*, 84 : 393–399.

WANG, L., ZHAO, J., HE, X., GAO, J., LI, J., WAN, C. AND JIANG, C. 2012. Electrochemical

impedance spectroscopy (EIS) study of LiNi1/3Co1/3Mn1/3O2 for Li-ion batteries, *International Journal of Electrochemical Science,* 7 (1) : 345–353.

YANG, Y., WANG, P., SHI, S. AND LIU, Y. 2009. Microwave enhanced Fenton-like process for the treatment of high concentration pharmaceutical wastewater, *Journal of Hazardous Materials*, 168 (1): 238 - 245

ZAZOULI, M.A. AND TAGHAVI, M. 2012. Phenol removal from aqueous solutions by electrocoagulation technology using iron electrodes: Effect of some variables.

ZHOU, M., TAN, Q., WANG, Q., JIAO, Y., OTURAN, N. AND OTURAN, M.A. 2012. Degradation of organics in reverse osmosis concentrate by electro-Fenton process, *Journal of Hazardous Materials, 215* : 287 - 293.

ZHANG, C., FAN, F.R.F. AND BARD, A.J. 2009. Electrochemistry of oxygen in concentrated NaOH solutions: solubility, diffusion coefficients, and superoxide formation. *Journal of the American Chemical Society,* 131 (1): 177-181.

Chapter 6: General Conclusions and Recommendations

6.1 General Conclusions

This study deals with the application of EF, with a carbonaceous cathodic electrode for the degradation of the pharmaceutical antiretroviral drugs. It has generally been demonstrated that EF-BDD, are very efficient in the removal of pharmaceuticals in an aqueous medium. The use of a carbon cloth as a cathodic cathode amid oxygenation makes certain the continuous electrogenerated of H_2O_2 and Fe^{2+} needed to produce homogeneous $OH^{\bullet}$ in the bulk solution. The synthesis of iron supported CC electrode was done by electrodeposition of iron (II) onto the surface of the CC electrode through cyclic sweeping from -1.8 to 1 V and back at 0.05V/s for 90 cycles in an N_2-enriched working solution containing 0.1M $FeSO_4.7H_2O$ and 50 mM (millimole) of K_2SO_4 at a pH of 3.

The BDD anode also produces large amounts of active heterogeneous BDD ($OH^{\bullet}$) radicals, making the EF-BDD (with BDD anode) processes one of the most efficient processes for the mineralization of pharmaceuticals. For the characterization of the synthesized iron supported electrode, the SEM and EDX analysis show the formation of iron nanoparticles within the matrix structure of the prepared CC electrode. The XPS analysis highlights the presence of oxygen functional groups in the synthesized electrode's structure. EIS result depicts a decrease in charge transfer resistance (Rct) value as compared to the bare CC electrode. Finally, the CV result of the modified electrode fosters good conductivity, enhances current and large surface area. After characterization, the synthesized Fe/CC electrode was tested in the electro-Fenton degradation of prepared synthetic NVP, LVD and ZVD antiretroviral wastewater solution with

an initial concentration of 20 mg/L and a pH of 3. The aqueous solution of the antiretroviral organics was prepared using 50 mM of K_2SO_4 supporting electrolyte to increase their conductivity. The result of the degradation of electrolysis experiments by UV-vis analysis shows a decrease in the normalized concentration (C_t/C_o) of the organics with respect to reaction time.

Deductions from the obtained data show that ZVD degrades faster with a removal efficiency of 31% as compared to 25% removal efficiency recorded for NVD and LVD respectively. This result is very promising when compared to the removal efficiency obtained by Gouthami *et al.* 2013 and Pottabathini *et al.* 2016. The apparent degradable rate constants (K_{app}) obtained were 1.52 x 10^{-3} $mol^{-1}min^{-1}$ for ZVD, 1.20 x 10^{-3} $mol^{-1}min^{-1}$ for NVP and 1.18 x 10^{-3} $mol^{-1}min^{-1}$ for LVD. Further analysis of degradation samples of NVP, LVD, and ZVD using HPLC, indicates peaks which were assigned to the intermediate products of I, II, III, IV, V, and VI with retention times of 3.27, 3.78, 2.64, 2.98, 1.24, and 3.13 minutes, respectively. Generally, the obtained result heightens the potentiality of EF as environmentally benign technologies for the remediation of wastewaters containing pharmaceutical organics and their oxidation by-products.

6.2 Recommendation

For future studies, researchers should be encouraged to put more effort into exploring ways of improving the catalytic activity, stability, and selectivity of iron supported electrode since it encourages the continuous *"in-situ"* electrogenerated H_2O_2 and Fe^{2+} needed to produce homogeneous hydroxyl radicals ($OH^{\bullet}$) for total mineralization of micro organics. Also, there is a need to study the chemistry of electrodeposition on the solid electrode support.

APPENDICES

Appendix I

CALCULATING THE CONCENTRATIONS OF THE ARVDS

Mass of ARVDs measured = 0.1 g = 100 mg

Vol of deionised water = 100 ml

Concentration of ARVDs stock solution = $\frac{100mg}{100ml} = \frac{1mg}{ml} = 1000\ mg/l$

Concentration of stock ARVDs solution = 1000 mg/l

To prepare a working ARVDs solution having 20 mg/l of concentration in 100 ml volumetric flask, we use dilution method as expressed in equation as: $C_1V_1 = C_2V_2$

20 mg/l x 100 ml = 1000 mg/l x V

$\frac{20\ 00\ mg.ml.l}{1000\ mg.l} = 2\ ml$

So we measure 2 ml from stock solution into 100 ml volumetric flask and top it up with deionised water.

Initial Concentration (C_0) of NVP, ZVD and LVP that degraded = 20 mg/L

Preparation of Iron (II) Solution of different concentration.

Prepare 0.1M, 0.01M, 0.001M and 0.0001M of Iron (II) in 100ml of solution.

- 0.1M 100ml Iron (II) sulfate heptahydrate

1M I000mL $FeSO_4.7H_2O$ ≡ 278.01g/mol $FeSO_4.7H_2O$

0.1M I000mL $FeSO_4.7H_2O$ ≡ 27.8 g/mol $FeSO_4.7H_2O$

0.1M 100mL $FeSO_4.7H_2O \equiv 2.78$ g/mol $FeSO_4.7H_2O$

Therefore, measure 2.78 g of $FeSO_4.7H_2O$ and pour it into 100mL volumetric flask.

- 0.01M 100ml Iron (II) sulfate heptahydrate are prepared as

0.1M 100mL $FeSO_4.7H_2O \equiv 2.78$ g/mol $FeSO_4.7H_2O$

0.01M 100mL $FeSO_4.7H_2O \equiv 0.278$ g/mol $FeSO_4.7H_2O$

0.001M 100ml $FeSO_4.7H_2O \equiv 0.0278$ g/mol $FeSO_4.7H_2O$

0.0001M 100 ml $FeSO_4.7H_2O \equiv 0.00278$ g/mol $FeSO_4.7H_2O$

Smaller concentrations require smaller masses, which the weighing balances cannot measure. As such, we use Dilution method, hence:

- $C_1V_1 = C_2V_2$

To prepare 0.001M 100 ml $FeSO_4.7H_2O$ from 0.1M 100mL $FeSO_4.7H_2O$ solution we will have:

0.001M x100 ml = 0.1M x V_2

V_2 = 1 ml (We measure 1ml from 0.1M 100 ml solution into a 100ml vol. flask)

To prepare 0.0001M 100 ml $FeSO_4.7H_2O$ from 0.1M 100mL $FeSO_4.7H_2O$ solution we will have:

0.0001M x 100 ml = 0.1M x V_2

V_2 = 0.1 ml (We measure 0.1ml from 0.1M 100 ml solution into a 100ml vol. flask)

Different Con. of Fe^{2+} precursor used during iron electrodeposition on CC electrode

Fe^{2+} Molar Con. (Mol)	Mass (g)	Vol. Measured (mL)
0.1	2.78	-
0.01	0.278	-

0.001	0.0278	1
0.0001	0.00278	0.1

Values obtained when CC is loaded with different Fe^{2+} concentration to degrade ZVD wastewater solution

For ZVD

Time	C_t/C_0 for different Fe^{2+} Loading			
	0.1MFe	0.0001MFe	0.01MFe	0.001MFe
0	1	1	1	1
10	0.93525	0.95345	0.94525	0.95345
20	0.88826	0.94571	0.92015	0.94431
30	0.84801	0.94321	0.89021	0.92211
60	0.79434	0.94191	0.85733	0.91689
90	0.78704	0.93979	0.85221	0.89902
120	0.73806	0.93457	0.81112	0.89321
150	0.7266	0.93029	0.79239	0.89012
180	0.71076	0.92413	0.75713	0.88831
210	0.68803	0.92869	0.72112	0.88122

Degradation removal efficiency (RE) obtained for ZVD at different iron dose loading

For 0.1M Fe^{2+}, RE = (1 – 0.68803/1) x 100 = 31%

For 0.0001M Fe^{2+}, RE = (1 – 0.92869/1) x 100 = 7%

For 0.01M Fe^{2+}, RE = (1 – 0.72112/1) x 100 = 28%

For 0.001M Fe^{2+}, RE = (1 – 0.88122/1) x 100 = 12%

For NVP

	C_t/C_0			
Time	0.1MFe^{2+}	0.01MFe^{2+}	0.001MFe^{2+}	0.0001MFe^{2+}
0	1	1	1	1
10	0.93763	0.96983	0.99083	0.99183
20	0.92243	0.95463	0.98662	0.98941
30	0.90322	0.93542	0.97879	0.98821
60	0.86518	0.89738	0.96563	0.98501
90	0.84433	0.87653	0.95112	0.97663
120	0.80891	0.84111	0.95758	0.97431
150	0.79379	0.82599	0.94321	0.97079
180	0.77972	0.81192	0.93597	0.95979
210	0.75366	0.78556	0.93312	0.94879

Degradation removal efficiency (RE) obtained by degrading NVP

For 0.1M Fe^{2+}, RE = (1 – 0.75366/1) x 100 = 25%

For 0.01M Fe^{2+}, RE = (1 – 0.78556/1) x 100 = 21%

For 0.001M Fe^{2+}, RE = (1 – 0.93312/1) x 100 = 7%

For 0.0001M Fe^{2+}, RE = (1 – 0.94879/1) x 100 = 5%

For LVD

0	1	1	1	1
10	0.94873	0.98093	0.99661	0.99881
20	0.93592	0.96812	0.98381	0.98601
30	0.92615	0.95835	0.97404	0.97623
60	0.87311	0.90531	0.97042	0.97261
90	0.86831	0.90399	0.95121	0.96913
120	0.81567	0.88135	0.93915	0.95746
150	0.81151	0.87719	0.93887	0.95213
180	0.79171	0.85739	0.92837	0.94914
210	0.76213	0.82781	0.90879	0.94888

Degradation removal efficiency (RE) obtained by degrading LVP

For 0.1M Fe^{2+}, RE = (1 – 0.76213/1) x 100 = 25%

For 0.01M Fe^{2+}, RE = (1 – 0.82781/1) x 100 = 17%

For 0.001M Fe^{2+}, RE = (1 – 0.90879/1) x 100 = 9%

For 0.0001M Fe^{2+}, RE = (1 – 0.94888/1) x 100 = 5%

Values obtained for calibration curves at λ_{max} 289 nm for NVP, 274 nm for LVD and 281 nm for ZVD

Conc.	Nevirapine Absorbance	Zidovudine Absorbance	Lamivudine Absorbance
5	0.43011	0.81871	0.91237
10	0.87007	1.33414	1.58011
15	1.29402	1.93957	2.40412
18	1.57401	2.29583	2.70114
20	1.75012	2.52361	3.02044

Obtained values for the degradation of NVP, LVD and ZVD at pH 3

	NVP		LVD		ZVD	
Time	Con. (C_t)	(C_t/C_0)	Con. (C_t)	(C_t/C_0)	Con. (Ct)	(C_t/C_0)
0	20	1	20	1	20	1
10	18.7526	0.93763	18.9746	0.94873	18.705	0.93525
20	18.4486	0.92243	18.7184	0.93592	17.7652	0.88826
30	18.0644	0.90322	18.5230	0.92615	16.9602	0.84801
60	17.3036	0.86518	17.4600	0.8730	15.8868	0.79434
90	16.8866	0.84433	17.3662	0.86831	15.7408	0.78704
120	16.1780	0.8089	16.3134	0.81567	14.7612	0.73806

150	15.8758	0.79379	16.230	0.8115	14.5320	0.7266
180	15.5944	0.77972	15.8340	0.7917	14.2152	0.71076
210	15.0732	0.75366	15.2426	0.76213	13.7606	0.68803

Degradation removal efficiency (%) = $\left(\frac{C_0 - C_t}{C_0}\right) x\ 100 = \left(1 - \frac{C_t}{C_0}\right) x\ 100$

For NVP, RE = $\frac{20-15.0732}{20}\ x\ 100$ = 25%

For LVD. RE = (1 – 0.76213/1) x 100 = 24%

For ZVD, RE = (1 – 0.68803/1) x 100 = 31%

Values for in-situ generated hydrogen peroxide (H_2O_2)

	Bare Electrode	Modified Electrode
Time	Con.	Con
5	2.20436	6.46463
10	2.23094	10.82966
15	2.25753	14.43996
20	2.28222	20.46539
30	2.3335	25.42118
40	2.53988	29.32005
50	2.74437	35.33308
60	3.25969	39.23256

Calculation for the Effect of pH on degradability

For NVP

Time	C_t/C_0 values at different pH		
	pH=3	pH=5	pH=7
0	1	1	1
10	0.93763	0.94763	0.95763
20	0.92243	0.93194	0.94176
30	0.90322	0.92134	0.93195
60	0.86518	0.89077	0.90231
90	0.84433	0.87123	0.89141
120	0.80891	0.85632	0.87831
150	0.79379	0.83312	0.84661
180	0.77972	0.80761	0.83132
210	0.75366	0.79851	0.82864

At pH = 3, Removal efficiency = (1 – 0.75366/1) x 100 = 25%

pH = 5, Removal efficiency = (1 – 0.79851/1) x 100 = 20%

pH = 7, Removal efficiency = (1 – 0.82864/1) x 100 = 17%

For ZVD

Time	C_t/C_0 values at different pH		
	pH =3	pH =5	pH =7
0	1	1	1
10	0.93525	0.94525	0.94425
20	0.88826	0.92015	0.93115
30	0.84801	0.90732	0.91615
60	0.79434	0.86121	0.89192
90	0.78704	0.84733	0.87767
120	0.73806	0.81121	0.86239
150	0.7266 1	0.79239	0.83141
180	0.71076	0.75736	0.80213
210	0.68803	0.74889	0.79769

At pH = 3, Removal efficiency = (1 – 0.64532/0.93525) x 100 = 31%

pH = 5, Removal efficiency = (1 – 0.725925/0.96790) x 100 = 25%

pH = 7, Removal efficiency = (1 – 0.782312/0.97789) x 100 = 20%

For LVD

Time	C_t/C_0 values at different pH		
	pH =3	pH =5	pH =7
0	1	1	1

10	0.94873	0.95873	0.96873
20	0.93592	0.94131	0.95717
30	0.92615	0.93592	0.94341
60	0.87311	0.89141	0.92174
90	0.86831	0.87731	0.89321
120	0.81567	0.84326	0.86745
150	0.81115	0.82345	0.85511
180	0.79171	0.80139	0.85311
210	0.76213	0.78887	0.84879

At pH = 3, Removal efficiency = (1 – 0.71155/0.94873) x 100 = 25%

pH = 5, Removal efficiency = (1 – 0.764649/0.96791) x 100 = 21%

pH = 7, Removal efficiency = (1 – 0.801935/0.97797) x 100 = 18%

Effect of initial AVRDs Conc. On degradability

For NVP

	C_t/C_0		
Time	20mg/L	40mg/L	60mg/L
0	1	1	1
10	0.93763	0.96881	0.97921
20	0.92243	0.96122	0.97414
30	0.90322	0.95161	0.96774
60	0.86518	0.93259	0.95506

90	0.84433	0.92217	0.94811
120	0.80891	0.90445	0.9363
150	0.79379	0.8969	0.93126
180	0.77972	0.88986	0.92657
210	0.75366	0.87683	0.91789

At 20mg/L NVP, Removal efficiency = (1 – 0.75366/1) x 100 = 25%

40mg/L NVP, Removal efficiency = (1 – 0.87683/1) x 100 = 12%

60mg/L NVP, Removal efficiency = (1 – 0.91789/1) x 100 = 8%

For ZVD

0	1	1	1
10	0.93525	0.96762	0.97841
20	0.88826	0.94413	0.96275
30	0.84801	0.92401	0.94934
60	0.79434	0.89717	0.93145
90	0.78704	0.89352	0.92901
120	0.73806	0.86903	0.91269
150	0.7266	0.8633	0.90887
180	0.71076	0.85538	0.90359
210	0.68803	0.84401	0.89601

At 20mg/L ZVD, Removal efficiency = (1 – 0.68803/1) x 100 = 31%

40mg/L ZVD, Removal efficiency = (1 – 0.84401/1) x 100 = 16%

60mg/L ZVD, Removal efficiency = (1 – 0.89601/1) x 100 = 10%

For LVD

0	1	1	1
10	0.94873	0.95873	0.96873
20	0.93592	0.94131	0.95717
30	0.92615	0.93592	0.94341
60	0.87311	0.89141	0.92174
90	0.86831	0.87731	0.89321
120	0.81567	0.84326	0.86745
150	0.81115	0.82345	0.85511
180	0.79171	0.80139	0.85311
210	0.76213	0.78887	0.84879

At 20mg/L LVD, Removal efficiency = (1 – 0.76213/1) x 100 = 25%

40mg/L LVD, Removal efficiency = (1 – 0.78887/1) x 100 = 21%

60mg/L LVD, Removal efficiency = (1 – 0.84879/1) x 100 = 15%

Appendix II: General and specific standard for effluent being discharged into a water resource (DWA, 2013).

Substances/Parameters	**General limit**	**Special limit**
Faecal coliforms (per 100ml)	1000	0
Chemical oxygen demand (mg/l)	75	30
pH	5.5 – 9.5	5.5 – 7.5
Ammonia (ionized and unionized as nitrogen (mg/l)	6	2
Nitrate/nitrite as nitrogen (mg/l)	15	1.5
Chlorine as free chlorine (mg/l)	0.25	0
Suspended solids (mg/l)	25	10
Electrical conductivity (mS/m)	70 ms/m above intake to a maximum of 150 mS/m	50 mS/m above background receiving water, to a maximum of 100 mS/m
Ortho-phosphate as phosphorous (mg/l)	10	1 (median) and 2.5 (maximum)
Fluoride (mg/l)	1	1
Soap, oil or grease (mg/l)	2.5	0
Dissolved arsenic (mg/l)	0.02	0.01
Dissolved cadmium (mg/l)	0.005	0.001
Dissolved chromium (vi) (mg/l)	0.05	0.02
Dissolved copper (mg/l)	0.01	0.002
Dissolved cyanide (mg/l)	0.02	0.01

Dissolved iron (mg/l)	0.3	0.3
Dissolved lead (mg/l)	0.01	0.006
Dissolved manganese (mg/l)	0.1	0.1
Mercury and its compounds (mg/l)	0.005	0.001
Dissolved selenium (mg/l)	0.02	0.02
Dissolved zinc (mg/l)	0.1	0.04
Boron (mg/l)	1	0.5
OTHERS		
Dissolved Oxygen (mg/L)	75% saturation	75% saturation (8 – 10)
Temperature (°C)	35	25
Total Suspended Solids (mg/L)	90	10

Appendix III: Maximum Contaminant Level (MCL) for chemicals according to (NPDWR, 2016)

Contaminant	MCL (mg/L)
Acrylamide	TT
Acetaminophen	-
Alachlor	0.002
Ampicillin	-
Aspirin	-
Atenolol	-
Atrazine	0.003

Benzene	0.005
Bezafibrate	
Benzo(a)pyrene (PAHs)	0.0002
Bisphenol-A, BPA	
Carbofuran	0.04
Carbon Tetrachloride	0.005
Caffeine	
Carbamazepine	
Chlorobenzene	0.1
Chloramphenicol	
Clozapine	
Ciprofloxacin	
2,4-D	0.07
Dalapon	0.2
1,2-Dibromo-3-chloropropane (DBCP)	0.0002
o-Dichlorobenzene	0.6
p-Dichlorobenzene	0.075
1,2-Dichloroethane	0.005
1,1-Dichloroethylene	0.007
cis-1,2-Dichloroethylene	0.07
Polychlorinated Dibenzofurans (PCDFs)	
Trans-1,2-Dichloroethylene	0.1
Trans-1,2-dichloroethylene	
Dichloromethane	0.005

4,4'-Dichlorodiphenyl sulfone	
1,2-Dichloropropane	0.005
Di(2-ethylhexyl) adipate	0.4
Di(2-ethylhexyl) phthalate	0.006
Dinoseb	0.007
Dioxin (2,3,7,8-TCDD)	0.00000003
Diclofenac	
Diquat	0.02
Endothall	0.1
Endrin	0.002
Epichlorohydrin	TT
Ethylbenzene	0.7
Ethylene dibromide	0.00005
Erythromycin	114-07-8
Glyphosate	0.7
Heptachlor	0.0004
Heptachlor epoxide	0.0002
Hexachlorobenzene	0.001
Hexachlorocyclopentadiene	0.05
Ibuprofen	
Ketoprofen	
Lindane	0.0002
Methoxychlor	0.04
Metronidazole	

Nalidixic acid	
Nonylphenols	
Oxamyl (Vydate)	0.2
Polychlorinated biphenyls (PCBs)	0.0005
Pentachlorophenol	0.001
Picloram	0.5
Simazine	0.004
Styrene	0.1
Sulfamethoxazole	
Sulfamethazine	
Streptomycin	
Toxaphene	0.003
Tetracycline	
Trimethoprim	
Triclosan	
Tylosin	
1,1,2-Trichloroethane	0.005
Trichloroethylene	0.005
Vinyl chloride	0.002
Xylenes (total)	10